Development of an optical measurement method for determining the filling degree of double emulsions by in-line Raman spectroscopy

Zur Erlangung des akademischen Grades eines

DOKTORS DER INGENIEURWISSENSCHAFTEN (Dr.-Ing.)

von der KIT-Fakultät für Chemieingenieurwesen und Verfahrenstechnik des Karlsruher Instituts für Technologie (KIT)

genehmigte

DISSERTATION

von

M. Sc. Thomas Martin Hufnagel

Aus Brühl – Rohrhof, Deutschland

Tag der mündlichen Prüfung:	26.03.2024
Erstgutachterin:	Prof. Dr.-Ing. Heike P. Karbstein
Zweitgutachter:	Prof. Dr.-Ing. Matthias Rädle

Table of content

1 General Introduction

1.1 Introduction

Emulsions have been used by humans in various applications for more than a century. One of the most prominent examples is cow's milk. The patent for its homogenization dates back to 1899 [1].

In 1925, a new class of emulsions, the so-called double emulsions, was mentioned for the first time by William Seifriz in a technical journal [2]. As the name implies, this is a dual emulsion. This means that an existing emulsion is emulsified a second time. For example, a water-in-oil (W/O) emulsion is emulsified into a water-in-oil-in-water (W/O/W) emulsion [3].

This additional emulsification step offers new opportunities for product development. In the inner emulsion phase, value-giving, sensitive ingredients can be safely encapsulated until the emulsion is used [4]. In addition, the middle emulsion phase can be solidified, which offers increased protection against external influences. Also, properties of emulsions can be specifically influenced by the further emulsification step. For example, in the food industry, fat-reduced dairy products are manufactured by reducing the fat content of an O/W emulsion by adding water to the oil, which corresponds to a W/O/W emulsion [3].

However, besides their advantages, double emulsions also have decisive disadvantages. First and foremost, the need to keep double emulsions stable over a longer period of time still confronts researchers with a major challenge. Once a double emulsion has been produced, several instability mechanisms may take place, driven mainly by "diffusion" and "coalescence" [5]. When these mechanisms occur, both the internal and the average droplet size as well as the phase ratios and their composition can change, which will ultimately lead to phase separation [3].

Sophisticated measurement techniques are needed to understand and find adequate solutions to counteract the instability mechanisms. These must be able to precisely measure essential parameters of a double emulsion. In particular, the various droplet sizes, the filling degree and the time to coalescence are of great interest [6]. Today, there are already several methods that can determine these parameters. However, each method comes with specific limitations.

Raman spectroscopy offers a suitable alternative for a new measurement technique. This optical measurement technology is non-invasive, suitable for aqueous samples, does not require specific sample preparation and is highly selective. In addition, measurements can be performed both in-line and off-line [7, 8]. However, the numerous interphases within a double emulsion can be disadvantageous, since multiple reflections of the exciting laser as well as of the resulting Raman signal can occur here [9]. At the beginning of this work, only a few papers

had been published combining the two topics "double emulsions" and "Raman spectroscopy" [10].
In the following, the basics of double emulsions and Raman spectroscopy, which are necessary to understand this thesis, will be explained. In the case of double emulsions, the W/O/W double emulsion is always meant. At the end of this chapter the further structure of this thesis is explained.

1.2 Double emulsions

Double emulsions are complex multiphase systems consisting of three nested phases. The most common types are water-in-oil-in-water (W/O/W) or oil-in-water-in-oil (O/W/O) emulsions [6]. To distinguish between the inner and outer phases, indices are commonly used. For the inner phase 1, for the outer phase 2. A W/O/W double emulsion is therefore also called $W_1/O/W_2$ double emulsion [11].
Due to their specific structure, double emulsions can encapsulate valuable substances inside them until their application. The food industry, the cosmetics industry, and the pharmaceutical industry are the main markets for these products [12]. The encapsulation can be done in various ways. For example, the middle phase can be cured by a chemical reaction or crystallized due to solvent evaporation [13] or temperature reduction [14].
There are various methods to produce double emulsions. If the double emulsion is produced by conventional emulsification techniques, such as rotor-stator machines or high-pressure homogenizers, a two-stage process has been established. The process is based on the top-down principle [15]. First, a crude emulsion of large, non-uniform droplets is produced, which is then emulsified under high energy input to form small, uniform droplets. Subsequently, with significantly lower energy input, the produced emulsion is emulsified into the outer phase, creating the double emulsion. The significantly lower energy input is essential, otherwise the inner emulsion droplets can coalesce with the outer phase [4].
Depending on the emulsification technique, the properties of the resulting inner emulsion and the double emulsion can be controlled. All conventional emulsification techniques are characterized by a non-uniform droplet size. Therefore, the drop size is given in a drop size distribution. In order to determine the drop size distribution, various characteristic drop diameters are available [6].
In addition to conventional emulsification techniques, microfluidic emulsification systems have become increasingly used over the recent years. These work according to the bottom-up principle, whereby the droplets are produced directly from the separately present emulsion phases [15]. For this purpose, the emulsion phases are brought together in channel geometries that are typically smaller than 1mm in diameter. The very small channel geometries result in laminar flow conditions. As a result, identical forces act on all droplet breakups, leading to a

monodisperse droplet size distribution [16]. have been established for the microfluidic production of double emulsions [17].

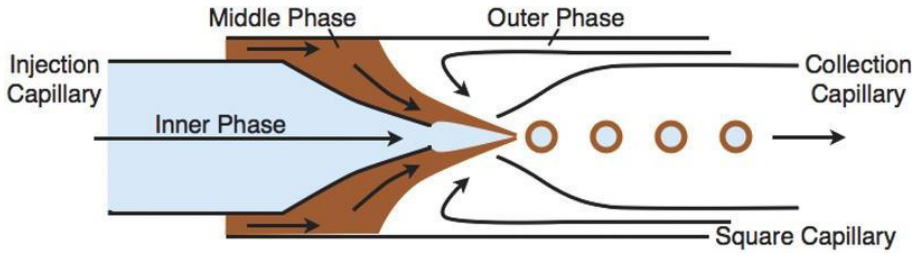

Figure 1-1 Schematic structure of a glass capillary device for the production of double emulsions [18].

Although production rates of 20 kHz can be achieved in microfluidic systems, the absolute throughputs are limited due to the narrow channel geometries. This contrasts with an unmatched precision in adjusting the droplet sizes [19]. These are dependent on various material and process parameters, such as viscosity, the flow rates of the emulsion phases, and the channel geometry [20].

As double emulsions are thermodynamically instable, their structure can be affected by a number of instability mechanisms, which can be driven by diffusion and coalescence [11, 12]. Coalescence occurs when two insufficient stabilized droplets come into contact with each other and merge into one droplet. This can happen both between the inner droplets (W_1-W_1 – coalescence) and between the outer double emulsion droplets (O-O – coalescence). In addition, coalescence occurs when an inner water droplet coalesces with the outer phase (W_1-W_2 – coalescence) [11].

W_1-W_1 – Coalescence does not change the properties of double emulsions significantly. However, different sized inner water droplets can lead to increased diffusion within the oil droplet as well as increased water droplets can influence the coalescence rate between the two water phases. If coalescence occurs between two double emulsion droplets (O-O – coalescence), the properties of the double emulsion, such as its viscosity and oil droplet size distribution, are significantly changed. In addition, larger oil droplets lead to increased creaming. The coalescence between inner water droplets and the outer water phase is also critical, since this ultimately leads to a breakdown of the double emulsion, resulting in an O-W emulsion [3].

Diffusion occurs between inner water droplets (W_1-W_1 – diffusion), the inner water droplets and outer phase (W_1-W_2 – diffusion) and between the oil phase (O-O – diffusion). Here, the driving forces result from the capillary pressure and the osmotic pressure. If both pressures are in equilibrium, diffusion processes do not occur [5].

The capillary pressure is calculated using the following equation 1-1 [6]

$$\Delta p_k = \Delta p_{k1} - \Delta p_{k2} = \frac{4 \cdot \gamma}{x_1} - \frac{4 \cdot \gamma}{x_2} = 4 \cdot \gamma \cdot \frac{x_2 - x_1}{x_1 \cdot x_2}. \qquad 1\text{-}1$$

Herein, p_k represents the capillary pressure, γ the interfacial tensions and x the diameter of one droplet. The equation shows that, the bigger the difference in diameter of two droplets, the bigger the capillary pressure difference between those droplets.
The osmotic pressure is given by the next equation 1-2 [13]

$$\Pi_{Osmotic} = C \cdot R \cdot T = C_0 \cdot \left(\frac{r_0}{r}\right)^3 \cdot R \cdot T. \quad 1\text{-}2$$

Where C is the molar concentration of the solute and C_0 represents the initial concentration. R is the ideal gas constant, T is the temperature and r, respectively r_0, give the actual, respectively the initial, radius of one droplet. Because of the exponent over the fraction, a changing droplet radius has significant influence on the osmotic pressure. Furthermore, it can be influenced by changes in molar concentration induced by adding osmotically active substances.
In double emulsions, diffusion mainly occurs between the inner water droplet and the outer water phase [21]. The direction of diffusion between the two phases depends on the ratio of the osmotic pressures. If the osmotic pressure in the outer phase is lower than in the inner phase, water diffuses from the outside to the inside. As a result, the inner droplets swell and the solvate concentration present in them as well as the inner osmotic pressure decrease [13]. In addition, the oil droplet size changes. To suppress diffusion, osmotically active substances such as salts can reduce the osmotic pressure gradient, and the inner water phase can be gelled [5].
The driving force of W1-W1 diffusion is the capillary pressure difference between two droplets. The smaller the droplet, the higher the capillary pressure. This results in water diffusion from smaller to larger droplets, which is referred to as Oswald ripening [6]. Effective countermeasures include uniform droplet sizes, by producing the inner water droplets microfluidically or by membrane emulsification, and adding osmotically active substances, which can also reduce capillary pressure. In addition, gelation of the water phase also has a reducing effect on Ostwald ripening [13]. Figure 1-2 shows the instability mechanisms which can occur in double emulsions.

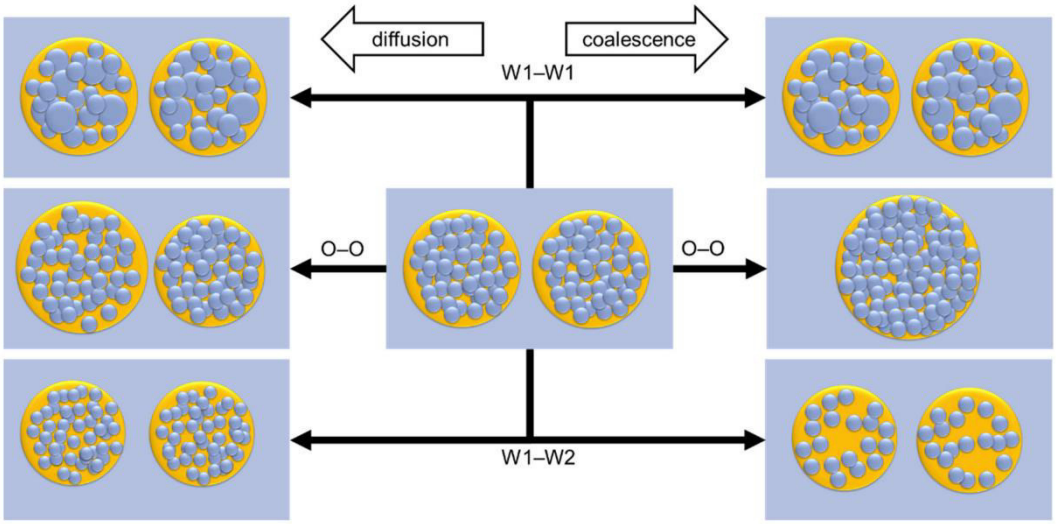

Figure 1-2 Summary of the various instability mechanisms that can occur in double emulsions. The diffusion mechanisms are shown on the left, the coalescence-based mechanisms on the right [5].

Common for all instability mechanisms is that emulsifiers can counteract them. Most often, hydrophilic emulsifiers are used in the outer water phase to stabilize the O/W interface, while hydrophobic emulsifiers are added to the oil phase to stabilize the W/O interfaces [3]. Ideally, both emulsifiers are present only at the intended interface. However, since emulsifier molecules are amphiphilic, they are often present at both interfaces, resulting in interactions between the emulsifiers [22].

In order to investigate the stability and structure of double emulsions experimentally, several methods are already available, which can be used, for example, to determine the droplet sizes, their distribution or the filling degree [5].

Dynamic and static light scattering are established methods for measuring droplet sizes. The measurement is performed offline with strong dilution of the emulsion. For this reason, the sample is disposed after the measurement. In the case of double emulsions, the droplet size of the inner emulsion must be measured before the second emulsification step, since these are no longer accessible in the final double emulsion [4].

Likewise, widely established are microscopic methods, such as confocal laser scanning microscopy, that can be used to confirm the multiple character of a double emulsion or to measure the droplet size and the filling degree. Both offline and inline systems can be used. However, a major disadvantage is the time it takes to obtain enough data for a statistically relevant result [5, 23]. While measuring droplet sizes, all droplets are measured at an unknown position. Therefore, the apparent droplet sizes must be corrected after measurement. For this correction, at least 2000 droplet diameters need to be measured to achieve a precise result.

Besides imaging methods, there are other analytical methods that can be used to determine structural parameters of double emulsions.

Differential scanning calorimetry can also be used to determine the filling degree of a double emulsion by supercooling it. Usually, the inner water phase has less impurities than the outer

water phase, and therefore, needs stronger supercooling and both water peaks can be distinguished. Furthermore, If the emulsion is measured several times, it is also possible to monitor qualitative changes of the inner water droplet size, since the necessary supercooling depends on the droplet size [24]. However, this method is only applicable for freeze stable emulsions, because otherwise, there can be a significant release of inner water to the outer water phase, which falsify the result [25].

Furthermore, the filling degree and the inner droplet size can also be calculated based on the diffusion coefficients of the inner and outer water phase, which are determined by pulse field gradient - nuclear magnetic resonance. If the measurement is performed successfully, this method gives great insight into double emulsion droplets. However, for this offline method, the requirements for the sample are high. The inner water droplets must be monodisperse with a droplets size of less than 1 µm and all diffusion within the double emulsion must be suppressed [26].

In summary, there is currently no measurement method that can reliably determine the filling degree of double emulsions inline. All available methods are usually performed offline without the possibility of real time measurements and require extensive sample preparations. Furthermore, some methods can only provide qualitative data and the sample is often not suitable for further investigations after the measurement. Consequently, there is a constant demand for new measurement technologies, which can overcome those limitations.

1.3 Raman spectroscopy

Raman spectroscopy is an increasingly popular analytical method used in a wide variety of applications [7]. The Raman effect is based on the interaction of exciting electromagnetic radiation with molecular bonds. The exciting radiation induces the change of vibrational states in a molecule. Depending on the vibrational state, both the polarizability α and the dipole moment µ can be changed. Figure 1-3 shows which vibrations are Raman active and which are infrared (IR) active [27].

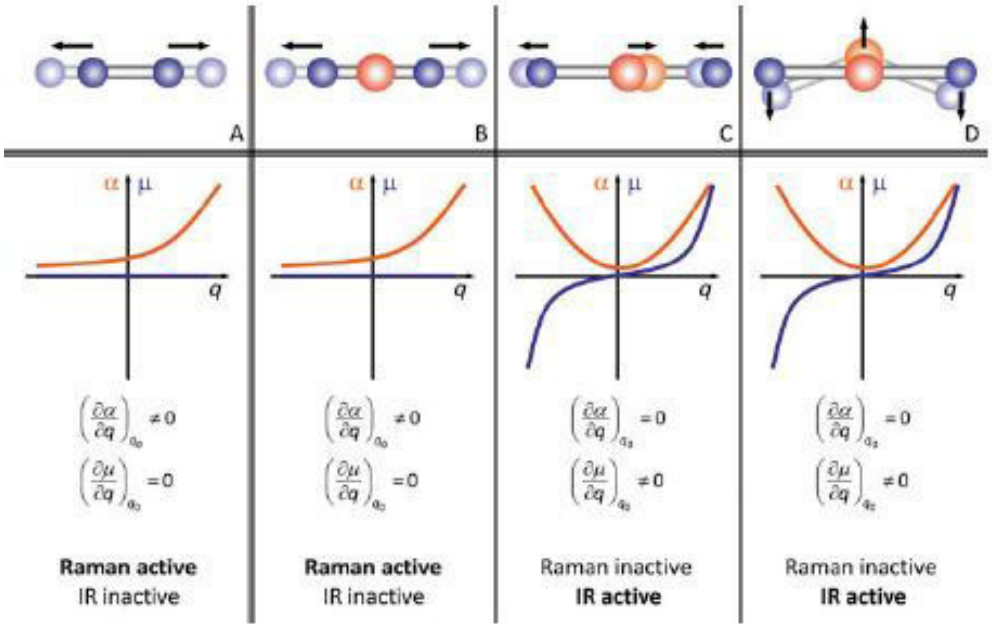

Figure 1-3 Different molecular vibrations lead to Raman or IR activity [27]

If only the polarizability of the excited molecular bond changes, it is Raman-active. This is the case for symmetrical stretching vibrations. If asymmetric stretching vibrations or deformation vibrations are present, the dipole moment changes and the molecular bond is IR-active [27]. Regarding the energy level of a molecule during excitation and de-excitation, three processes can be distinguished. If the molecule is excited to a virtual intermediate state and then falls back to the same vibrational state by emitting a photon, this is referred to as Rayleigh radiation. The wavelength of the emitted photon is identical to that of the exciting radiation. If the molecule returns to a higher vibrational state, the emitted photon has less energy than the energy introduced to raise it to the virtual state. The wavelength of the photon is shifted to longer wavelengths compared to the exciting radiation which is referred to as Stokes radiation. If the molecule is subsequently excited into the virtual state a second time and then falls back to the original ground state, the emitted photon has more energy than was introduced during the second excitation. As a result, its wavelength is shorter than that of the exciting radiation. This is called anti-Stokes radiation [28]. The Jablonski diagram shown in Figure 1-4 illustrates the energetic processes.

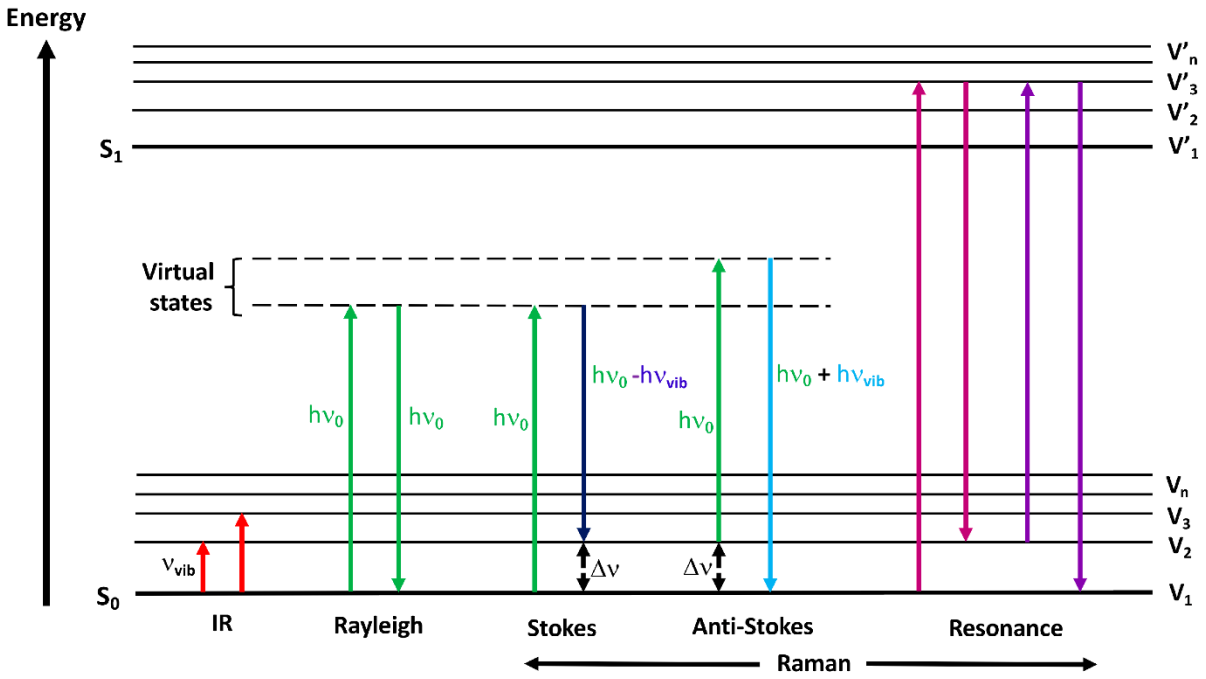

Figure 1-4 The Jablonksi diagram shows the energetic changes when optical radiation is present. Shown are the changes of state with IR radiation, Rayleigh, Stoke, Anti-Stokes as well as resonance Raman [28].

The intensity of the resulting Raman scattering is described by equation 1-3 [28]

$$I_R \propto I_0 \cdot \left(\omega_0 - \omega_{0,q}\right)^4 \cdot |\alpha|^2. \qquad 1\text{-}3$$

Herein I_R represents the Raman intensity, I_0 describes the intensity of the laser, ω_0 indicates the frequency of the laser and $\omega_{0,q}$ the resonant frequency of the excited molecular bond. α describes its polarizability.

Based on this formula, it can be seen that a shorter laser wavelength can generate a higher signal. However, with shorter wavelengths, fluorescence can also occur, which superimposes the Raman signal [29].

Raman spectra are composed of bands whose position results from the respective frequencies of the molecules present in the sample. Since the analyte concentration correlates with the band intensity, quantitative measurements can also be performed [8].

Raman spectroscopy offers several additional advantages compared to other spectroscopic methods. It has a higher spectral resolution than e.g. IR and is best suited for aqueous samples [7]. In addition, it is a non-invasive measurement method that does not affect the quality of the sample and does not rely on specific sample preparation or specific markers [30]. Since it is also possible to use fiber-optic coupled optical probes, Raman measurement points can be installed flexibly.

Figure 1-5 shows an exemplary setup of a Raman spectrometer. The Raman spectrometer contains a laser which is focused on the sample by an optical system. The resulting Raman

signal is also collected by the optical system and fed into the monochromator via a notch filter, which filters out the Rayleigh signal [31]. The monochromator consists of a dispersive element, often an optical grating, which disperses the Raman signal by wavelength [30]. Subsequently, it hits the detector, usually a CCD camera, which measures the signal wavelength-selectively with the help of a computer.

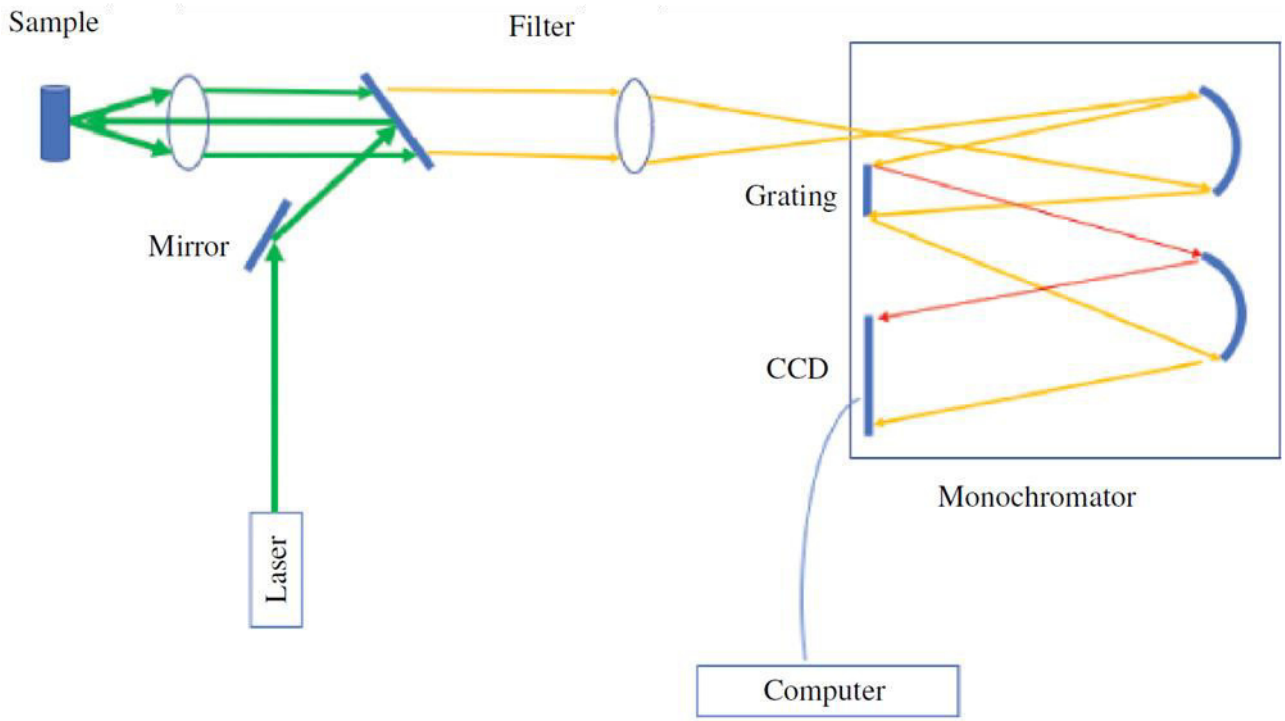

Figure 1-5 Schematic setup of a Raman spectrometer [31]**.**

Besides spectrometers, photometers can also be used for the detection of the Raman signal. These are not wavelength-selective, but count all photons striking in their sensitivity range. In doing so, they are able to amplify the signal of a single photon by a multiple, making extremely weak signals measurable. This is achieved by the characteristic design of photometers, which is shown in Figure 1-6 [32].

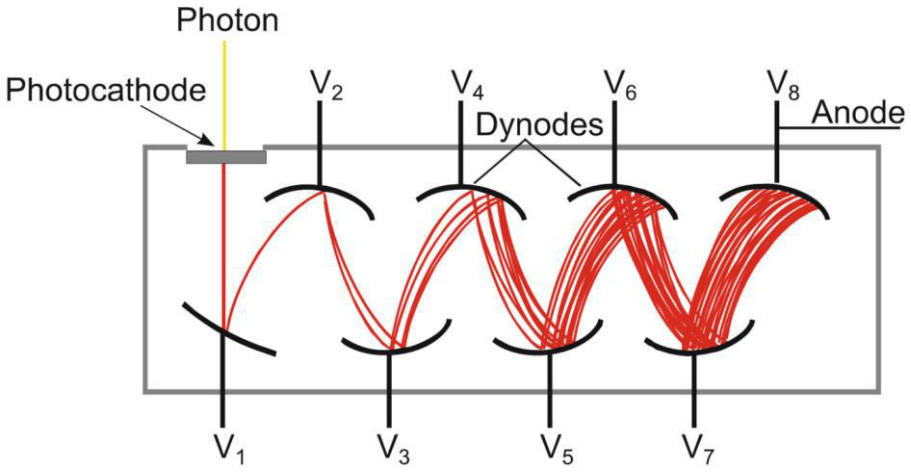

Figure 1-6 Concept of a photomultiplier. With each dynode the number of electrons multiplies, which finally hit the anode and generate an electrical output signal [32].

When a photon hits the photocathode, an electron is released from it and is accelerated in the direction of the first dynode (V1). Acceleration voltages are applied to all dynodes, and increase with each successive dynode. When an electron hits a dynode, it releases further electrons from it. All electrons are accelerated to the next dynode, releasing more and more electrons, until finally a multitude of electrons hits the photoanode. The growing number of electrons can be quantified by the amplification factor [33], which is defined as

$$G = g \cdot \delta^m \qquad 1\text{-}4$$

The individual parameters describe the collection probability g of the photoelectrode, the average amplification factor δ and m the number of dynodes. Usually, amplification factors of 10^6 - 10^7 are achieved.

It must be noted that not each photon releases an electron from the photocathode. This is defined by the quantum efficiency [33] as follows

$$\eta(\lambda) = \frac{N_{PE}}{N} \qquad 1\text{-}5$$

N_{PE} describes the number of photoelectrons released from the photocathode, N the number of photons hitting the photocathode. The quantum efficiency depends on the cathode material [32].

Although both detectors have some differences, both are equally suitable for Raman measurements [34]. This was proven by Nachtmann et.al. in a study in which they compared a commercial Raman spectrometer with a self-developed Raman measuring instrument, which is equipped with a photometer. For demonstration purposes, a dilution series of hydrogen peroxide in distilled water was measured and the reaction of CO_2 with an amine to carbamate was tracked. The results are shown in Figure 1-7.

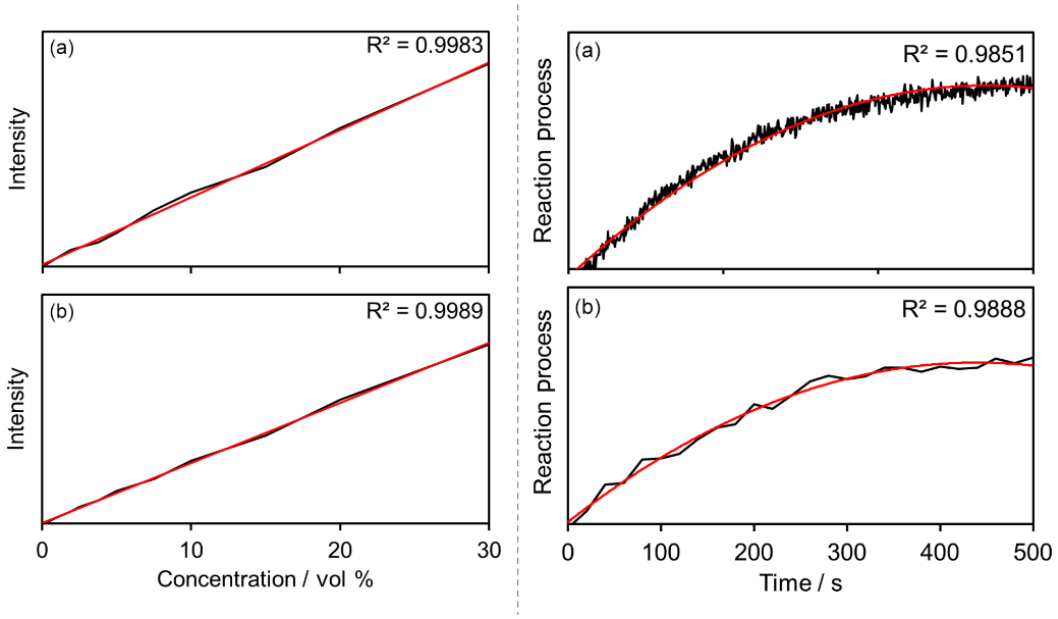

Figure 1-7 Results of the dilution series of hydrogen peroxide in distilled water (left) and the reaction tracking of an amine with CO_2 to carbamate (right). Top, labeled (a), shows the photometric data, and bottom (b) shows the spectrometric data. Data were taken from [34].

The dilution series covers a concentration range of 0% - 30% hydrogen peroxide. Figure 1-7 left shows that both the photometric (a) and spectrometric signals (b) increase linearly with the same slope. The Pearson coefficients of the respective trend lines are R^2 = 0,9983 (a) and R^2 = 0,9989 (b).

The measured data of the reaction tracking in Figure 1-7 right also show a congruent curve. After a sharp increase in the signal, it flattens out in the further course and approaches a maximum. Here, too, the Pearson coefficients are almost identical with R^2 = 0,9851 und R^2 = 0,9888 [34].

1.4 Motivation: Objective and outline of this thesis

The present thesis shows the development of a new measurement method which uses Raman spectroscopy to measure the filling degree of double emulsions. The following requirements were set for a successful development of the method:

- The method provides quantitatively comparable data reliably.
- The measurement method should be integrated in-line into existing emulsification processes.
- The measurement must not affect the emulsion structure
- The method should offer several application possibilities

Accordingly, the focus of this thesis is on the development of the measurement methodology and its application. Furthermore, the strengths and limitations of the measurement method will be analyzed and thus its general suitability for double emulsion based systems will be

investigated. It is not an objective to find new formulations for double emulsions or to optimize existing formulations.

Raman spectroscopy is a promising method for the analysis of double emulsions due to several characteristics. Double emulsions are a multiphase entity wherein each phase usually has a different composition. Accordingly, there are several components in a double emulsion that must be distinguished from each other. Therefore, a new measurement method must have a correspondingly high selectivity. Raman spectroscopy is characterized by excellent selectivity and has already been used for multicomponent samples.

Furthermore, optical measurement methods often struggle with aqueous samples. Raman spectroscopy, on the other hand, is not negatively affected by water. In the region of highest selectivity, the so-called fingerprint region, water is not visible in the spectrum. At higher Raman shifts, defined water peaks appear in the spectrum.

Additionally, the Raman signal scales with the sample mass present. Therefore, based on a suitable calibration, the measurement data can be compared quantitatively.

Since it is possible to use commercially available fiber optic probes for Raman spectroscopic measurements, they can usually be integrated on-line or in-line into existing processes.

Besides the advantages, there are also arguments against the use of Raman spectroscopy for the analysis of double emulsions. To circumvent these, appropriate boundary conditions must be observed during the experiments.

One relevant problem is the occurrence of light scattering at the phase boundaries of the double emulsion. In double emulsions there are innumerable phase boundaries at which light is scattered and the measurement is affected. The extent of scattered light depends on the refractive indices of the two phases. Therefore, it is expected that the refractive indices must be aligned at a minimum for successful Raman measurements of double emulsions. This would make more light available for excitation and the resulting Raman signal could also be better detected by the probe.

In addition, the two water phases of the double emulsion must be distinguishable spectrally, since both the internal water content and the oil content must be measured to determine the filling degree. For this purpose, a tracer molecule should be added to the inner water phase, which is used to indirectly measure the water phase. Ideally, the tracer molecule can also be used to vary the refractive index of the water phase to match the refractive index of the oil phase. In theory, it is possible to add the tracer to the outer water phase, too, but this will lead to the necessity of further calibrations and calculations in order to achieve a quantitative result for the amount of the inner water phase.

In principle, double emulsions could be affected by the thermal energy introduced by the laser. This cannot be predicted with universal validity, as it depends on several factors. Firstly, it depends on the emitted laser power. Secondly, as equally important, it also depends on the

energy absorption capabilities of the double emulsion. This, in turn, relies on two factors. First, the transparency of the double emulsion. The more transparent the double emulsion, less heat is absorbed. Second, the contact time between the laser and the double emulsion must be long enough to transfer enough heat energy to affect it.
However, the most significant and generally applicable disadvantage of Raman spectroscopy exists for fluorescent samples. In this case, the Raman signal is superimposed by the much stronger fluorescence and can no longer be evaluated. Therefore, when designing the substance system, care must be taken to ensure that fluorescence-free to minimally fluorescent substances are used.
Although Raman spectroscopy appears to be well suited for the analysis of emulsions, it has hardly been used for this purpose to date. Raman spectroscopy has only been used for reaction monitoring of emulsion polymerizations. However, these are water-in-oil or oil-in-water emulsions. For the combination of Raman spectroscopy and double emulsions, there is only one study so far, which, however, pursues a different approach as well as a different goal.
Due to the lack of literature, the overall hypothesis of this work is based on the generally accepted knowledge of Raman spectroscopy and the physical principles of light refraction at phase boundaries.

The overall hypotheses are:

GH1 *Raman spectroscopy can be used to determine structural parameters of double emulsions, such as their filling degree*

GH2 *Raman spectroscopy is suitable for studying the stability of double emulsions*

The study reported in Chapter 2 investigates the effect of different refractive indices on the strength of the Raman signal of the inner phase. For this purpose, the refractive indices of the two aqueous phases are varied by adding ammonium nitrate (inner water phase) or glycerol (outer water phase). Likewise, the filling degree of the double emulsions is systematically adjusted so that the total mass of ammonium nitrate is identical in all double emulsions. This ensures that differences in signal strength are caused solely by different refractive indices. Concretely, the study addresses the following working hypotheses:

H2.1 *The Raman signal strength of the inner phase increases as the difference in refractive indices between the inner water phase and the oil phase decreases*

H2.2 The Raman signal strength of the inner phase increases with decreasing refractive index differences between the outer water phase and the oil phase

Based on the results of the first study, the next study presented in chapter 3 investigates the accuracy of determining the structural parameters filling degree and outer droplet size by Raman spectroscopy. For this purpose, the following working hypothesis was formulated:

H3.1 Filling degrees of double emulsions, whose refractive indices are identical, can be quantitatively measured and differentiated precisely

H3.2 If a measurement technique with high temporal resolution is used, the outer droplet diameters of individual double emulsion droplets can be determined

After demonstrating the general suitability to use Raman spectroscopy to analyze double emulsions, the study presented in Chapter 4 presents an application method for investigating the stability of double emulsions as a function of their filling degree. For this purpose, the osmotically induced water diffusion between the two water phases was investigated on the basis of the following two working hypotheses:

H4.1 The lower the osmolality of the inner water phase, the lower the relative filling degree change

H4.2 With increasing osmolality of the outer water phase, the relative filling degree change is also increasing

2 Influence of Refractive Index Differences on the Signal Strength for Raman-Spectroscopic Measurements of Double Emulsion Droplets

This chapter was published as: Hufnagel, T.; Rädle, M.; Karbstein, H.P. Influence of Refractive Index Differences on the Signal Strength for Raman-Spectroscopic Measurements of Double Emulsion Droplets. *Appl. Sci.* **2022**, *12*, 9056. https://doi.org/10.3390/app12189056

2.1 Abstract

Double emulsions show great potential for encapsulating active substances and protecting them against external influences. However, they tend to become unstable during storage. Research on double emulsions, therefore, focuses on maintaining their microstructure during their shelf life. Optical measurement methods, such as Raman spectroscopy, have hardly been used to date to analyze the microstructure of double emulsions, mainly due to multiple scattering effects. This study investigates the influence of refractive index matching of double emulsion phases by measuring the Raman signal strength of the inner water phase for different refractive index combinations. Ammonium nitrate and glycerol are added to the inner and outer water phase, respectively, to change the refractive indices of both phases. Additionally, polyvinyl alcohol serves as an emulsifier in the outer water phase. The oil phase consists of silicone oil and Dowsil Resin XR 0497 as the emulsifier. The refractive index of the oil phase is kept constant. For individual phase boundaries of single droplets, the refractive index matching plays a minor role. However, if there are many droplets with correspondingly numerous phase boundaries, which leads to multiple scattering during the measurement, the matching has a significant influence on the signal strength of the inner phase. When measuring double emulsions, the phases should always be matched, as this results in higher signals and improves the sensitivity of the measurement.

2.2 Introduction

Emulsions are widely used in food, pharmaceutical, and chemical industry [20]. Compared to homogeneous systems, emulsions are more complex regarding their structure and resulting properties [35]. Their higher complexity arises from various parameters, such as the size distribution of the inner droplet phase and the interfacial properties, as well as the compositions of each phase [36]. The requirements for the measurement techniques used are therefore high. The interfaces between the phases can be especially challenging [37, 38].

To monitor chemical reactions, optical measurement technologies are a widely used tool [39]. Raman spectroscopy has started to play a more important role during recent years [40]. In industry, Raman spectroscopy is used to monitor emulsion polymerization processes [41], to ensure food quality [42, 43] and for the development of new pharmaceuticals [44].

One major advantage of Raman spectroscopy is its high selectivity for molecular bonds [8]. Furthermore, the intensity of the Raman signal correlates with the concentration of the sample [8]. Both characteristics suggest that Raman spectroscopy is ideally suited for measuring heterogeneous systems such as emulsions.

However, a special problem arises when measuring emulsions [45]. The interface between the continuous phase and the dispersed phase leads to elastic scattering of the incident light [46]. This is because the refractive indices of the disperse and continuous phases differ. This results in refraction and reflection at the interfaces [9]. Due to these effects, the light does not enter the emulsion droplets unhindered, but is scattered away from the primary direction. Depending on the measuring device, this effect leads to strong disturbances in the measurement process and makes interpretation of the results more difficult.

The strength of the reflections can be quantified using the reflectance R [9]. To calculate the reflectance, two cases, the reflectance of perpendicular polarized light R_{per} and parallel polarized light R_{par}, need to be considered. The equations for both parameters can be derived from the Fresnel's formula. In the following, the case of the same magnetic permeability of the emulsion phases, which is generally valid for emulsions, is shown:

$$R_{per} = \frac{sin^2(\alpha-\beta)}{sin^2(\alpha+\beta)}, \tag{2-1}$$

$$R_{par} = \frac{tan^2(\alpha-\beta)}{tan^2(\alpha+\beta)}. \tag{2-2}$$

To determine the reflectance for non-polarized light, the mean value [9] of the perpendicular and parallel polarization needs to be calculated.

$$R = \frac{R_{per} + R_{par}}{2} \tag{2-3}$$

For the special case of perpendicular polarized light, $\alpha = \beta = 0°$, which results in cosine functions of 1 and simplifies the formula [9] as follows:

$$R = \left(\frac{N_1 - N_2}{N_1 + N_2}\right)^2. \qquad 2\text{-}4$$

Due to the high disperse phase fractions of more than 70% commonly found in emulsions [47], multiple scattering occurs caused by the numerous phase interfaces [45]. An important role is played by the refractive index difference: the phase ratio and the droplet size distribution; and also by the geometry of the incident light, its focusing at the focal point and other imaging conditions.

This challenge is increased further when the microstructure of double emulsions has to be evaluated. Double emulsions are emulsions within emulsions, i.e., complex multiphase systems in which both water-in-oil (W/O) and oil-in-water (O/W) emulsions exist simultaneously [48]. The most common case is a water-in-oil-in-water (W/O/W) emulsion, where one to innumerable water (W_1) droplets are dispersed within oil (O) droplets, which form an emulsion themselves by being dispersed within the second water (W_2) phase [4].

One key advantage of the double emulsion structure is the ability to encapsulate active or sensitive substances [49], as e.g., enzymes, vitamins or crop protection agents. The middle phase can be solidified and used as a protective shell [18]. In addition, the release of encapsulated substances can be controlled precisely, which is particularly beneficial for encapsulated active ingredients in drugs [50]. Furthermore, WOW double emulsions are used to reduce the fat content in foods [51]

On an industrial scale, double emulsions are produced using classical methods, such as rotor-stator machines [4]. Here, the inner emulsion is produced under high energy input, resulting in very small W_1 droplets [52]. The second emulsification step is carried out at lower energy input so that the inner emulsion is affected as little as possible [53]. Industrial emulsification methods have the disadvantage of producing wide droplet size distributions [15].

Microfluidic systems offer the chance to provide nearly monodisperse droplet size distributions [19]. It uses miniscule channels to produce emulsions in laminar flow profiles [16]. For double emulsions, glass capillary devices have proven to be very useful [17]. However, the fabrication of a single device is costly and difficult to reproduce [54]. Therefore, an optimized glass capillary device has recently been developed [55]. It follows the same emulsification principle but is much easier to manufacture and can also be modified during operation [56]. It offers the possibility of producing double emulsions, having a wide range of internal and external droplets in terms of size and degree of filling, both parameters being independently variable [43].

Due to their complex structure, double emulsions tend to undergo various instability mechanisms [5]. Besides diffusional losses of encapsulated water or actives, inner as well as

outer droplets may coalesce with each other, or inner droplets may coalesce with the outer water phase.

Improving the stability of double emulsions is the focus of many research groups today [4]. However, research is limited as e.g., real-time measurement of structure-related parameters, as inner and outer droplet size distributions, and their filling degree, is extremely challenging. Usually, to measure those parameters, non-real-time measurement methods, such as dynamic and static scattered light methods [4], differential scanning calometry [24], or nuclear magnetic resonance NMR spectroscopy [57], are used. Those methods are usually performed offline and require sample preparation. Furthermore, the measured emulsion sample is usually unusable for other measurements.

Therefore, there is a need for a new measurement method suitable for double emulsions, which can be performed in- or online to deliver real-time results without sample preparation and which does not affect the double emulsion [30].

Raman spectroscopy fulfils these requirements. Furthermore, because of its high selectivity and its suitability for water [58], it is expected that each double emulsion phase can be detected individually. The only challenge for Raman measurements of double emulsion, will be multiple light scattering, caused by different refractive indices of the three double emulsion phases.

Thus, the scope of this work is to investigate whether the method of refractive index matching creates the possibility to suppress the cross-influences resulting from phase boundaries in Raman measurements of double emulsions and the effect of refractive index differences between the three double emulsion phases on the Raman signal strength. Therefore, the signal of the inner water phase is measured using Raman spectroscopy, while the refractive indices of the inner and outer water phases are varied. It is expected that the signal strength of the inner water phase increases as the differences between the refractive indices of the inner water phase, the oil phase and the outer water phase, decrease.

Furthermore, the work investigates the possibility to compensate refractive index differences by mathematical corrections via simple functional relationships.

We found one publication with a similar scope, which is about the molecular mapping of multiple emulsions using coherent anti-Stokes Raman scattering (CARS) microscopy [10].

2.3 Materials and Methods

2.3.1 Emulsions System

With a view to Raman spectroscopy, ammonium nitrate (CarlRoth, Karlsruhe, Germany) is additionally used as a tracer in the inner water phase. M10 silicone oil (CarlRoth, Karlsruhe, Germany) serves as the oil phase. As the emulsifier, 2% Dowsil Resin XR 0497 (DowCorning,

Midland, MI, USA) is added therein. The outer water phase consists of 2% polyvinyl alcohol Kuraray Poval 26–80 (Kovayal, Hattersheim am Main, Germany) and glycerol.

In total, forty different W/O/W double emulsions are investigated. All of the different emulsion phases are listed in Table 2-1. To achieve this, all eight outer water phases are combined with all five inner water phases.

Table 2-1 lists the refractive indices of all emulsion phases. They were determined in triplicate with a digital refractometer (Type: ORF 1RS, KERN Optics, Bahlingen, Germany). The refractive index of the oil phase serves as a reference for the water phases. The smallest deviation between all refractive indices is found for the combination of 49% ammonium nitrate and 49% glycerol.

Table 2-1 Summary of the refractive indices for each phase. Each mean value is based on three measurements. Each set of measurements has a standard deviation of less than 0.0001. ΔN is the difference between the refractive index of the oil phase compared to the water phases.

	Phase	Mean Value	ΔN
W_2	00.00% Glycerin	1.3385	0.0642
	10.00% Glycerin	1.3513	0.0514
	20.01% Glycerin	1.3635	0.0392
	30.01% Glycerin	1.3782	0.0245
	40.00% Glycerin	1.3917	0.0110
	49.04% Glycerin	1.4044	−0.0017
	60.00% Glycerin	1.4189	−0.0162
	70.00% Glycerin	1.4317	−0.0290
O	2.02% Dowsil Resin XR 0497	1.4027	
W_1	16.33% Ammonium nitrate	1.3569	0.0458
	24.50% Ammonium nitrate	1.3662	0.0365
	32.46% Ammonium nitrate	1.3771	0.0256
	48.91% Ammonium nitrate	1.4007	0.0020
	61.25% Ammonium nitrate	1.4200	−0.0173

2.3.2 Raman Measurement

The RNX1-532 Raman spectrometer (Kaiser Optical Systems, INC., Ann Arbor, MI, USA) is used for the Raman measurements. It is equipped with a laser at a wavelength of 532 nm and a laser power of 150 mW. The associated backscatter probe (Kaiser NCO-0.5-VIS) irradiates the sample with a half-inch lens, producing a focal diameter of 55 µm with a focal length of 500 µm.

Spectra of all phases have been measured, see Figure 1. These were measured at 1s integration time with 3 accumulations in a standard spectroscopy cuvette (Type: 100-10-40,

Hellma Analytics, Müllheim, Germany), allowing the spectra to be quantitatively compared. Ammonium nitrate shows one dominating peak in the fingerprint region [29] at 1047 cm^{-1} [59], which is the highest peak of all phases in this area. The oil phase has only minor peaks in the shorter shifted fingerprint region at 489 cm^{-1} and 707 cm^{-1} [60], while the outer water phase shows multiple smaller peaks in the range between 800 cm^{-1} to 1200 cm^{-1} which are attributable to glycerol [61]. Specifically, there is a peak at 1060 cm^{-1}, which overlaps significantly with the ammonium nitrate peak at 1047 cm^{-1}. Therefore, a baseline correction is applied in the evaluation to reduce the influence of glycerol.

For the different concentrations of both water phases, the linearity of the peak height at 1047 cm^{-1} (ammonium nitrate) and 1060 cm^{-1} (glycerol) is investigated. The respective Pearson coefficients are $R^2 = 0.992$ (ammonium nitrate) and $R^2 = 0.983$ (glycerol).

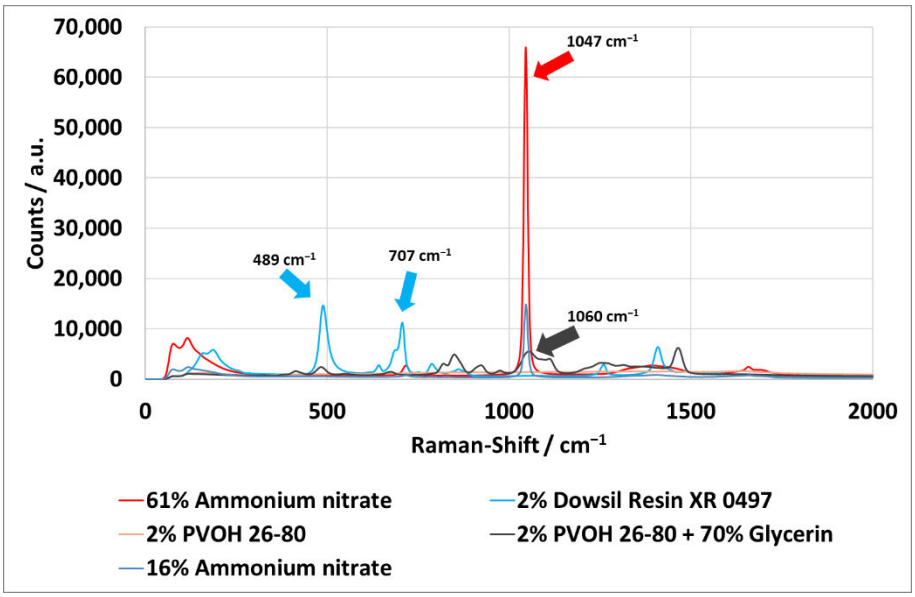

Figure 2-1 Raman spectra of all phases. For the inner and outer water phase, only the lowest and highest concentrations of ammonium nitrate and glycerol are shown.

For the baseline correction, the two endpoints are determined from a spectrum of ammonium nitrate solution. These are located at 1030 cm^{-1} and 1060 cm^{-1}. First, the total integral is calculated in this range. Subsequently, the slope of the baseline is determined using the measured values at 1030 cm^{-1} and 1060 cm^{-1} and the integral between the x-axis and the baseline is calculated. The difference of the two integrals gives the integral of the baseline corrected ammonium nitrate peak.

To measure a significant number of droplets per experiment, each experimental set is measured for 400 s in total. This time is divided into five individual measurements of 80 s, which in turn are divided into 4 accumulations of 20 s. In the end, five spectra are obtained of each experimental set, which are combined into one data point.

2.3.3 Emulsification

The double emulsion was produced in a two-step process, using different emulsification techniques. First, five different W_1/O emulsion were produced with the rotor-stator system "Megatron MT3000" (Kinematica AG, Malters, Switzerland) using a two row gear ring at a rotational speed of 20,000 min^{-1} (circumferential speed = 27.2 m/s) for 90 s. These emulsions serve as the inner emulsion in the subsequently produced double emulsions.

The droplet size distribution of the emulsions with 16%, 24%, 33% and 61% ammonium nitrate was measured by static laser light scattering using a particle analyzer HORIBA LA-950 (Microtrac Retsch GmbH, Haan, Germany). The Sauter mean diameter of the inner emulsions are in the range of 2.07 µm (33% ammonium nitrate) to 2.67 µm (16% ammonium nitrate). The respective droplet size distributions are shown in Figure 2-2. The emulsion containing 49% ammonium nitrate in the water phase could not be measured as a result of the similar refractive indices. Since all other emulsions show similar droplet size distributions, it is assumed that the droplet sizes do not deviate in this set.

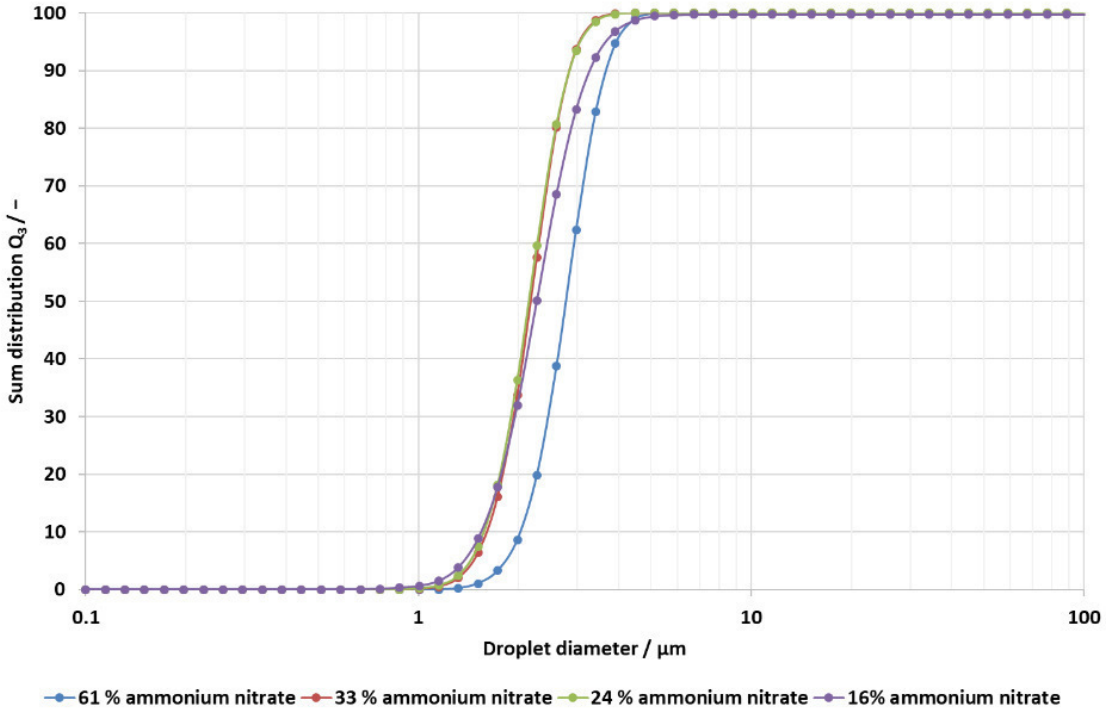

Figure 2-2 Droplet size distribution of the inner emulsions.

Figure 2-3 shows the five different inner emulsions. The emulsions become more and more transparent with the increasing concentration of dissolved ammonium nitrate. At the best matching (ΔN = 0.002 at 49% ammonium nitrate), the emulsion is optically clear. At 61% ammonium nitrate, the optimum is exceeded, and the emulsion appears milky.

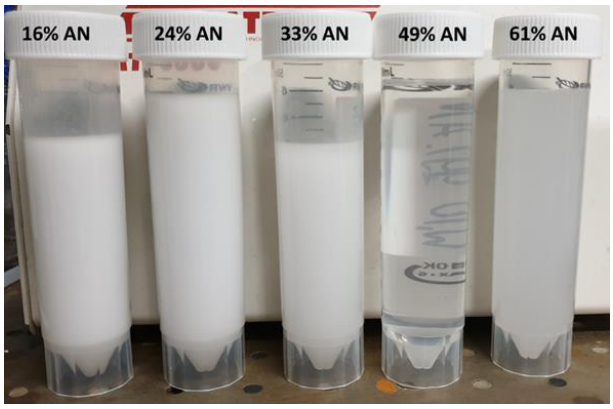

Figure 2-3 The investigated W_1/O emulsions with the respective ammonium nitrate (AN) concentrations.

In order to obtain monodispersed W_1/O droplets in a double emulsion, these inner emulsions were then emulsified in the outer water phase using a microfluidic glass capillary system [30]. The glass capillaries used are placed in two Teflon blocks, which are connected to each other by a plug-in connection. Syringe pumps (Legato 100, kdScientific Inc., Holliston, MA, USA) were used to inject the inner W_1/O emulsions and the outer water phases into the microfluidic device. The inner emulsion was pumped at 2 mL/h and the outer water phase at 10 mL/h. This leads to a droplet breakup rate of 3 Hz to 5 Hz with a droplet diameter of 1.15 mm. Figure 2-4 shows a double emulsion droplet flowing through the larger squared capillary.

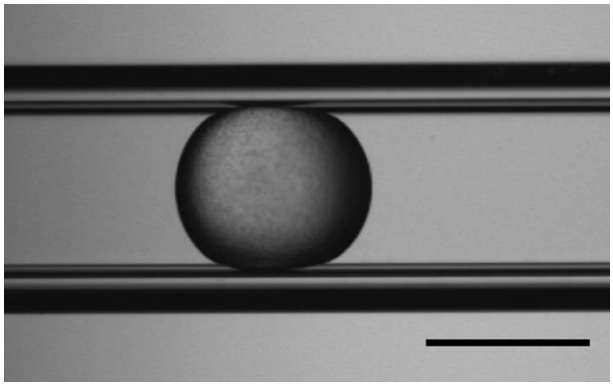

Figure 2-4 An individual double emulsion droplet flowing through the squared capillary. The scale bar is equal to 1 mm.

The microfluidic device is designed in a co-flow system, i.e., the inner emulsion and the outer phase flow parallel to each other. When both phases come into contact, the inner emulsion breaks up into droplets in the outer phase. Since the breakup to the double emulsion takes place in a round borosilicate glass capillary (ID: 1.12 mm, WPI, Sarasota, FL, USA), a square quartz capillary (ID: 1.00 mm, CM Scientific Ltd., Silsden, UK) is connected to the round capillary via an internally designed 3D-printed nylon adapter. For online Raman measurements, a square quartz capillary was mounted. Thus, neither the capillary material nor its curvature has a negative influence on the Raman measurement. A schematic of this setup is shown in Figure 2-5. On the right side, the conical, green, vertical bar indicates the

laser beam for Raman excitation. It is emitted by the backscatter probe, which also detects the Raman signal.

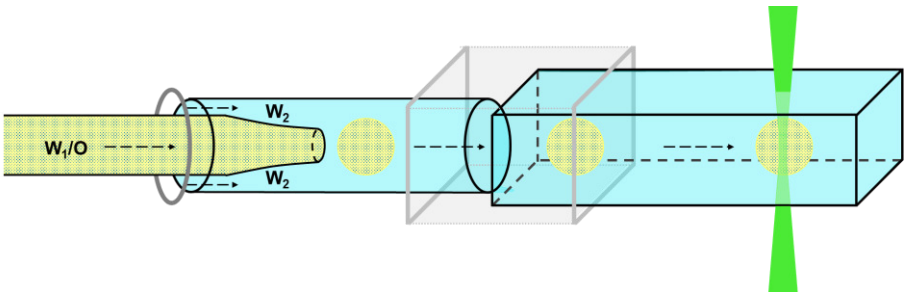

Figure 2-5. Scheme of the capillary system including the measuring point.

2.3.4 Set of Experiments

Five sets of experiments have been carried out. In each set, a different inner emulsion was investigated. The inner emulsions differ in their ammonium nitrate concentration and filling degree. Both parameters are calculated to ensure that the same mass of ammonium nitrate is present in the inner emulsion in all sets. The oil phase remains identical in its composition during all measurements. Only its amount is adjusted depending on the filling degree. The outer phase is varied during the test series by adjusting the glycerol content between 0% and 70%.

Table 2 shows the individual experiments with the respective concentrations of ammonium nitrate and filling degrees. In addition, the amounts of the inner phase, which are emulsified in the Megatron, and the resulting mass of ammonium nitrate in the individual inner emulsions are listed. Each emulsion contains almost exactly 6 g of ammonium nitrate, thus fulfilling the fundamental idea of this set of experiments.

Table 2-2 Survey of the test series with corresponding weights and concentrations.

	Set of Experiment				
	#1	**#2**	**#3**	**#4**	**#5**
Filling degree / w-%	8.17	10.21	15.31	20.40	30.61
Ammonium nitrate concentration / w-%	61.25	48.91	32.46	24.50	16.33
Amount W_1 / g	36.731	24.482	18.366	12.257	9.811
Amount ammonium nitrate / g	6.01	6.00	5.96	6.00	6.00

2.4 Results

2.4.1 Influence of the Refractive Index Matching on the Raman Signal

Figure 2-6 show the results of the set of experiments, each as a function of the refractive index differences between the inner water and oil phase and the outer water and oil phase, respectively.

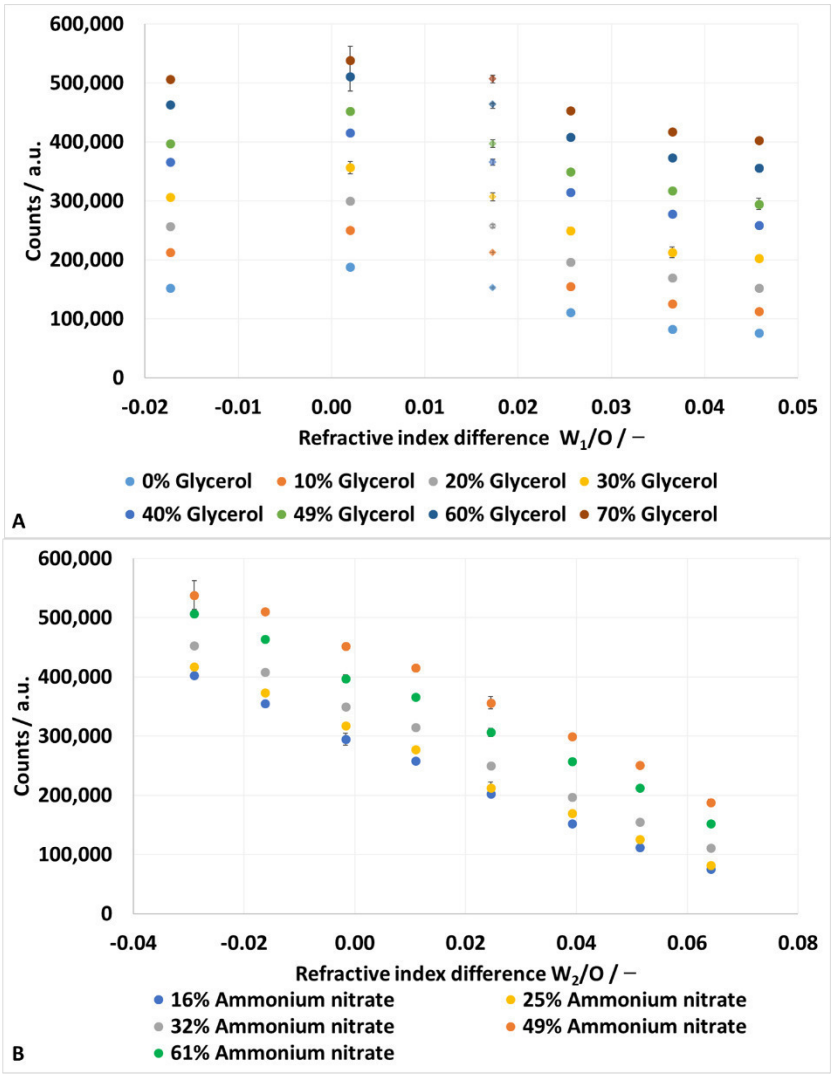

Figure 2-6 Results of the experiments presented as a function of refractive index differences between the oil phase and the inner water phase (A) and the outer water phase (B).

In Figure 2-6A, each column of data points represents one ammonium nitrate concentration. Thereby, the ammonium nitrate concentration decreases from left (61%) to right (16%). The only exemption is the column at ΔN = 0.0173 (diamonds instead of circles). The ammonium nitrate concentration of this column is 61%. For this column, the signals are plotted over the absolute refractive index difference to illustrate the linear dependency between the signal and the refractive index difference. The linear trend lines for each glycerol concentration have Pearson coefficients of more than $R^2 = 0.95$.

The emulsions with 49% ammonium nitrate, respectively the smallest refractive index difference, show the highest signals within a constant glycerol concentration. When the refractive index difference increases, in both positive and negative directions, the signal gets weaker. Within one column, the signal increases with increasing glycerol concentration.
In Figure 2-6B, each column of data points represents one glycerol concentration, and the concentration decreases from left (70%) to right (0%). The signals decrease with decreasing glycerol concentration. Within one column, the signal increases with increasing ammonium nitrate concentration. The exception is the ammonium nitrate concentration of 61% (green dots). It is past the point of best matching and the values are below the maximum. The maximum is at 49% ammonium nitrate (orange dots) and is the best matching.
Furthermore, the measured values show a linear dependence on the glycerol concentration. The Pearson coefficients of the linear trend lines of all glycerol concentrations are all above $R^2 = 0.99$.

2.4.2 Linear Multiple Regression

For emulsions whose refractive indices cannot be adjusted, a simple 2-parametric function is computed to provide correction results. Therefore, a multiple linear regression was performed using a spreadsheet. All measured data points, 200 in total, are included in this regression. The result is the following equation:

$$I = 448595.53 - 3681943.73 \cdot \Delta N_{W_2/O} - 3499292.90 \cdot \Delta N_{W_1/O}. \quad 2\text{-}5$$

The Pearson coefficient of this equation is $R^2 = 0.99$, with a standard error of 12,568.54. Using Equation 2-5, the calculated results for the signal strengths of the inner water phases are in the range of 51,947.13 (0% glycerol and 16% ammonium nitrate) to 548,373.31 (70% glycerol and 49% ammonium nitrate), with most of the calculated signal strength being above 100,000. That means, compared to the calculated signal strengths, the relative standard error is between 24% and 2%, but mostly less than 10%. This, in turn, means the discrepancy between the regression and measured values are mostly less than 10%, which indicates a good correlation between the regression and measured values. Therefore, the regression is suitable to compensate for refractive index differences, mathematically.
To further test the goodness of correlation, the relative residuals were considered in relation to the corresponding measured values, see Figure 2-7.

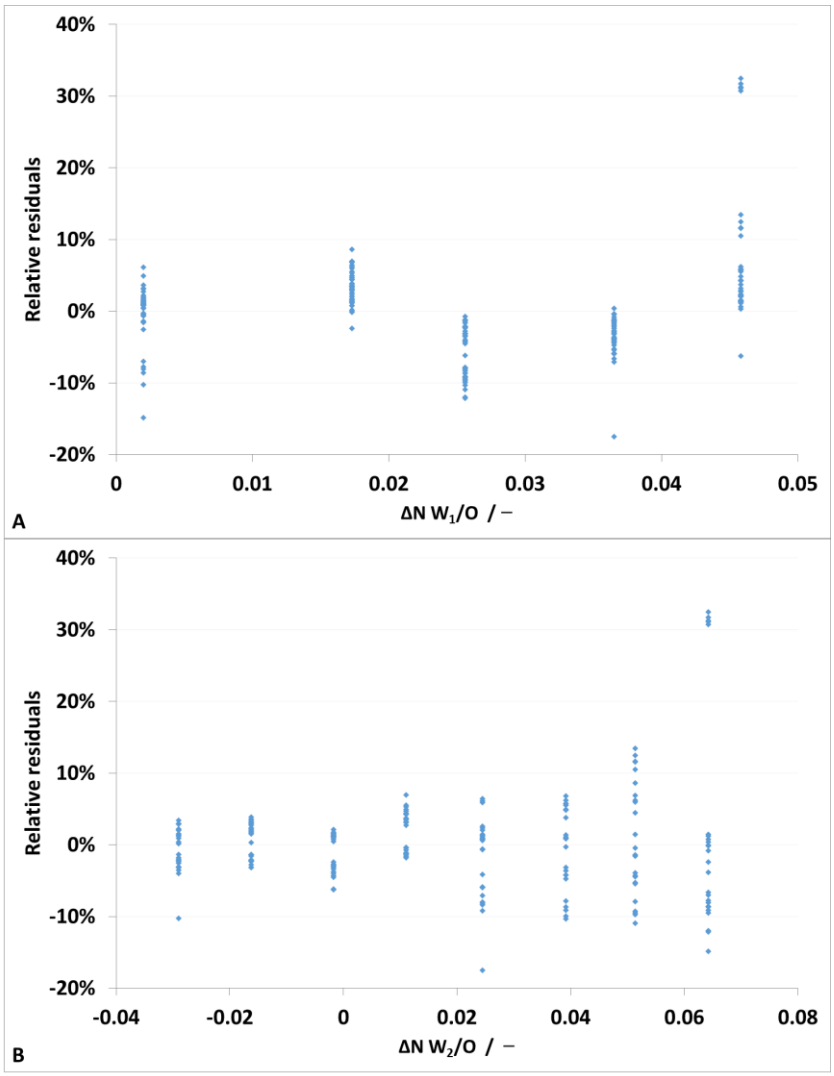

Figure 2-7 Residues as a function of refractive index difference between the inner water and oil phase (A) and the outer water and oil phase (B).

In general, the residuals show larger values at low concentrations of ammonium nitrate and glycerol. By far the largest deviation is found at 0% glycerol ($\Delta N\ W_2/O = 0.0642$) and 16% ammonium nitrate ($\Delta N\ W_1/O = 0.0458$). In Figure 2-6B, this data point is the lowest one in the right column. In this column, the data point of 16% ammonium nitrate is too high and overlaps with the data point of 25% ammonium nitrate. This means, the spread of the ammonium nitrate concentration in this column is smaller compared to the other columns. The correlation, in turn, assumes an approximately equal spread within the individual ammonium nitrate concentrations. However, there is no justification for this deviation from the raw data. The five individual measurements of this concentration combination have a variance of 0.96%.

Overall, 80% of the relative residuals are in the range of −8% to +6%. The average relative deviation of the individual residuals is 0.16% with a standard deviation of 7.15%. Both underline the high accuracy of the correlation.

2.5 Discussion

The experiment is designed to measure the double emulsion droplets individually. This means, one after another the double emulsion droplets pass through the laser, which runs constantly during the measurement. This ensures that the measurement of one droplet is not influenced by another one.

When light is irradiated into highly filled double emulsions, multiple scattering occurs at the interfaces. This results in a weak signal of the inner phase. Figure 2-6 shows that the light's ability to reach the inner water phase, represented by the signal of ammonium nitrate, depends on the refractive index matching.

To interpret the results, we start from a single droplet. The light enters the drop, which acts as a converging lens when the refractive index of the outer phase is low. The more the refractive index of the outer phase increases, and thus the refractive index difference becomes smaller, the lower the reflectance at the phase interface. This can be calculated using Equations 2-1 – 2-4.

In the case of a double emulsion, the incident light is somewhat focused by the first phase boundary. In the oil droplet, it strikes the inner phase, whose refractive index relative to the oil phase was varied in the experiments. The experiments are designed so that the total amount of ammonium nitrate is constant. If the inner phase always allows all of the light to pass, the displayed ammonium nitrate signal should remain constant for all measurements.

As expected, the ammonium nitrate signal increases with increasing ammonium nitrate concentration, respectively lowering the refractive index difference and reaching its maximum at 49% ammonium nitrate; the best matching. At 61% ammonium nitrate, the refractive index difference is larger, and respectively, the signal is smaller.

A similar behavior is seen with the variation of the glycerol concentration. The measured values increase with increasing glycerol content, respectively decreasing the refractive index difference. However, they continue to increase above the best matching at 49% glycerol.

To explain both observations, the reflectance during each experiment are considered. These are shown in Table 2-3. The reflectance at an incidence angle of 0° is calculated using Equation 2-4, and for 45° using Equation 2-3.

To estimate the reflectance in the case of multiple scattering, the following equation, derived by the authors, is used. It is assumed that reflected radiation is lost and one phase interface is passed after the other.

$$R_{ms} = 1 - (100\% - R)^{n_{phase\ transitions}}. \qquad 2\text{-}6$$

Table 2-3 Reflectance between the water phases and the oil phase. For the inner phases, the reflectance for multiple scattering of 1000 phase transitions is calculated.

Glycerol / w-%	**Single Interface Transition**		**Multiple Scattering**	
	0°	**45°**	**0°**	**45°**
0%	0.05%	0.12%		
10%	0.03%	0.08%		
20%	0.02%	0.04%		
30%	0.01%	0.02%		
40%	0.00%	0.00%		
50%	0.00%	0.00%		
60%	0.00%	0.01%		
70%	0.01%	0.02%		
Ammonium nitrate / w-%				
16%	0.03%	0.06%	24.08%	44.64%
24%	0.02%	0.04%	15.95%	30.74%
32%	0.01%	0.02%	8.13%	16.16%
49%	0.00%	0.00%	0.09%	0.10%
61%	0.00%	0.01%	3.69%	7.07%

Each oil droplet contains numerous inner water droplets. Therefore, a correspondingly large number of phase passes of the incident light occur here. With only 1000 water droplets, the reflectance increases significantly. Table 2-3 shows that for 16% ammonium nitrate and 1000 phase passes, the reflectance is 24.08% (0°) and 44.64% (45°), respectively. In contrast, for 49% ammonium nitrate, the reflectance is 0.09% (0°) and 0.10% (45°). In other words, matching the refractive indices of the inner water and oil phases reduces the reflectance by a factor of 279.95 (0°) and 437.50 (45°). Therefore, the matching of the inner phase boundaries has a significant effect on the measurement signal.

There is only one phase boundary between the outer water phase and the oil droplet. Accordingly, the reflectance is calculated for one phase transition. In the worst case, for 0% glycerol and a 45° angle of incidence, the reflectance is 0.12%. At 49%, practically no light is reflected at the phase interface. This indicates a negligible influence of the external matching. In addition, Figure 2-6 shows that there is always approximately 100.000 counts difference between 16% and 49% ammonium nitrate, regardless of the glycerol concentration. Accordingly, there is no influence of the external matching here either. Furthermore, the signal increases linearly with increasing glycerol concentration. This can most likely be explained by the overlap of the ammonium nitrate and glycerol peaks, which cannot be completely separated using a baseline correction.

2.6 Conclusions

The presented results indicate that it is advantageous for the application of optical spectroscopic measurement methods to match the refractive indices of the inner phase, thus creating a beam of light of maximum power that enters the inner phase.
It should be noted that the conclusion on the matching of the outer phase is valid for single drop measurements. If several double emulsion drops are measured simultaneously, e.g., in a beaker, it can be assumed that the matching of the outer phase has a similar influence as that of the inner phase.
This work shows that Raman spectroscopy offers an opportunity to determine microstructural parameters in double emulsions in situ. With the aid of this measurement technology, the influences of formulation or process parameters on the structure and stability of emulsions, for example, can be investigated quickly and easily in future.

2.7 Acknowledgments

The authors thank Goran Vladisavljevic from Loughborough University for the kind donation of the microfluidic device.

3 Measurement of the Filling Degree and Droplet Size of Individual Double Emulsion Droplets Using Raman Technologies

This chapter was published as: Hufnagel, T.; Stoy, R.; Rädle, M.; Karbstein, H.P. Measurement of the Filling Degree and Droplet Size of Individual Double Emulsion Droplets Using Raman Technologies. *Chemosensors* **2022**, *10*, 463. https://doi.org/10.3390/chemosensors10110463

3.1 Abstract

Double emulsions arouse great interest in various industries due to their ability to encapsulate value-adding ingredients. However, they tend to be unstable due to their complex structure. Several measurement techniques have already been developed to study and monitor the stability of double emulsions. Especially for the measurement of the filling degree of double emulsions, so far there is no reliable method available. In this paper, a measurement system is presented that can measure the filling degree of water-in-oil-in-water (W/O/W) double emulsions by both spectrometrical and photometrical means. The method is based on the Raman effect and does not require any sample preparation, and the measurement has no negative influence on the double emulsion. It is shown that both spectrometric and photometric Raman techniques can reliably distinguish between double emulsions with filling degrees that have a 0.5% difference. Additionally, oil droplet sizes can be photometrically measured. Furthermore, the measurement system can be integrated into both inline and online emulsification processes.

3.2 Introduction

A compound where two immiscible liquids are mixed so that one liquid is formed into small droplets is referred to as an emulsion [47]. In addition to the described emulsions, there can also be multiple emulsions. In this case, an already existing emulsion is emulsified for a second time [47].This emulsion is called a double emulsion, the most common types being water-in-oil-in-water ($W_1/O/W_2$) or oil-in-water-in-oil ($O_1/W/O_2$) emulsions [5].

Double emulsions are mainly used in food, cosmetics, and pharmaceutical industries [62]. Due to their characteristic structure, double emulsions are used to encapsulate value-giving ingredients, such as active ingredients in the pharmaceutical industry [49] or vitamins in foods [63]. As a result, they are protected from external influences during storage and can be released in a targeted manner as required [53].

Conventional emulsification equipment, such as rotor-stator machines or high-pressure homogenizers, operate on the top-down principle [15]. A two-stage process has been established for producing double emulsions. First, the inner emulsion is produced under high shear forces, resulting in very small droplets. In the second step, the double emulsion is produced using much lower shear forces. It is important that the acting forces are not too strong, otherwise the inner emulsion can be damaged and inner droplets can coalesce with the outer phase [4]. However, this method does not allow for a precise adjustment of the droplet size [15].

Microfluidic emulsification operates on the bottom-up principle. In this process, double emulsions are produced in small channels with little shear force in one- or two-stage processes. Due to the narrow channel geometries, microfluidic flow is laminar, resulting in an almost monodisperse droplet size distribution. In recent years, glass capillary devices for the production of double emulsions have been established, in which both droplet breakups take place in parallel [17]. Both the sizes of the inner and outer droplets as well as the type and number of inner droplets can be precisely adjusted in the process [20].

Regardless of the production method, all double emulsions can undergo different instability mechanisms [5]. A fundamental differentiation must be made between reversible and irreversible instability mechanisms. Reversible mechanisms, such as creaming or sedimentation, do not permanently damage the double emulsion structure and can be undone by, e.g., shaking the product prior to use.

Irreversible instability mechanisms, however, cannot be reversed. These mechanisms involve diffusion between the inner and outer phases. Moreover, outer droplets can coalesce with each other, and inner droplets can coalesce with each other or with the outer phase.

In general, there are numerous measuring methods that can be used to monitor and analyze double emulsions during production and storage. One of the most important parameters for double emulsions is the droplet size, which determines the morphology and microstructure of

double emulsions. Furthermore, changing droplet sizes indicate occurring instability mechanisms [64]. Additionally, the encapsulation efficiency and rheological properties are of great importance [4], and often change significantly with the change in droplet sizes over storage time. Typical measurement techniques known from single emulsion, however, often fail in double emulsions due to the emulsion-in-emulsion structure [65] or the need for sophisticated sample preparation [66].

Optical measuring methods can be used to make statements about the droplet size and filling degree; microscopy examinations play a particularly important role here. Among other things, it is the method of choice for confirming the multiple characteristics of a double emulsion [23]. In addition, any changes in the double emulsion, such as the loss of internal water phase or changes in oil droplet size, can be qualitatively monitored over time.

To measure the droplet size distribution of emulsions, dynamic and static scattered light methods have been established as the most common laboratory methods. Here, the size of the inner water droplets is usually measured before the second emulsification step, which is otherwise not accessible with common measurement methods. Accordingly, after the second emulsification step, only the oil droplet size can be measured [4].

The amount of inner water can be determined using a differential scanning calometry (DSC) analysis [24]. Here, the double emulsion is strongly supercooled until the outer water phase freezes, followed by the inner water phase. The mass of inner water can be calculated from the heat released during the freezing. In addition, the supercooling required to freeze the inner water phase delivers information on the droplet size of the inner water phase. The smaller the droplet size, the deeper the necessary supercooling. However, there are some limitations to DSC measurements [25].

NMR-based methods have also been proposed to determine both the amount of encapsulated water and inner droplet size in W/O/W emulsions [57]. To date, they are limited to inner droplet sizes > 1 µm with a monodisperse droplet size distribution and the need to suppress any diffusion during the measurement period [67].

Double emulsions are also characterized by rheological measurements. These are used to determine the filling degree of a double emulsion based on its viscosity. For this purpose, correlations such as the Krieger–Dougherty equation, which describes the viscosity as a function of the filling degree, are used. The higher the filling degree, the higher the viscosity of the double emulsion [68].

The described methods for measuring the filling degree as well as the droplet size all share a common point in that they are usually performed offline. This requires sample preparation, and the sample is not suitable for further investigations after the measurement process. We therefore want to present a new optical measurement method based on the Raman effect. It can be performed both in- and online, so that the emulsion is not affected by the measurement.

The Raman effect is based on the interaction of molecules and electromagnetic radiation. When radiation hits a molecule, it is excited into a virtual state until the molecule is de-excited by emitting a photon. If the photon has the same energy as the exciting radiation, it is known as elastic Rayleigh radiation [29].

However, for the Raman effect, the energy of the emitted photon is unequal to the exciting radiation, which is the reason why inelastic radiation is present here. The shift of the wavelength is called a Raman shift, and it is proportional to the energy difference between the incident and emitted light [29].

In general, the Raman effect is a very weak effect, because compared with Rayleigh scattering, only one in every 10^8 photons show inelastic Raman scattering. Therefore, modern Raman spectrometers are equipped with an optical filter that separates the Rayleigh scattering from the Raman signal [69].

The Raman intensity I_R can be calculated using the following correlation

$$I_R \propto I_0 \nu^4 N \left(\frac{\partial \alpha}{\partial Q}\right)^2, \qquad 3\text{-}1$$

where I_0 and ν describe the intensity and frequency of the excitation laser, respectively, N is the number of scattering molecules, α describes the polarizability, and Q is the amplitude of the vibrational coordinate [7].

Based on Equation 3-1, the strongest possible short wavelength laser will provide the strongest Raman signal. However, it should be noted that fluorescence excitation can also occur with short wavelength lasers, which produces a much stronger signal than the Raman signal [7].

Raman spectrometers are used for most Raman measurements as they measure a complete spectrum of the sample, but are expensive to purchase. However, often only a small part of the spectrum is of interest. Therefore, there is the alternative of using photometers in combination with a dispersive element for detection [34]. Photometers are not wavelength-selective and only detect the part of the spectrum that can pass through the dispersive elements. The speed and sensitivity are usually higher than with spectrometers, and the costs are significantly reduced.

For emulsions, Raman spectroscopy is used in monitoring emulsion polymerizations, usually in those using single emulsions [70]. To the best of our knowledge, there are currently only two publications that address Raman spectroscopy measurements of double emulsions. First, coherent anti-Stokes Raman scattering microscopy was used to acquire an image of a double emulsion [10]. Second, one of our previous papers dealt with the influence of refractive index matching in double emulsions on the Raman signal strength [71].

This paper presents a new measurement method that combines Raman spectrometry and photometry to measure the filling degree and oil droplet size of individual W/O/W double

emulsion droplets. The two measuring methods are combined in a way that they simultaneously operate without any time delay between the measurements.

3.3 Materials and Methods

3.3.1 Emulsion System and Experimental Setup

We dissolved 49% ammonium nitrate (CarlRoth, Karlsruhe, Germany) in the inner water phase, which served as a tracer for the Raman measurement. In addition, the ammonium nitrate aligns the refractive index of the inner water phase with that of the oil phase, which means that the inner water phase provides a stronger Raman signal [71]. The oil phase was based on M10 silicone oil (CarlRoth, Karlsruhe, Germany), in which 2% Dowsil Resin XR 0497 (DowCorning, Midland, MI, USA) was dissolved as an emulsifier. In the outer water phase, 4% emulsifier was dissolved in the form of polyvinyl alcohol Kuraray Poval 26-80 (Kovayal, Hattersheim am Main, Germany).

The measurement system is capable of simultaneous spectroscopic and photometric Raman measurements. For the spectrometric measurements, the “RNX1-532” Raman spectrometer (Kaiser Optical Systems, Inc., Ann Arbor, MI, USA) was used. Three “CM 92N” custom photon multipliers (CPMs) (ProxiVision, Bensheim, Germany) were used for the photometric measurements. The “Kaiser NCO-0.5-VIS” backscatter probe, which is part of the spectrometer, was used for the measurements. The “gem532” laser (Novanta, Bedford, MA, USA) was used as excitation source. It emits a wavelength of 532 nm at a maximum power of 400 mW.

Figure 3-1 shows a scheme of the experimental setup. The detection signal was first passed through a long-pass filter after the Raman probe to block the laser wavelength. It was then split into four equally strong signals via a system of three 50:50 beam splitters (Thorlabs, Newton, NJ, USA). One signal was focused into an optical fiber, which was connected to the Raman spectrometer. The other three signals were each coupled into a CPM module. Because photometers are not wavelength-sensitive, bandpass filters were placed in front of the CPMs to isolate the signal from ammonium nitrate, silicone oil, and a reference. Details regarding the bandpass filters are listed in Table A1 (Appendix to chapter 3).

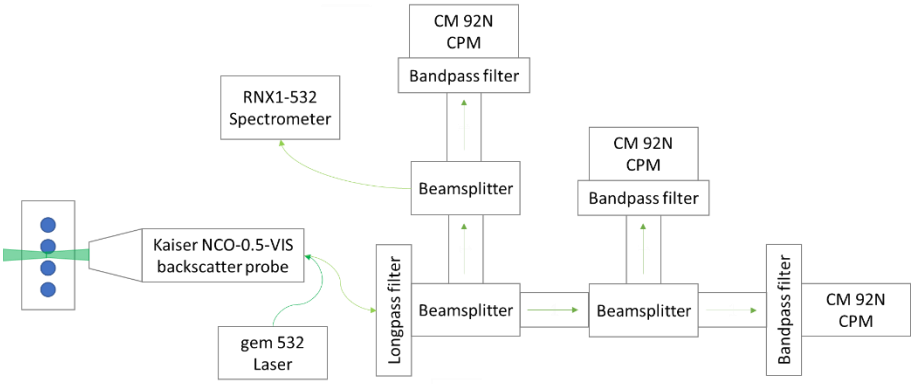

Figure 3-1 Schematic illustration of the measurement system. The focus is on the measurement technology components; details of the emulsification technology are not included.

The limits of the optical filters are shown in Figure 3-2. The filters for ammonium nitrate and the reference were located directly next to each other, while the filter for the oil phase was located separately.

The spectra of the individual phases were measured using the Kaiser spectrometer. For the measurements, a spectroscopy cuvette (Type: 100-10-40, Hellma Analytics, Müllheim, Germany) was used, which was placed in a cuvette holder belonging to the spectrometer. Due to this procedure, the spectra shown in Figure 2 are quantitatively comparable.

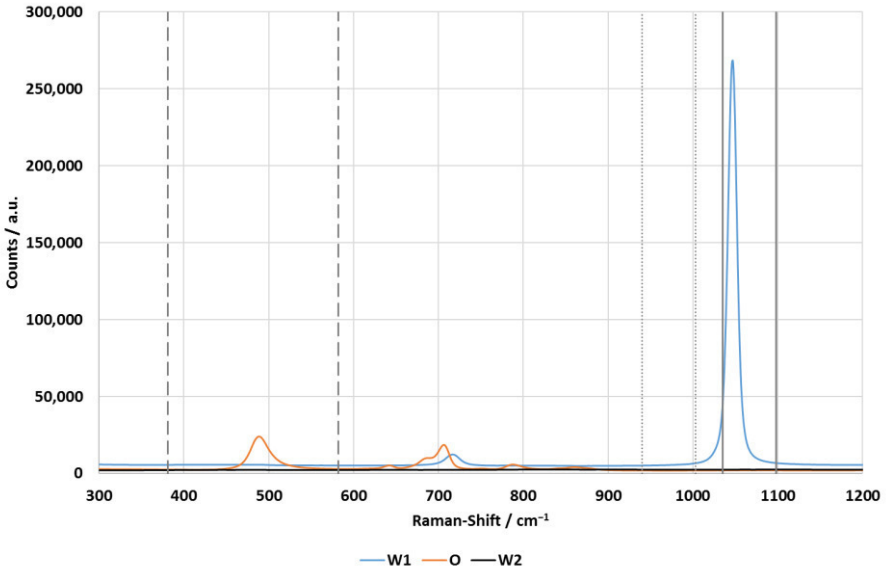

Figure 3-2 Spectra of the individually measured phases of the double emulsion. The spectra were measured using the Kaiser spectrometer at 1 s integration time and with five accumulations. The vertical lines visualize the limits of the oil phase filter (dashed lines), reference filter (dotted lines) and inner water phase filter (solid lines).

The spectra show that the outer water phase had no peaks in the relevant region of the spectrum. The inner water phase had a dominant peak due to ammonium nitrate at 1047 cm^{-1}, which was not overlapped by the oil phase. The oil phase was characterized by two peaks. The shorter wavelength peak at 489 cm^{-1} was also not affected by the other phases, while the longer wavelength peak around 700 cm^{-1} was overlapped by a small ammonium nitrate peak.

However, this is not a concern, as the bandpass filter of the oil phase transmits light in the range of 381–582 cm^{-1}. The superposition is also irrelevant for the evaluation of the spectroscopic data, as the larger oil peak at 489 cm^{-1} was used for this purpose. Table 3-1 summarizes the measured Raman bands, including the respective excited molecular bond.

Table 3-1 Summary of detected Raman bands, including the respective excited molecular bond.

Substance	Raman Band	Excited Molecular Bond
Ammonium nitrate	1047 cm^{-1}	NO_3^-
Silicone oil	489 cm^{-1}	Si-O

In principle, Raman spectroscopy is able to detect water bands and, therefore, directly measure water. For the measurement method presented in this article, this is not useful, as it is not possible to distinguish between the water signals of the inner and outer water phase.

3.3.2 Data Evaluation

The measured spectra were evaluated using a baseline correction. A base point is set in front of and behind the peaks, which form the start and end point of the baseline. First, the total integral between the selected boundaries is calculated. Then, the integral under the baseline is calculated and is subtracted from the total integral, resulting in the baseline-corrected integral of the peak. The boundaries are determined from the spectra of the double emulsions. For the oil phase, the boundaries are 400–600 cm^{-1}, for the inner water phase, the boundaries are 1015–1065 cm^{-1}.

The measurement of one filling degree took eight minutes. The spectrometer took four measurements at a speed of two minutes each during this time. For statistical evaluation, a spreadsheet software was used to calculate the mean value and standard deviation of the four measurements per filling degree.

Three photometric signals were measured: one for the inner water phase, oil phase, and as a reference, respectively. During the measurement time of eight minutes per filling degree, the CPMs were constantly measuring with an integration time of 2 ms. The number of counts measured over time is the output. Each peak in the photometric results corresponds to a double emulsion drop, which was individually evaluated.

An internally programmed Matlab software was used for the evaluation. The software read the data, calculated the integrals of the peaks, and subsequently, using the following equation

$$FD = \frac{Int._{AN} - Int._{Ref}}{Int._{O}}, \qquad 3\text{-}2$$

calculated the filling degree of each individual double emulsion droplet. In Equation 3-2, the three parameters are the calculated integrals of ammonium nitrate ($Int._{AN}$), silicone oil ($Int._{O}$), and the reference ($Int._{Ref}$). To obtain statistical information for the accuracy of the

measurement, the mean value of the measured filling degrees of all double emulsion droplets, as well as the respective standard deviation, was calculated using a spreadsheet software.

The “Peak detection” function was used for the peak detection analysis. This outputs the position of the peak top as well as the position of the flanks at half-peak height. To find the position of the peak base before and behind the peak, the function has been edited. This allows the peak flank to be examined for an inflection point. To avoid setting a local minimum in the flank as the position of the peak base, a maximum Y-value for the peak base can be manually set in the user interface. This procedure was only carried out for the signal of the oil phase, as the largest peaks occurred here. The X-values of the peaks found here were utilized for the peak evaluation of the inner phase as well as the reference.

To determine the Y-value of the peak base, the mode of the baseline between two peaks was determined. Once the base points of the peak were found, a baseline was interpolated between them.

The measurement duration of a drop can be calculated from the X-positions of the peak. The volume flow in the capillary and its cross-sectional area were also known, so that the diameters of the droplets could be calculated using Equation (3)

$$d_{Drop} = \frac{\dot{V} \cdot t}{a}. \qquad 3\text{-}3$$

where d_{Drop} describes the oil droplet diameter, $\dot{V}$ is the volume flow in of the capillary, a is its cross-sectional area, and t describes the measurement duration of one oil droplet.

3.3.3 Emulsification

The double emulsion was produced in a two-stage process. First, an inner emulsion with a filling degree of 40% was produced using a “Megatron MT300” rotor-stator system (Kinematica AG, Malters) with a double-row ring gear. The rotational speed was set to 20,000 min^{-1}, which corresponds to a peripheral speed of 27.2 m/s. The produced W_1/O emulsion served as the stock emulsion for the other internal emulsions with lower filling degrees. To obtain the lower filling degrees, the corresponding quantities of oil phase and stock emulsion were mixed in laboratory bottles using stirred mixers.

The droplet size distribution of the stock emulsion cannot be measured using light scattering as a result of the similar refractive indices of the inner water phase and oil phase. Therefore, two further inner emulsions were produced: one with 40% ammonium nitrate in the inner water phase and the other with 60% ammonium nitrate. The oil phase was not changed. The filling degree of both emulsions was 40%, and the emulsification procedure was the same as for the stock emulsion. Both emulsions were measured by static laser light scattering using a HORIBA LA-950 particle analyzer (Microtrac Retsch GmbH, Haan, Germany).

The second emulsification step was performed using a new variant of microfluidic glass capillary devices [17], the so-called “Lego®-Device” [55]. Inside, the droplet break-up takes place in a co-flow regime, i.e., inner emulsion and outer water phase flow parallel to each other. Two syringe pumps (Legato 100, kdScientific Inc., Holliston, MA, USA) were used for pumping. The applied flow rates were 10 mL/hr for the inner emulsion and 20 mL/hr for the outer phase. The inner emulsion was fed into the Lego-Device in a round borosilicate capillary (ID: 0.58 mm; OD: 1 mm; World Precision Instruments, Friedberg, Germany). The outer phase flowed in the sheath stream between the mentioned capillary and another round borosilicate capillary (ID: 1.12 mm, WPI, Sarasota, FL, USA). Droplet breakup occurred at the tip of the thinner capillary, which was tapered and grounded to an orifice diameter of 200 µm. The set flow rates led to a production rate of more than 5 Hz, so that at least 2400 drops were produced per filling degree. Because round borosilicate capillaries can negatively influence Raman measurements, an internally developed 3D-printed nylon adapter was used to transfer the double emulsion into a square quartz capillary (ID: 1.00 mm, CM Scientific Ltd., Silsden, UK). The Raman measurement took place in this capillary, which means that negative material influences or reflections due to the curvature of the round capillary can be excluded.
To demonstrate the filling degree measurement, a total of nine double emulsions were measured. The weights and resulting filling degrees are shown in Table A2 (Appendix to chapter 3).

3.4 Results

3.4.1 Droplet Size Distribution of Inner Emulsion

Figure 3-3 shows the droplet size distribution (DSD) for 40% ammonium nitrate and 60% ammonium nitrate in the inner water phase. Both DSDs are very similar, and the Sauter diameters are 3.18 µm (40% ammonium nitrate) and 3.05 µm (60% ammonium nitrate). Therefore, it can be assumed that the Sauter diameter for the stock emulsion containing 49% ammonium nitrate is in the same range.

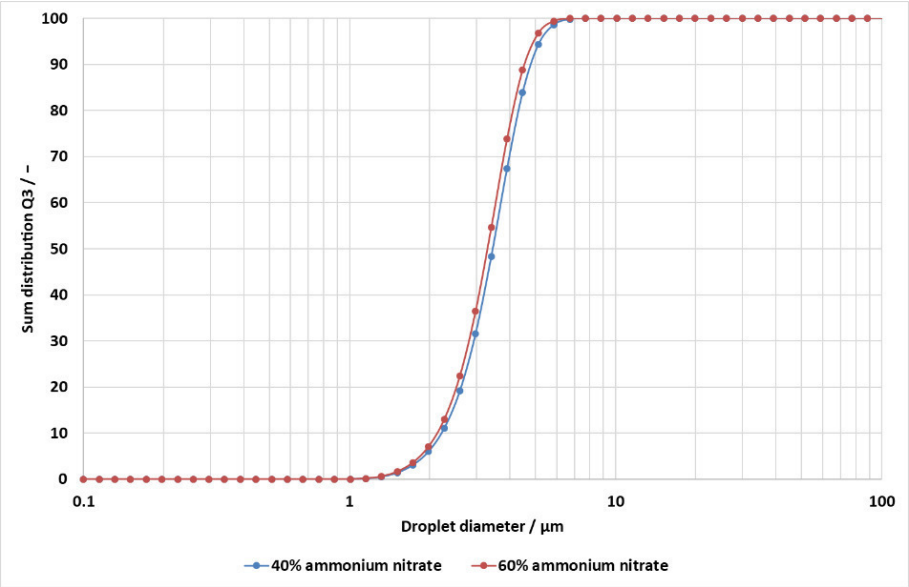

Figure 3-3 Droplet size distributions of two inner emulsions containing 40% ammonium nitrate and 60% ammonium nitrate, respectively, in the inner water phase.

3.4.2 Spectrometric Results

Figure 3-4 shows the spectra of three representative samples of the double emulsions, with filling degrees of 0%, 20%, and 40%, respectively. The two oil peaks at 490 cm^{-1} and 700 cm^{-1} decreased with the increasing filling degree, which results from the increasing proportion of the internal water phase. Correspondingly, the ammonium nitrate peak at 1047 cm^{-1} becomes larger as the filling degree increases.

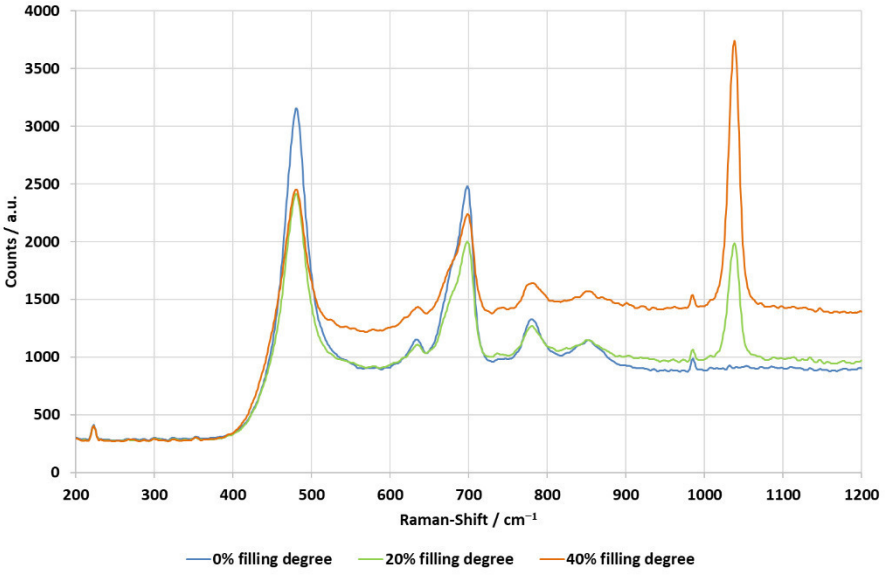

Figure 3-4 Section of three representative Raman spectra samples of the filling degrees of 0%, 20%, and 40%.

After the baseline correction, the filling degree was calculated as described in Section 3.3. In Figure 3-5, the filling degrees calculated from the measured data are plotted against the set filling degrees. The data points follow a linear trend with a Pearson coefficient of $R^2 = 0.9992$.

Each data point is based on four measurements. The standard deviations for each data point are also given. In relation to the absolute mean values, the respective percentual standard deviations are below 10% for the filling degrees when the internal water phase is present, and they decrease with the increasing filling degree. In contrast, for absolute numbers, the standard deviations are in the same scale, ranging between 0.001 and 0.003. Only the 0% filling degree is out of range, with a standard deviation of 0.008. This is equivalent to a standard deviation percentage of 31.9%.

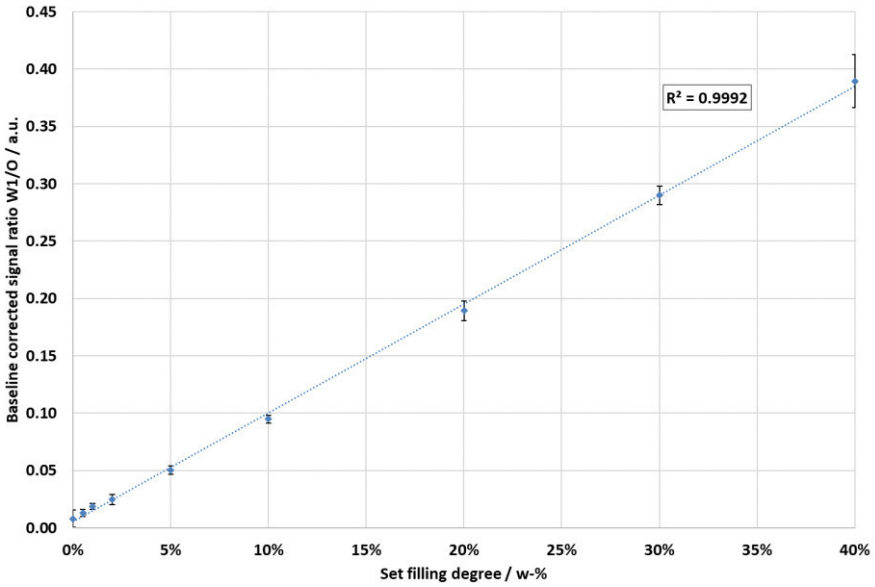

Figure 3-5 Result of the filling degrees calculated from the measured data plotted against the set filling degrees. Each data point is based on four measurements. The data show a very high linearity with a coefficient of determination of $R^2 = 0.9992$. The associated standard deviations are shown. However, all standard deviations are multiplied by a factor of three for improved visibility.

3.4.3 Photometric Results

3.4.3.1 Filling degree

The photometric results are shown in Figure 3-6. The filling degrees calculated from the measured data are also plotted against the set filling degrees. The data also have a high linearity, with a Pearson coefficient of $R^2 = 0.9900$. The data points are the average filling degrees of all double emulsion drops, which were calculated according to Equation 3-2.

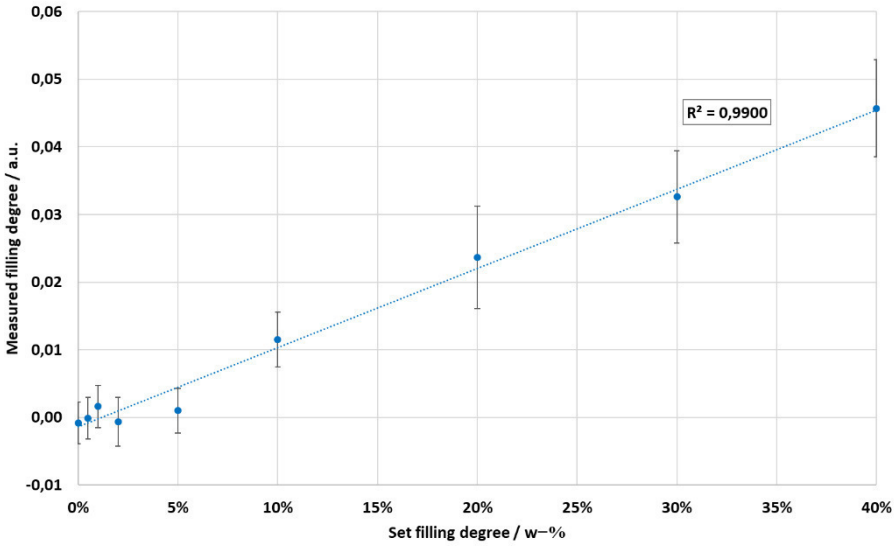

Figure 3-6 Result of the photometric measurements. The data points are based on all individually calculated filling degrees of the analyzed double emulsion droplets. A high linearity with a Pearson coefficient of $R^2 = 0.9900$ is shown.

The standard deviations for each data point are also shown. Compared with the standard variations of the spectrometric results in Figure 3-5, the photometric standard deviations appear significantly larger; in absolute numbers, however, they have the same order of magnitude. Because of the approximately tenfold smaller absolute mean values for the filling degrees, the standard deviation percentages are significantly larger. In general, the standard deviations for the photometric results follow the trend of increasing with the increasing filling degree from 0.003 to 0.008.

3.4.3.2 Oil Droplet Size and Oil Droplet Size Distribution

Figure 3-7 shows the oil droplet sizes for each filling degree. The diameters of the individual droplets are combined into an average value. Between the 0% and 10% filling degree, the droplet diameters were between 0.8 mm and 0.9 mm in size. The standard deviations are less than 20% in each case. In the further course, the droplet sizes continued to increase until, at the 40% filling degree, they averaged 2.1 mm in size. It is striking that the droplet diameter of 1.8 mm at the 20% filling degree was significantly larger than observed in the 30% filling degree; here, the average diameter was 1.3 mm. In addition, for the 20% filling degree, the standard deviation of 69% was significantly larger than for the other filling degrees.

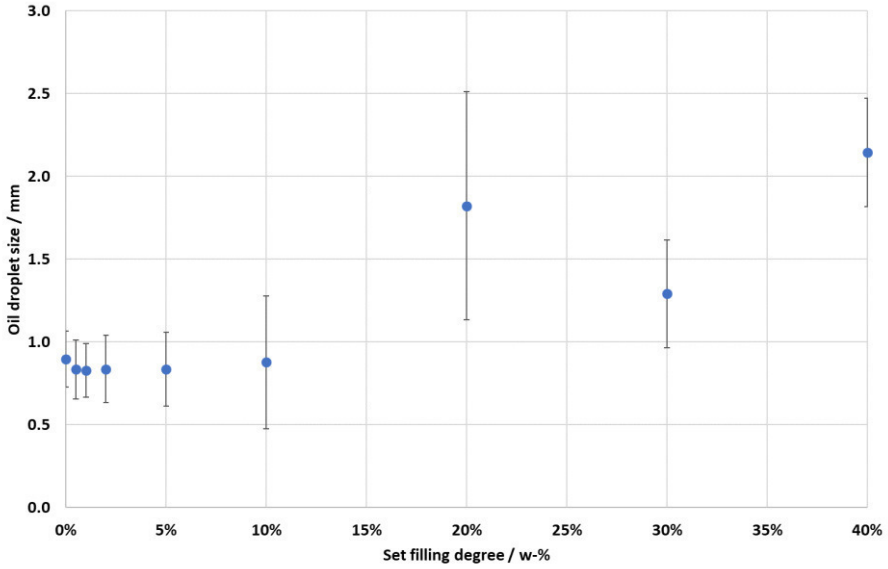

Figure 3-7 Plot of mean oil droplet sizes versus filling degrees. The droplet sizes remained constant up to the 10% filling degree before increasing.

From the individual droplet sizes, the individual droplet size distributions per filling degree can be calculated. As an example, the sum distributions of the 1% (lowest polydispersity) and 20% (highest polydispersity) filling degrees are plotted in Figure 3-8.

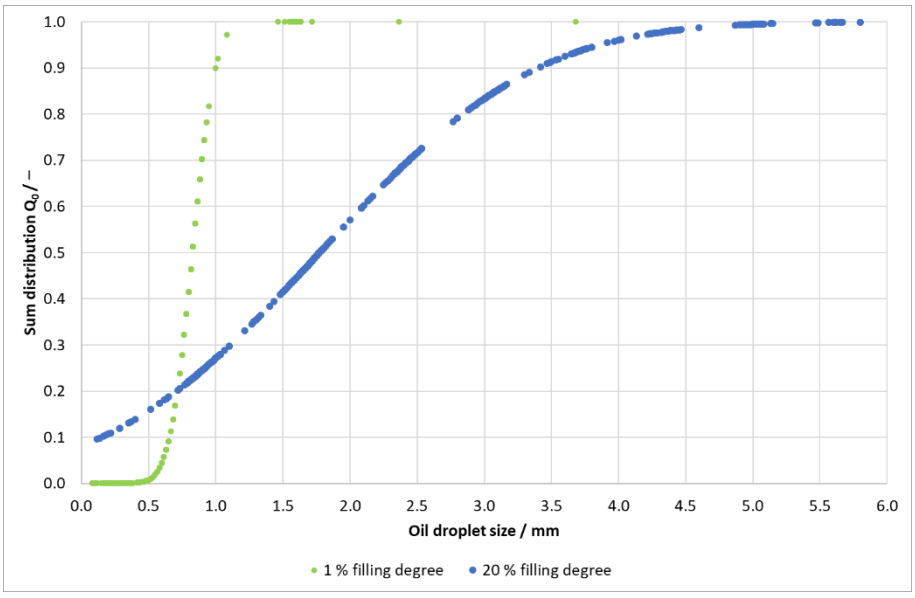

Figure 3-8 Sum distributions of the 1% (lowest polydispersity) and 20% (highest polydispersity) filling degrees.

Figure 3-8 illustrates the different standard deviations or the clearly more polydisperse oil droplet breakup at the 20% filling degree. At the 1% filling degree, 80% of the droplet diameters ranged between 0.6 mm and 1.0 mm, while at a filling degree of 20%, the droplet diameters varied between 0.4 mm and 3.6 mm.

3.5 Discussion

The measurement results together with their calculated Pearson coefficients show that the filling degrees of double emulsions can be measured and distinguished with both Raman measuring methods, i.e., spectroscopically and photometrically.

The data recorded with the spectrometer show almost perfect linearity. The standard deviations decreased with the increasing filling degree. At the 0% filling degree, by far the largest standard deviation of 31.9% was present. This can be explained by the absence of an ammonium nitrate peak, which means that only the signal noise is included in the integral calculation. The larger the ammonium nitrate peak with increasing filling degree, the more constant the integrals and the smaller the standard deviations, i.e., it is method-related, and the measurement accuracy increases with the filling degree of the sample.

The oil integrals hardly varied over all filling degrees, with their maximum standard deviation being 2.0%. This means that they only had a minor influence on the standard deviations of the filling degrees.

The filling degrees calculated from the photometric results showed a slightly worse linearity, with $R^2 = 0.9900$. Accordingly, the filling degrees can also be distinguished with this method, but with a lower sensitivity compared with the spectrometric measurements.

The standard deviations per filling degree were significantly larger for the photometric measurements, which is due to several aspects. For each filling degree, the shortest measured measurement durations were 10–20 ms, corresponding to droplets in the size range of about 20–40 µm. Theoretically, it can be ruled out that these are individual, very small oil droplets that are produced, as oil droplet size values just below the size of the capillary's inner diameter are to be expected with the co-flow arrangement of the capillaries that were used. In fact, such droplets did not exist in all samples, as could be verified by microscopic images. These measured signals can only be explained by particulate impurities which are present in the continuous phase and reflect the excitation light.

Another reason is the very short integration time of 2 ms. In general, the longer the integration time, the more stable the result. The strong fluctuations can be seen in the section of the evaluated peaks at the 5% filling degree shown in Figure 3-9.

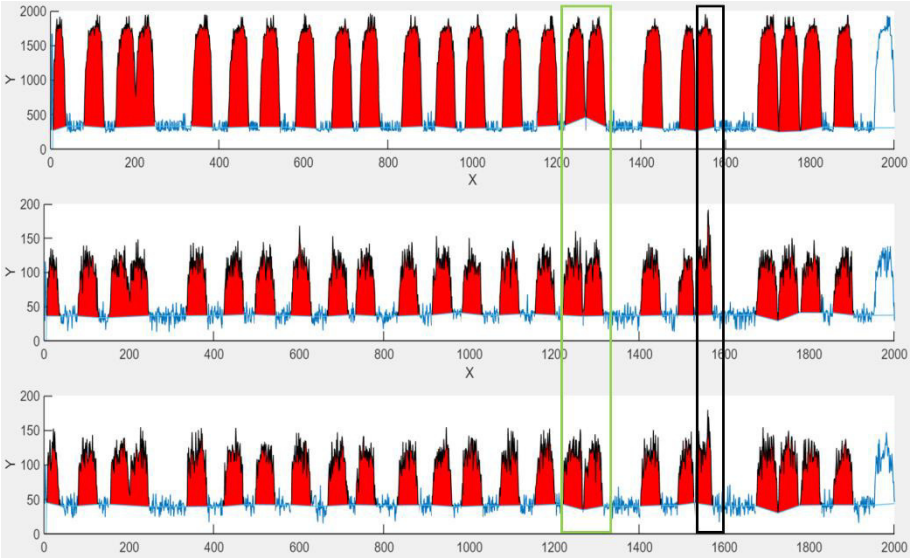

Figure 3-9 Section of the peak evaluation of the double emulsions at the 5% filling degree. The top column shows the peaks of the oil phase, the middle column those of the inner water phase, and the bottom column those of the reference.

Considering both the baselines between the peaks and the areas of the peak maxima, a clear scattering of the measured values can be seen. In addition, the baselines were individually determined for each peak. This disadvantage becomes clear with the double peak that is highlighted by the green rectangle. The double peak results from two drops which were measured in very short succession. Consequently, the baseline was calculated from extremely few measured values. In this case, this results in the slope of the first baseline being positive and the slope of the second baseline being negative for the oil signal. For the inner water phase, both baselines have no significant slope. For the reference, the first baseline has a negative slope, and the second baseline has a positive slope.

In addition to the baselines, there are numerous outliers on the peaks, such as on the peak within the black rectangle. The oil signal has a small outlier in the middle, but it is of this magnitude on most peaks. On the corresponding peaks of the inner water phase and the reference, the outliers are much more pronounced.

Even without outliers, the scattering on all peaks is different and does not follow a pattern. Even between three superimposed peaks that all originate from the measurement of the same droplet, there are differences in the scattering pattern around the peak maxima.

In general, an increase in oil droplet size from the filling degrees above 10% can be explained by the associated increase in the viscosity of the inner emulsion [17]. The increased viscosity makes it more difficult for the outer phase to break the inner emulsion into double emulsion droplets, which results in increased oil droplet sizes. Up to a filling degree of 10%, the increase in viscosity is small and thus has no significant influence.

At the 40% filling degree, a uniform drop break-up was no longer possible. Instead, up to five individual droplets formed a droplet chain, which meant that the individual droplets could not

be individually measured. This can be seen in Figure 3-10, which shows a section of the evaluated oil peaks.

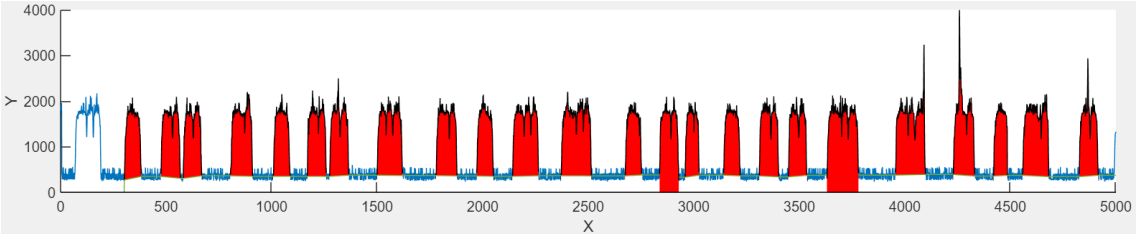

Figure 3-10 Section of the evaluated oil peaks at the 40% filling degree. The individual peaks have different distances, which illustrates the non-uniform flow. Many peaks have black vertical lines in their upper half. The line indicates the boundary between two drops in a drop chain.

Figure 3-11 shows a similar behavior of the droplets in the channel for the 20% filling degree. The droplets flow in non-uniform intervals, with some flowing as single droplets, and others in a chain of several droplets.

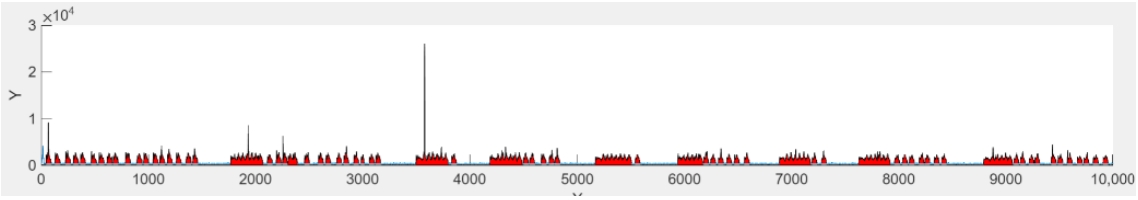

Figure 3-11 Section of evaluated peaks at the 20% filling degree, which shows an unsteady flow pattern with single droplets as well as droplet chains.

Based on the droplet chains, which are recognized as one droplet by the software, the significantly larger oil droplet diameters as well as wide oil droplet size distribution can be explained.

3.6 Conclusions

In summary, both measuring methods are able to measure the filling degree of W/O/W double emulsions. The photometric measurement method can also reliably measure the oil droplet sizes. Which measurement method is more suitable therefore depends on the experimental goal, required accuracy, and budget available.

The spectrometric method should be chosen if information on the droplet size is not important. With this method, filling degrees with a 0.5% difference can be distinguished with high accuracy.

If information on the droplet size is also required, the photometric method must always be used, as only this method measures individual oil droplets. However, this measurement method is subject to greater fluctuations, which is why small percentage differences in the filling degree cannot be as reliably measured here as with the spectrometric method. However, the very short sampling rate of 2 ms, which is the basis of the measurement of each individual

drop, has a share in this. In addition, further optimizations to the software, such as a global baseline for all peaks or a minimum measurement duration, could make the results more precise

3.7 Acknowledgments

Special thanks is given to Goran Vladisavljevic for providing the Lego-Device and for providing numerous productive discussions. The authors would also like to thank Nico Leister for all of the helpful discussions and for his professional advice.

4 Monitoring of Osmotic Swelling Induced Filling Degree Changes in WOW Double Emulsions Using Raman Technologies

This chapter was published as: Hufnagel, T.; Leister, N.; Stoy, R.; Rädle, M.; Karbstein, H.P. Monitoring of Osmotic Swelling Induced Filling Degree Changes in WOW Double Emulsions Using Raman Technologies. *Chemosensors* **2023**, *11*, 206. https://doi.org/10.3390/chemosensors11040206

4.1 Abstract

Due to their nested structure, double emulsions have the potential to encapsulate value-adding substances until their application, making them of interest to various industries. However, the complex, nested structure negatively affects the stability of double emulsions. Still, there is a lack of suitable measurement technology to fundamentally understand the cause of the instability mechanisms taking place. This study presents a novel measurement method to continuously track filling degree changes due to water diffusion in a water-in-oil-in-water ($W_1/O/W_2$) double emulsion droplet. The measurement method is based on the Raman effect and provides both photometric and spectrometric data. No sample preparation is required, and the measurement does not affect the double emulsion droplet.

4.2 Introduction

Double emulsions are complex multiphase systems in which one emulsion is emulsified a second time. The most prominent types of double emulsions are water-in-oil-in-water ($W_1/O/W_2$) and oil-in-water-in-oil ($O_1/W/O_2$) double emulsions [47].

Due to their structure, they offer great potential for encapsulating valuable, sensitive substances, which can be released in a targeted manner during application. The main areas of application are cosmetics, pharmaceuticals and foods [53]. In these industries, the typical droplet diameter for the inner and outer droplets are 1 µm and 10 µm, respectively. However, due to their multiphase structure, double emulsions are prone to various instability mechanisms. Therefore, to date, there is no product on the market based on double emulsions [35].

The instability mechanisms that occur can be divided into two groups: Coalescence between or within one emulsion phase and diffusion between two phases [5].

To achieve good stability in double emulsions, coalescence and diffusion must be suppressed. Concerning diffusion, it is mainly the diffusion between the outer W_2 phase and the inner W_1 droplets which is observed in application systems as a destabilizing process [21]. The capillary pressure of the encapsulated water droplets leads to the diffusive release of inner water. Whether the encapsulated substances are also transported from the inner water phase to the outer water phase depends on their solubility in the oil phase and on the applied surfactants [72]. In common formulations, the diffusion from W_1 to W_2 is hindered by balancing the capillary pressure with an osmotic pressure by dissolving e.g. salts in the W_1 phase [73]. The concentration of the osmotic active substances must be chosen with care, since too high osmotic pressure leads to the diffusion of water molecules from W_2 to W_1, which results in a swelling of the water droplets within the oil droplets. When this transport exceeds a certain level, osmotic swelling breakdown occurs [74, 75]. This means, the double emulsion droplets invert their phases and an O/W emulsion with much smaller oil droplets remains, while the inner phase is released completely.

To hinder coalescence, both interfaces must be stabilized by surfactants. At the inner W_1/O interface, oil soluble surfactants are used. At the outer O/W_2 interface, more hydrophilic surfactants are applied [76]. Since the presence of the surfactant cannot be strictly limited to its corresponding interface, the interactions of the surfactant play a major role in double emulsion research [11, 22].

Plenty of review papers are available that summarize the efforts of researchers in optimizing the formulations of double emulsions [4, 13, 35, 64, 76–78]. In brief, no general rules can be formulated how to produce a stable double emulsion. In the outer phase, polymeric surfactants are often preferred in comparison to short chain surfactants [79]. Strongly interfacial active short chain surfactants were found to increase W_1–W_2 coalescence and therefore limit the

encapsulation efficiency in combination with some lipophilic surfactants [3]. However, many applications need short chain surfactants, either for fast stabilization in the production process or to avoid the increase in viscosity polymers bring with them. For polymeric surfactants, specific formulations with good stabilities are reported [80, 81]. In terms of lipophilic surfactants, the choices are often limited, depending on the oil phase used. For triglycerides, PGPR and Span 80 are most widespread used [13]. Furthermore, for silicone oil, copolymers made of a silicone backbone in combination with a hydrophilic moiety are proposed [82].

The stability of double emulsions is usually determined by tracking the changes of both water and oil droplet sizes, as well as measuring the encapsulation efficiency of tracer substances [5].

Tracking the release of a marker substance gives interesting information for the application of a system. However, the diffusion of water is not detectable with this method. The release of the encapsulant may happen via diffusion [83] or via coalescence [52]. The responsible mechanism is not easily named and troubleshooting for a formulation is therefore often complicated and not target oriented. A major limitation is the dependence of the encapsulation efficiency on the encapsulated substance [84, 85]. Therefore, systematic studies are always limited to the encapsulated substance examined.

A more elaborate method is the measurement of droplet sizes by confocal laser scanning microscopy (CLSM). The droplets are tagged with fluorescent markers and the droplet sizes are measured from the pictures. Since the pictures of the droplets are cross-sections of the droplets at an unknown position, the apparent droplet size must be corrected, which needs at least 2000 droplets to be examined [36]. When this is done properly, the double emulsion is completely described, and changes can be tracked reliably.

With pulsed-field-gradient nuclear magnetic resonance (PFG-NMR), the droplet sizes of the inner droplets can also be assessed [26]. By measuring the diffusion coefficients of inner and outer water, both the amount of inner water and the droplet sizes can be calculated [86]. While this method gives great insights into double emulsion droplets, the requirements for the samples are rather high. During the measurements, no creaming of the oil droplets should occur und a good overall stability of the emulsion is demanded [87].

Differential scanning calorimetry (DSC) also allows the measurement of the amount of inner water [24]. Since the small inner water droplets are unlikely to have any impurities to act as a heterogenous nucleus for crystallization, they need a higher supercooling than the outer water phase. Therefore, the peaks for W_1 and W_2 phase can be separated easily. As a limitation, this measurement technique can only be applied for freeze stable double emulsions, since many formulations show a significant release during the freezing of the W_2 phase [25].

Because of the limitations each measurement method poses on the detection of the amount of inner water of double emulsions, novel methods are constantly looked for. As an alternative,

Raman spectroscopy is promising, as it is a fast and non-destructive method [30], which can also be applied for inline measurements.

Raman spectroscopy is based on the electromagnetic interaction between photons and molecular bonds. The interaction raises the molecular bond to a virtual energy level. If it falls back to the initial energy level by emitting a photon, i.e., via Rayleigh radiation. If the molecular bond does not emit the complete energy through the emitted photon, the wavelength of the emitted photon is shifted to longer wavelengths compared to the excitation source. This shift is called Stokes shift. If the molecular bond is excited a second time after emitting a Stokes photon and, subsequently, emits more energy by a second photon, the wavelength of the second photon is shifted to a shorter wavelength compared to the excitation source. This is called anti-Stokes shift. [29]

The respective shift distance depends on the excited molecular bond. As a result, each molecular bond has characteristic peaks in the spectrum, which makes it possible to differentiate between different molecular species and leads to the high selectivity of Raman spectroscopy. Since the peak height as well as the peak area correlate with the sample amount, samples can also be investigated quantitatively [8].

The properties of Raman spectroscopy are also advantageous for the analysis of double emulsions since the high selectivity enables distinguishing the individual phases and water does not negatively influence the measurements [10]. The oil phase itself and different solvates in both water phase can therefore be detected and quantified with their respective Raman peaks. One disadvantage, however, is the susceptibility to fluorescence of some materials that can overlay the Raman signal [29].

Two of our previous works already deal with the analysis of double emulsions using Raman spectroscopy. First, we investigated the influence of refractive index differences between the three phases on the signal strength of the inner phase [71]. In addition, we have shown that the filling degree of different double emulsions as well as the oil droplet diameter can be measured reliably [88].

This work presents another measurement method, based on Raman spectroscopy, which can be used to continuously monitor filling degree changes within a single double emulsion droplet. To demonstrate its usefulness, we investigate whether the following known mechanisms for water diffusion within a double emulsion can be monitored:

- The lower the osmolality of the inner water phase, the lower the relative filling degree change.
- With increasing osmolality of the outer water phase, the relative filling degree change is also increasing.

4.3 Materials and Methods

4.3.1 Emulsion System and Material Properties of the Phases

The outer water phase consists of 2% polyvinyl alcohol Kuraray Poval 26—88 (Kovayal, Hattersheim am Main, Germany) and ammonium chloride, which was added at 5%, 10% and 15%. As oil phase, silicone oil (M10, CarlRoth, Karlsruhe, Germany) was used with 2% Dowsil Resin XR 0497 (DowCorning, Midland, MI, USA) as emulsifier. For the inner water phase, two variants were used. As first variant, 49% ammonium nitrate (CarlRoth, Karlsruhe, Germany) in water and, as second variant, 24.5% ammonium nitrate and 24.5% polyethylene glycol (CarlRoth, Karlsruhe, Germany) in water were applied.

This emulsion system is not based on an existing application but solely developed for the development and demonstration of the new measurement method, and therefore, it is optimized for Raman measurements. For example, the high solvate content of the inner water phase increases its refractive index to the same level as the oil one. As a result, the double emulsion droplet is transparent for the human eye and the interfaces between the inner water droplets and the oil phase don't affect the Raman measurement.

The osmolalities of the different water phases could not be determined directly with a freezing point osmometer due to the high solvate concentrations. Corresponding solutions with a maximum solvate content of 7.5% were measured with the osmometer "Advanced® Micro Osmometer Model 3320" (Advanced Instruments Inc., Norwood, MA, USA) and the respective osmolalities of the used aqueous emulsion phases were extrapolated from these data.

The Raman spectra of the different emulsion phases were acquired with the Raman spectrometer "RNX-532" (Kaiser Optical Systems, Inc., Ann Arbor, MI, USA). The integration time was 0.5 s with three accumulations. The phases were placed in a standard spectroscopy cuvette (type: 100-10-40, Hellma Analytics, Müllheim, Germany), which was placed in a cuvette holder belonging to the spectrometer. This procedure allows the quantitative comparison of the spectra.

4.3.2 Optical Setup

A "gem532" laser (Novanta, Bedford, MA, USA) was used for excitation. The wavelength is 532 nm with an output power of 400 mW. The laser is focused into the "Kaiser NCO-0.5-VIS" backscatter probe (Kaiser Optical Systems, Inc., Ann Arbor, MI, USA), which in turn focuses it into the double emulsion droplets. The spot size of the probe is 55 µm, and the length of the focal volume is 500 µm. After the probe, the light is passed through a collimator (Thorlabs, Newton, NJ, USA) into a system of three 50:50 beam splitters (Thorlabs, Newton, NJ, USA). This splits the Raman signal into four equal parts. In addition, between the collimator and the

first beam splitter, a long-pass filter is placed (AHF analysentechnik AG, Tübingen, Germany), which blocks the laser.

One of the four signals is focused into an optical fiber connected to the Raman spectrometer "RNX1-532" (Kaiser Optical Systems, Inc., Ann Arbor, MI, USA). The other three signals are applied directly to "Custom Photon Multipliers" (CPM) (ProxiVision, Bensheim, Germany). CPMs work much faster than a spectrometer, allowing much more time-resolved measurements. However, CPMs are not able to distinguish between different wavelengths. Therefore, a bandpass filter is mounted in front of each CPM, which transmits only one signal of the inner water phase, one signal of the oil phase and one signal of a reference. Details about the filters can be found in the appendix in Table B1. A scheme of the measurement setup is displayed in Figure 4-1.

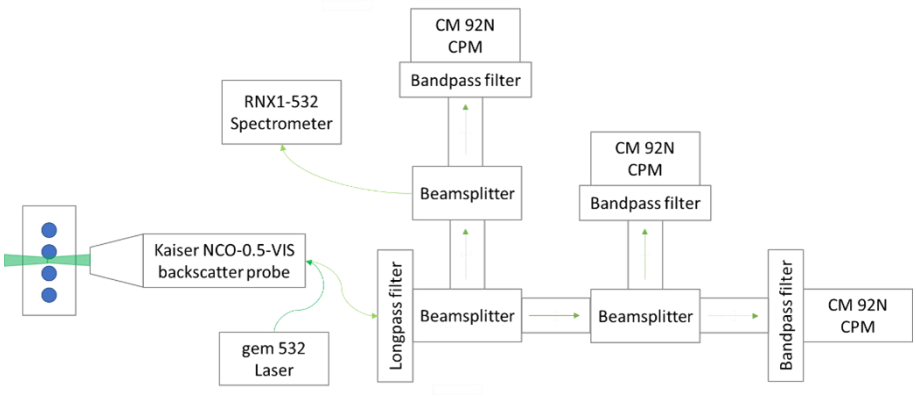

Figure 4-1 Schematic illustration of the measurement system. The focus is on the measurement technology components; details of the emulsification technology are not included [38].

4.3.3 Production of the Double Emulsion

The inner emulsions were produced in the "Megatron MT300" rotor-stator system (Kinematica AG, Malters, Switzerland) using a double-row gear rim geometry. It was set to 22,000 rpm, which corresponds to a maximum rotational speed of 29.9 m/s. During the ninety-second-long emulsification process, the emulsion was run in a closed circuit. The initial filling degree of the inner emulsions is 30%.

The droplet size distribution of the inner emulsions was determined by static light scattering using the "HORIBA LA-950 particle analyzer" (Microtrac Retsch GmbH, Germany). Since the refractive indices of the two applied water phases are matched with the refractive index of the oil phase, a direct measurement by static light scattering is not possible. Therefore, four inner emulsions with different solvate concentrations were prepared in the same way. For the first inner emulsion, the concentration of ammonium nitrate was 40% and 60%, respectively. For the second inner emulsion, the concentration of ammonium nitrate and polyethylene glycol was 20% and 30%, respectively. It can be assumed that the droplet size distributions of the two main inner emulsions are very similar.

The second emulsification step took place in the microfluidic LEGO® device [55], which is an optimization of the glass capillary devices [17]. The main components are two borosilicate capillaries (ID: 0.58 mm; OD: 1 mm; World Precision Instruments, Friedberg, Germany and ID: 1.12 mm, WPI, Sarasota, FL, USA), with the thinner capillary positioned inside the thicker one. The inner emulsion flows through the thinner capillary, and the outer water phase flows in the mantle flow between the capillaries. At the conical end of the inner capillary, both flows meet, resulting in the breakup of monodisperse double emulsions. Two syringe pumps (Legato 100, kdScientific Inc., Holliston, MA, USA) are used to feed both flows. The inner emulsion flows into the LEGO® device at 0.5 ml/h, the outer phase at 2.5 ml/h.
A square quartz capillary (ID: 1.00 mm, CM Scientific Ltd., Silsden, UK) is connected to the thicker capillary of the LEGO® device in which the Raman measurement is performed. The square quartz capillary prevents a negative influence on the measurement due to the curvature of the borosilicate capillary or the glass material.

4.3.4 Experimental Procedure

To start one experiment, the double emulsion is prepared according to the above description. When the syringe pumps are switched off, the time is recorded. As soon as a single double emulsion droplet is placed in the laser, the elapsed time is noted, and the measurement started.
The photometers measure continuously with an integration time of 100 ms at 10 iterations, resulting in one data point per second. The spectrometer starts a measurement every four minutes with an integration time of 2 min. After approximately one hour, the measurement is terminated.
Both inner emulsions are combined with all four outer water phases and measured in triplicate.

4.3.5 Data Analysis

To monitor changes in the filling degree, the signal of the oil phase is evaluated for both measuring methods.
For the spectrometric data, a baseline correction of the oil peak is first performed to obtain the integral of the oil peak without signal background [89]. For the baseline correction, one base point is set before the oil peak at 400 cm^{-1} and one behind the oil peak at 580 cm^{-1}. The baseline is drawn between the two base points. Subsequently, the integral of the entire area between the base points as well as the integral below the baseline is calculated. The difference of these integrals gives the baseline corrected integral of the oil peak. This was done for all spectra, which were collected during one measurement, and each spectrum provides one data point.
For the photometric data, it is not necessary to perform any kind of data preparation prior to the evaluation.

The calculation of the filling degree curve is performed analogously for both measuring methods. Both methods provide measurement data over time. First, the oil signals are normalized to the value of the first oil measurement. Subsequently, the relative change of the filling degree at a certain time t is calculated by means of equation 4-1

$$FD_{rel.,t} = \left(O_{0,norm.} - O_{t,norm.}\right) \times 100\%. \quad 4\text{-}1$$

The parameters in equation 4-1 are the relative filling degree change at time t ($FD_{rel.,t}$), the first data point at time t = 0 ($O_{0,norm.}$), to which all further data points are normalized and all further normalized data points at time t ($O_{t,norm.}$).

4.4 Results

4.4.1 Raman Spectra of the Emulsion Phases

Figure 4-2 shows the Raman spectra of the individual emulsion phases. In addition, the limits of the used bandpass filters are marked. The two inner water phases each have a significant peak at 1047 cm^{-1}, representing the binding of ammonium nitrate. For the inner phases containing only ammonium nitrate (light green), there are no further significant peaks. If polyethylene glycol is present (dark green) in addition to ammonium nitrate, the peak at 1047 cm^{-1} is proportionally smaller and the spectrum has a small offset.

The oil phase (red line) can be identified by two peaks at 400 cm^{-1} and 700 cm^{-1}. Only the first, larger peak at 400 cm^{-1} is evaluated.

The outer water phases (yellow and gold) have no characteristic peaks. However, the offset is strong compared to the other phases. For a better overview, only the spectra of the outer phases without and with 15% ammonium chloride are shown.

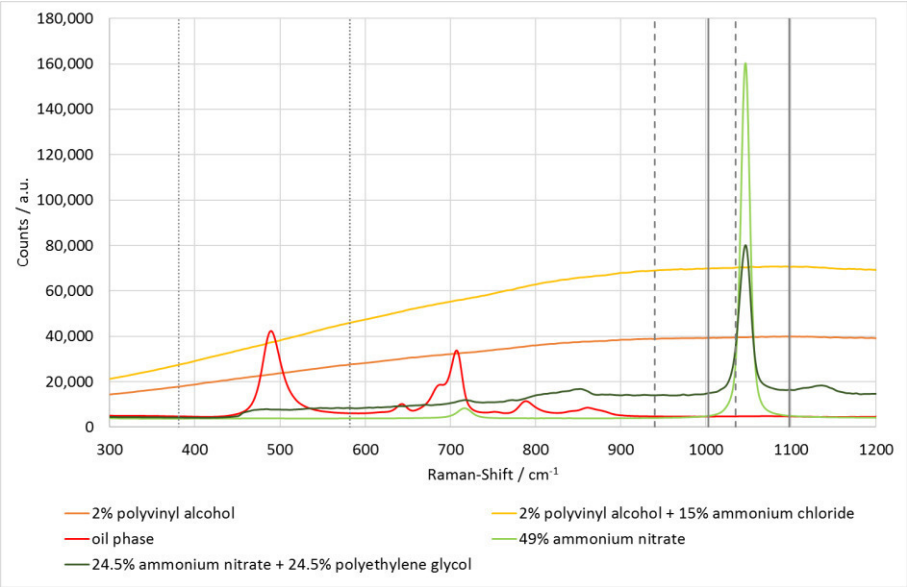

Figure 4-2 Section of the spectra of the individually measured phases of the double emulsions. In addition, the limits of the bandpass filters used are shown: dotted lines - oil phase; dashed lines - reference; solid lines - ammonium nitrate and inner water phase, respectively.

4.4.2 Osmolalities of the Aqueous Phases

The respective osmolalities were measured or extrapolated for all six aqueous phases of the double emulsions. For each phase, different solutions with a maximum of 7.5% solvate content were measured, from which corresponding correlations were determined. The respective osmolalities are listed in Table 4-1. The coefficients of determination of the different correlations are at least $R^2 = 0.9992$. Detailed data are publicly archived [90].

Table 4-1 Summary of the osmolalities of the individual aqueous emulsion phases. * These values are extrapolated. ** These values are measured.

Phase	Composition	Osmolality [mOsm/kg]
W_1	49% ammonium nitrate	10255*
	24.5% ammonium nitrate + 24.5% polyethyleneglycol	5788*
W_2	2% poly vinylalcohol 26—88	6**
	2% poly vinylalcohol 26—88 + 5% ammonium chloride	1877**
	2% poly vinylalcohol 26—88 + 10% ammonium chloride	3717*
	2% poly vinylalcohol 26—88 + 15% ammonium chloride	5581*

The osmolalities of the two inner water phases are significantly higher than those of all outer water phases. Only between the inner water phase with 24.5% ammonium nitrate and 24.5% polyethylene glycol and the outer water phase with 15% ammonium chloride is there a small difference.

4.4.3 Droplet Size Distribution of Inner Emulsions

Figure 4-3 shows the droplet size distributions of the analysed inner emulsions, which do not differ within standard deviation of a typical laser diffraction measurement [91]. This is also shown by the respective Sauter diameters, which are in the range of 2.87–2.96 µm. As a result, it can be assumed that the droplet size distributions of the two used inner emulsions are almost identical. Furthermore, differences in the droplet size of the inner water droplets can be excluded as a significant influencing factor on the measurements.

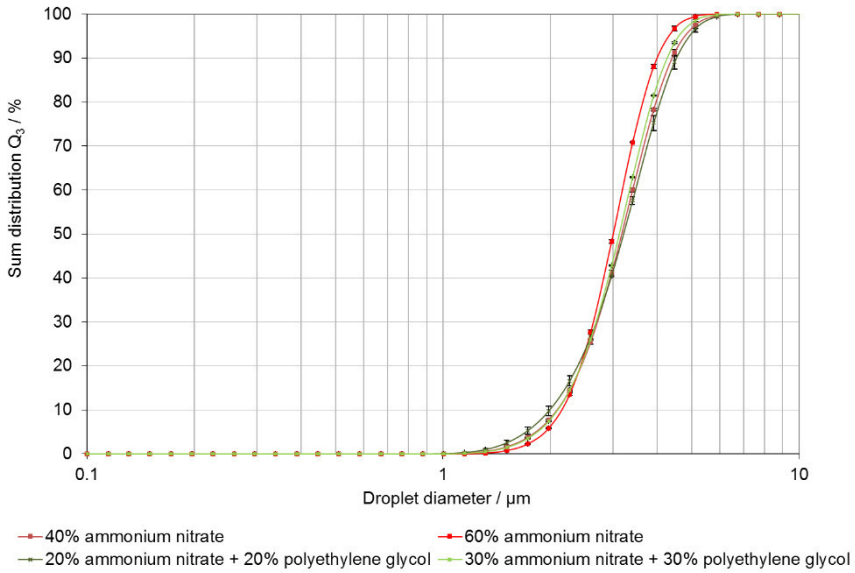

Figure 4-3 Sum distributions of the droplet sizes of all inner emulsions. Each emulsion was measured threefold.

4.4.4 Raman Spectra and Photometric Data of One Measurement

Figure 4-4 shows an example of the spectra from one measurement. The peak in the spectrum at 480 cm^{-1} is the oil peak, which is used to calculate filling degree changes. The changes in the internal water phase are tracked using the ammonium nitrate peak at 1047 cm^{-1}. The spectra follow the trend that the peak heights decrease with increasing experimental time. Likewise, the offset, which is largest for the first measurements, decreases continuously.

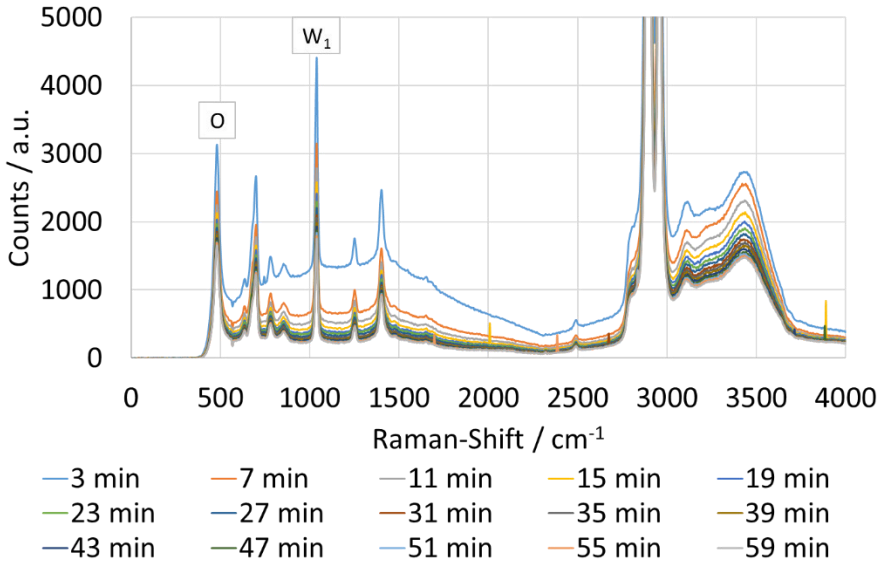

Figure 4-4 Progress of the spectra of one measurement series. The inner water phase contained 49% ammonium nitrate, the concentration of ammonium chloride in the outer phase was 10%.

Figure 4-5 shows the course of the photometric data during a measurement. In the beginning, the signal decreases strongly, which indicates a pronounced water diffusion. After 10 min, the signal decreases less strongly, which indicates a decreasing difference in osmolalities between both water phases. Therefore, water diffusion is less pronounced.

Since the absolute values of the oil phase are significantly higher than those of the photometric data, they are plotted on a second y-axis. All three curves show the same course. Possible fluctuations, such as after just under 10 min, can be seen in each curve and can therefore be neglected as measurement artifacts.

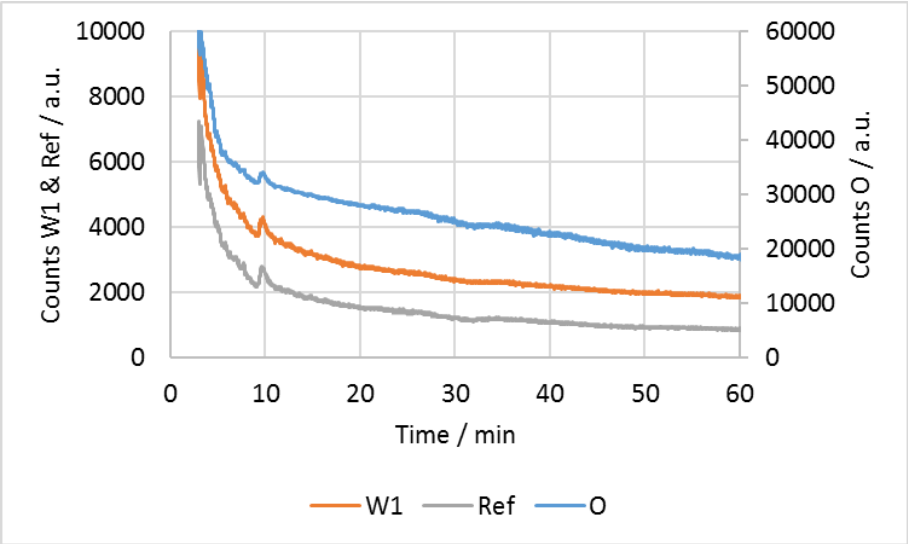

Figure 4-5 Courses of the three photometric channels during an exemplary measurement. The inner phase contained 49% ammonium nitrate, the outer phase 10% ammonium chloride. A second y-axis was implemented for the oil phase to make it easier to visually compare the data sets. W1: signal of ammonium nitrate in inner water phase, Ref: signal of the reference, O: signal of the oil phase.

4.4.5 Measured Relative Filling Degree Changes

The spectrometrically and photometrically measured relative filling degree change of a double emulsion droplet is shown in Figure 4-6. Both curves show a parallel progression, which initially rises sharply before changing to a slower growth. A clear maximum cannot be seen in either curve, which indicates an ongoing water diffusion.

Due to the significantly higher time resolution, the course of the photometric data is repeatedly subject to short-lived fluctuations, as can be seen, for example, after almost 10 min. These fluctuations are detected by all photometric channels and can therefore be neglected as measurement artifacts.

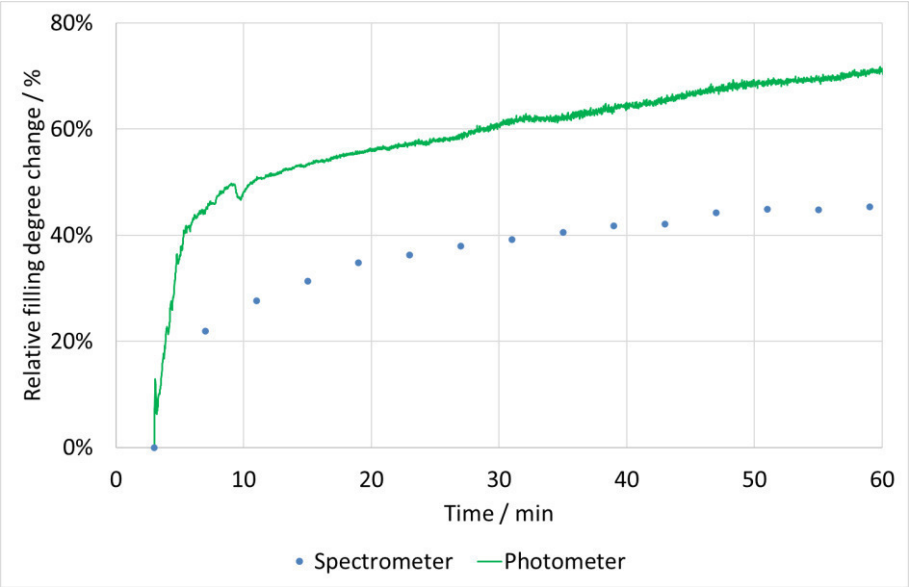

Figure 4-6 Results of the spectrometric and photometric measurements of the relative filling degree change of one droplet. The inner phase contained 49% ammonium nitrate, the outer phase, besides polyvinyl alcohol, 10% ammonium chloride.

4.4.6 Changes in Filling Degree of Double Emulsion

Figure 4-7 summarizes all experiments. With increasing ammonium chloride content in the outer water phase, the filling degree of the double emulsions increases less strongly. A linear trend can be seen in each measurement series. Only for 15% ammonium chloride in the outer water phase, the trend is not observed. No trend can be seen for the standard deviations. They vary between 3% and 26% with a mean of 10%.

There is a significant difference between the two inner water phases. In the presence of PEG, the relative filling degree changes are smaller. It is also noticeable that the filling degrees determined by the photometer are substantially higher than those determined by the spectrometer.

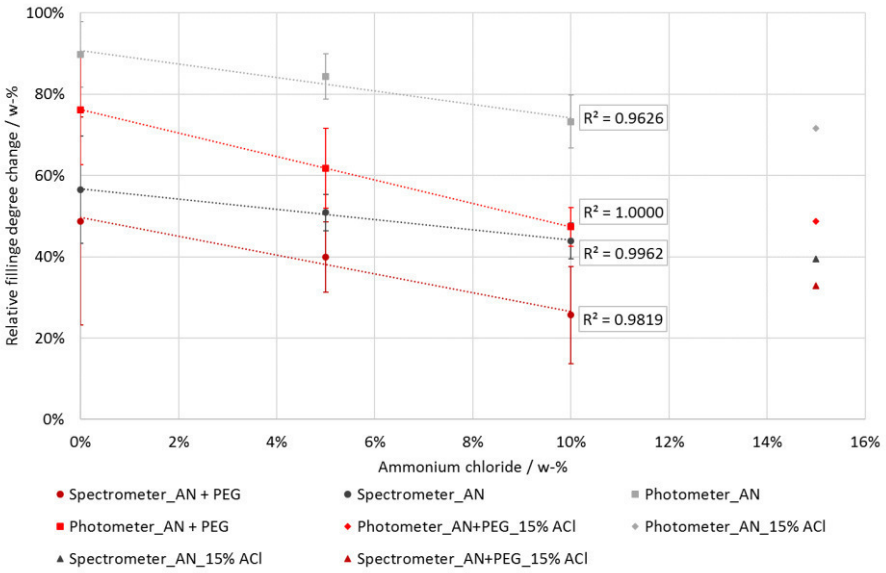

Figure 4-7 Summary of all performed experiments. The relative change in filling degree versus the ammonium chloride concentration of the outer water phase is plotted. For the concentration range 0% to 10%, linear trend lines are also present, all with a Pearson coefficient of at least R = 0.9626. At 15% ammonium chloride in the external water phase, the linear trends are interrupted, which is why they are plotted separately.

Furthermore, the relative filling degree changes in one double emulsion droplet can be compared to the respective osmolality difference between the inner and outer water phase. As seen in Table 4-2, with decreasing osmolality difference, the relative filling degree change is decreasing, too. Again, for 15% ammonium chloride, the trend is broken.

Table 4-2: Comparison of the osmolality difference and relative filling degree change for each investigated double emulsion. AN: ammonium nitrate. ACL: ammonium chloride. PEG: Polyethylene glycol.

W_1	W_2	Osmolality Difference $W_1 - W_2$ / mOsm/kg	Relative Filling Degree Change / %	
			Spectrometer	Photometer
49% AN	0% ACL	10249	56.5	89.8
	5% ACL	8378	50.9	84.3
	10% ACL	6538	43.8	73.3
	15% ACL	4674	39.5	71.7
24.5% AN + 24.5% PEG	0% ACL	5782	48.8	76.2
	5% ACL	3911	39.9	61.8
	10% ACL	2071	25.7	47.4
	15% ACL	207	32.9	48.7

4.5 Discussion

The measurement results in combination with the data evaluation in Figure 4-7 and Table 4-2 demonstrate the reliability of the Raman measurement method, both spectrometrically and photometrically. It is expected that the greater the difference in osmolalities, the greater the

relative change. For all four measurement series, this trend can be observed for ammonium chloride concentrations from 0% to 10%.

For 15% ammonium chloride in the outer water phase, the trend is broken because of interactions of polyvinyl alcohol and ammonium chloride. A more detailed explanation is given in section 4.5.1.

Therefore, the linear fit for each measurement series is based on three data points. However, since a linear fit with a Pearson coefficient of at least 0.96 is obtained four times, the linearity can be considered as valid.

4.5.1 Interactions of Ammonium Chloride and Polyvinyl Alcohol

The deviations of the relative filling degree changes at 15% ammonium chloride in the outer phase from the linear downward trend can be explained by an interaction between polyvinyl alcohol and ammonium chloride. In general, polyvinyl alcohol has a limited solubility for salts. Once the solubility limit is reached, polyvinyl alcohol coagulates, with the salt present above a specific threshold [92].

The solubility of ammonium chloride in a 2% PVOH solution was determined in advance of the experiments. At 15% ammonium chloride, a very weak and milky turbidity of the solution was observed, which represents the beginning of the coagulation. This is illustrated in Figure 4-8. At 17% ammonium chloride, a more pronounced turbidity can be seen, which indicates a progressive coagulation.

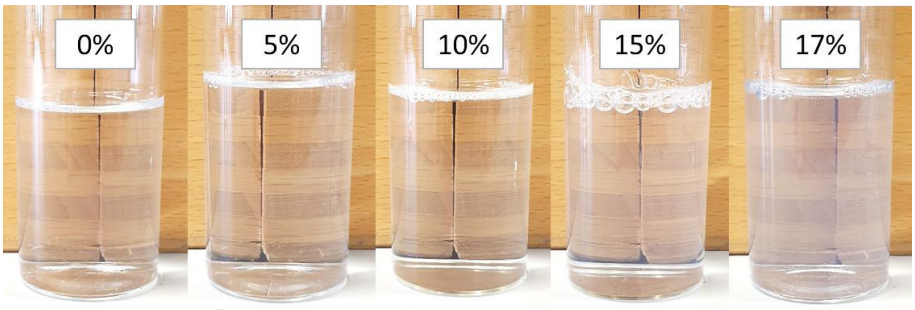

Figure 4-8 Comparison of the four outer water phases used plus another two percent polyvinyl alcohol solution with 17% ammonium chloride. No turbidity can be seen between 0% and 10%. At 15%, a very weak turbidity can be seen, which is more pronounced at 17%.

As a result of the coagulation, the measurements with 15% ammonium chloride in the outer water phase do not follow the downward trend as for 0%–10% ammonium chloride in the outer water phase. Since this is not a metrological but a chemical problem, the measurements with 15% ammonium chloride in the outer water phase are not considered in the evaluation.

4.5.2 Correlation Between Decreasing Signal and Increasing Filling Degree

With increasing filling degree, the oil signals decrease. This phenomenon can be explained by the two schemes in Figure 4-9, showing the focal volume of the Raman probe, which is located

inside the double emulsion droplets. Accordingly, the inner emulsion is in the focal volume. At the start of the experiment, small drops of water are present in the oil phase. When water diffuses from the outer water phase into these water droplets, these droplets become larger. As they swell, oil that was previously in the focus volume of the laser is displaced from it. Therefore, with increasing water diffusion, less oil is measured and its signal decreases accordingly.

The mass of solvate in the individual droplets remains constant during the measurement. However, while swelling, some inner water droplets will be displaced from the focal volume and the total solvate content in the focal volume decreases. This leads to a decrease in the ammonium nitrate signal.

The decreasing ammonium nitrate concentration leads to a decrease in the refractive index of the inner water phase. With increasing diffusion, an increasingly greater amount of laser emission is reflected at the phase boundary between the oil and the inner droplets, resulting in a decrease of the excitation and the Raman signal of the inner water phase. In order to exclude the refractive index influence on the filling degree change, only the signal of the oil phase is considered for the evaluation.

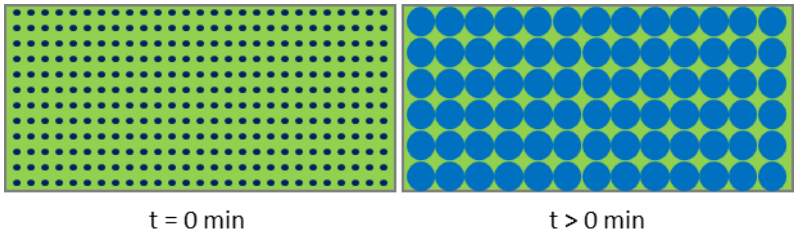

Figure 4-9 Schematic representation of the diffusion processes in the focal volume. At the start of the measurement, t = 0 min, smaller water droplets with a high solvate concentration (dark blue) are present. As the measurement time progresses, t > 0 min, water diffuses from the outer phase into the inner droplets. This causes the droplets to swell and the solvate concentration to decrease (light blue).

4.5.3 Difference Between Spectrometric and Photometric Filling Degree Changes

Figure 4-6 shows the relative filling degree changes measured spectrometrically and photometrically. The difference between both datasets is striking, as the photometric values are approximately 20% - 25% higher than the spectrometric ones.

This can be explained by the different integration times in combination with the evaluation based on equation 4-1. In general, spectrometers require longer integration times than photometers. Accordingly, the integration times are 1 s for the photometer and 2 min for the spectrometer. Thus, the photometer provides the first data point after one second, when hardly any relative filling degree changes had occurred. In contrast, the spectrometer measures a changing signal for two minutes and produces an averaged data point. During the measurement time, relative filling degree chances had already occurred, resulting in a different

first data point compared to the photometric one. Since all further data points are normalized to the respective first data point for evaluation, there will always be a difference between the two measurement methods. Because of the much higher time resolution, it can be assumed that the photometric signal is quantitatively more precise than the spectrometric signal. Nevertheless, with 2 min integration time, the spectrometric data provides accurate qualitative filling degree changes.

4.5.4 Decreasing Fluorescence During Measurement

The occasionally strong fluorescence in the first measurements followed by measurements with less intense fluorescence, as seen in Figure 4-4, is caused by the manual positioning of the droplet in the laser and the resulting detection of the outer water phase. Figure 4-10 shows three measurement conditions schematically. In case (a), the laser hits the double emulsion droplet perfectly in the centre, so that the influence of the external phase is negligible.
Due to the manual positioning of the double emulsion droplet in the laser, it is not always hit exactly in the centre. Case (b) shows schematically what happens at the beginning of the measurement. The laser hits the droplet in the upper area. This also excites the outer phase, which fluoresces, and causes fluorescence in the spectrum. In the further course of the experiment, case c, the droplet swells due to water diffusion, so that the outer phase is displaced from the laser. Accordingly, the fluorescence input by the outer phase decreases and the offset in the spectrum is smaller.

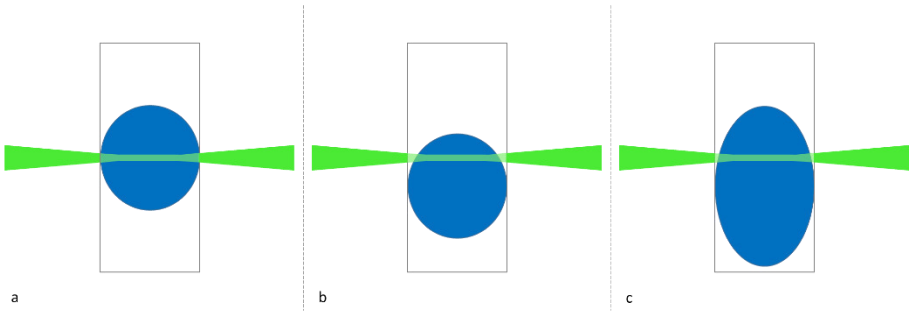

Figure 4-10 Effect of the positioning of the droplet in the laser. (a): The droplet is positioned centrally in the laser, thus the outer phase has no significant effect on the measurement. (b): The droplet is not positioned centrally in the laser. As a result, proportionally more outer phase is detected. (c): During the measurement, the droplet becomes larger, which means that less outer water phase is detected.

4.6 Conclusions

In conclusion, for both Raman measurement methods, spectrometrically and photometrically, it is possible to reliably monitor filling degree changes in $W_1/O/W_2$ double emulsion droplets caused by water diffusion. This can be undertaken during the development of new formulations of double emulsions and to analyze existing double emulsion formulations, thereby creating

more knowledge about diffusion in double emulsions and how it affects their stability. In doing so, both methods have their advantages and disadvantages.

Regarding the higher quantitative accuracy, the photometric method is preferred as it can track the filling degree changes more precisely due to its higher time resolution. However, the accuracy of the spectrometric method can be increased by reducing the integration time. Based on the size of the oil peak in Figure 4-4, it can also be expected that this can be significantly reduced. To obtain the shortest possible integration time for spectrometers, the signal to noise ratio needs to be considered for the oil peak. In general, a signal to noise ratio of 3 is sufficient for spectrometric measurements. Here, since the signal is decreasing, we would recommend a signal to noise ratio of 10.

An advantage of the spectrometer, on the other hand, is represented by Raman spectra, which, for example, also allow fluorescence influences to be detected. Possible improvements for fluorescence problems include, firstly, if possible, using non-fluorescent species in all double emulsion phase, which prevents the fluorescence input beforehand. Secondly, as long as the fluorescent species is only present in the outer water phase, initially larger double emulsion droplets or a smaller measurement capillary will reduce the impact of fluorescence.

Furthermore, the method of choice also depends on the experimental goal as well as the equipment and budget available, respectively.

4.7 Acknowledgments

We acknowledge support by the KIT-Publication Fund of the Karlsruhe Institute of Technology. Special thanks are given to Goran Vladisavljević for providing the Lego®-Device.

5 Discussion

This thesis shows the development of a new optical measurement method for the analysis of double emulsions by Raman spectroscopy. The main measurement objective is the filling degree of a double emulsion, which is determined spectrometrically as well as photometrically. In addition, the measurement of the outer droplet diameter using the new measurement method is also demonstrated. In Chapter 1, specific requirements were defined for the measurement method. It should reliably provide quantitatively comparable data, be integrable in-line into existing emulsification processes, must not interfere with the emulsion structure, and should offer several application options.
Before demonstrating the measurement method, a study is presented in chapter 2 which investigates the effect of different refractive index combinations on the signal strength oft he inner water phase. In chapter 3 and 4, studies are shown in which all requirements are met. In each, the method provides quantitatively comparable data, is integrated in-line into the microfluidic emulsification process and does not interfere with the emulsion structure. Furthermore, several applications of the method are also demonstrated. Chapter 3 shows the application in process control by monitoring the filling degree of double emulsions both spectrometrically and photometrically. In addition, it can be used to determine the droplet diameter based on the photometric data. Beyond that, chapter 4 shows an application of the method for stability studies of double emulsions. Additionally, to the aforementioned goals, the following two overall hypotheses were formulated at the beginning of this work, which serve as guidelines during the development of the measurement method:

GH1 *Raman spectroscopy can be used to determine structural parameters of double emulsions, such as their filling degree and the outer droplet size*

GH2 *Raman spectroscopy is suitable for studying the stability of double emulsions*

5.1 Experimental setup and procedure

To perform a successful measurement of the filling degree of double emulsions using the presented method, several aspects must be considered.

- The emulsion system
- The emulsification procedure
- The Raman setup
- The data evaluation

In general, for Raman spectroscopic measurements, having a non, or at least low, fluorescent system, is crucial. Therefore, a lot of work was done to design an emulsion system. The

challenge was to find an oil, which has a good Raman spectrum, which is not affected by fluorescence. Additionally, its refractive index must not be too high, otherwise it would not be possible to have higher refractive indices for both water phases. After testing several organic and synthetic oils, such as MCT oil or silicone oil, silicone oil was chosen for this work. Its Raman spectrum doesn't show any fluorescence, it has several distinguishable peaks and with 1.4027, its refractive index is lower than the ones of other oils.

For the inner water phase, a tracer must be found for the Raman measurements. Again, a good Raman spectrum without fluorescence, but with prominent Raman peaks is searched for. Furthermore, the solubility of the tracer must be high enough to increase the refractive index above the oil phase refractive index. A wide variety of substances, such as salts and sugars were tested, but most of them didn't fulfill the requirements. In the end, ammonium nitrate was chosen for the inner water phase. Its Raman spectrum is not affected by fluorescence and, among the tested substances, it shows the most prominent Raman peak at 1047 cm^{-1}. Furthermore, because of its high solubility in water, refractive indices higher than 1.4200 can be achieved.

Beyond the suitability for the Raman measurements, it is equally important to have a stable emulsion system, which is not affected by both tracers. Therefore, both interfaces, between the inner water phase and the oil phase as well as the oil phase and the outer water phase, need to be stabilized by emulsifiers. To stabilize the inner interface, Dowsil Resin XR 0497 was added to the oil phase. It is a well know emulsifier for oil-based emulsion and has no effect on the Raman spectrum. To find a suitable emulsifier for the outer water phase was challenging. Again, it has to fulfill all requirements regarding the Raman measurements but must also stabilize the oil droplet reliably as well as must be combinable with glycerol. Well known emulsifiers, such as various Lutensols or Tweens, don't fulfill all requirements. In the end, polyvinyl alcohols (PVAs) show the most promising results. But, depending on the degree of hydrolyzation and the chain lengths, some PVAs don't stabilize the double emulsion reliably or are highly fluorescent. Ultimately, among the tested PVAs, only the Kuraray Poval 26–80 polyvinyl alcohol as well as the Kuraray Poval 26–88 polyvinyl alcohol fulfil all requirements.

For both studies in chapters 2 and 4, additional substances were necessary to reach the experimental goals. In chapter 2, the refractive index of the outer water phase should be increased stepwise to a maximum of more than 1.4200, which is the refractive index of the oil phase. To do that, glycerol was added to the outer water phase. It is low fluorescent and has only minor peaks in the Raman spectrum. Furthermore, a solution of 2 % Kuraray Poval 26–80 polyvinyl alcohol and 70 % glycerol can be produced, which has a refractive index of 1.4317.

The third study in chapter 4 investigates filling degree changes caused by osmotic swelling. Therefore, different substances are necessary to modify the osmotic pressure of both water phases. Again, each substance must be combinable with the existing water phases, fulfil all

requirements regarding the Raman measurement and must not affect the emulsion stability. For the inner water phase, polyethylene glycol was added to change the osmotic pressure. Ammonium chloride was added to the outer water phase to modify its osmotic pressure.

To develop and evaluate a new measurement technique, it is necessary to have equal samples and to know the measurement result in advance. For double emulsions, this is not achievable using conventional emulsification system, such as rotor stator machines, because of the polydisperse droplet size distribution. Therefore, a microfluidic emulsification process offers the best possibilities to prepare the double emulsion. For the microfluidic production of double emulsions, glass capillary devices are the most promising tool. But it comes with a critical limitation for this work, since it is not possible to change the number of inner droplets, respectively the number of inner interfaces and, in the end, the filling degree, over a wide range. However, this is necessary for the planned experiments, and ultimately, for the development of the measurement method. To work around this limitation, the method of choice is a two-step emulsification process. First, the inner emulsion is prepared using a rotor-stator machine. This way, the filling degree can be set over a wide range. Examples of different inner emulsions can be seen in Figure 2-3. Second, the inner emulsion is fed into a glass capillary device to produce a double emulsion with monodisperse oil droplets. Exemplarily, one double emulsion droplet is shown in Figure 2-4. Regarding the Raman measurements, another limitation of glass capillary devices are the round borosilicate capillaries, which are used to make the device. Borosilicate glass shows fluorescence, which can superimpose smaller Raman peaks. Beyond that, for round capillaries, if the excitation laser beam does not hit the capillary precisely perpendicularly, parts of the laser's energy is deflected by the curvature of the capillary. To solve both issues, a squared quartz capillary was mounted at the end of the glass capillary. To connect both capillaries, a self-designed and internally 3D-printed adapter was used. A scheme of the setup is shown in Figure 2-5.

For the Raman measurement, the idea was to measure each droplet individually. To achieve that, measurement times of a few microseconds must be possible. However, standard Raman spectrometer are unable to perform a measurement within a few microseconds. Usually, minimum integration times start around 300 ms. Therefore, for single droplet measurements, a photometric solution is necessary. Again, this comes with limitations, since photometers are not wavelength specific, which means, it is not possible to measure different Raman peaks at the same time using only one photometer. Furthermore, a spectrometric measurement is nevertheless necessary to prove the correctness of the photometric measurements. As photometers, custom photon multipliers were chosen, which can work with integration times down to 1 ms and shorter. To be able to get wavelength specific results, bandpass filters are placed in front of the custom photon multipliers. Another challenge was to be able to measure all necessary Raman information – one signal of the oil phase, one of the inner water phase

and a reference – at the same time. To achieve that, the measured signal was splitted into four equal parts using three 50:50 beam splitter in combination with three custom photon multipliers. The fourth splitted signal was used to overcome the second limitation, to prove the correctness of the measurements. Here, the signal was refocused into a glass fiber and led to a Raman spectrometer. A scheme of the Raman setup is pictured in Figure 3-1.
After each experiment, the recorded data of all measurements must be evaluated. To evaluate the spectrometric data, all relevant Raman peaks were baseline corrected as well as its area calculated using a specifically design Microsoft Excel template. Subsequently, now having quantified data of all relevant Raman peaks, further calculations could be performed. For the photometric data, because of the huge number of individual data points, the evaluation could not be done using a Microsoft Excel template. Thus, a MatLab software was written, which calculated the area of all relevant Raman peaks as well as the measurement time of each individual droplets. A detailed description of the software is given in section 3.3.2.

5.2 Raman spectroscopy can be used to determine structural parameters of double emulsions, such as their filling degree and the outer droplet size

The overall hypothesis GH1 is used to investigate whether it is possible to measure specific structural parameters by Raman spectroscopy. The potentially biggest problem here is the multiple refraction of the laser at the numerous phase interfaces within one double emulsion droplet. Therefore, Chapter 2 first examines the extent to which multiple refractions affect the measurement. For this purpose, the two hypotheses H2.1 and H.2.2 are tested. The objective is to determine the changes in the strength of the Raman signal when the refractive indices of the two water phases are varied. Hypothesis H2.1 states that the Raman signal strength increases as the difference between the refractive indices of the inner water phase and the oil phase decreases. Hypothesis H2.2 states the same for the refractive index difference between the oil phase and the outer water phase. Similarly, the Raman signal strength of the inner water phase should increase with decreasing refractive index difference. The refractive indices of the inner water phase are in the range of 1.3569 to 1.4200, those of the outer water phase between 1.3385 and 1.4317. The refractive index of the oil phase remains unchanged at 1.4027 in all experiments. Table 2-1 lists all the emulsion phases used with the corresponding refractive indices.
If the refractive index of the inner water phase is increased, and thus the refractive index difference between the inner water phase and the oil phase decreases, the Raman signal strength of the inner water phase increases. The maximum Raman signal is measured when the refractive indices of the inner water phase and the oil phase are identical. If the refractive

index of the water phase is further increased above this optimum point, the refractive index difference also increases, reducing the Raman signal of the inner water phase. The results of these experiments can be seen in Figure 2-6A. Thus, hypothesis H2.1 is confirmed.

Hypothesis H2.2 is used to investigate whether the same behavior applies to the refractive index difference between the oil phase and the outer water phase. To vary the refractive index difference between the two phases, glycerol is added to the outer water phase. In this case, the Raman signal also increases with decreasing refractive index difference until there is no refractive index difference between the two phases. If the refractive index of the outer water phase is further increased beyond this, the Raman signal also becomes stronger. This contradicts hypothesis 2.2, which is why it cannot be confirmed. The corresponding measurement results are shown in Figure 2-6B.

An explanation for the unconfirmed hypothesis is given by the number of interfaces between the respective phases involved. Since a large number of inner water droplets are present in a double emulsion droplet, the light is very frequently refracted at the interfaces between the inner water phase and the surrounding oil phase. Adjustments to the refractive index of the inner water phase thus have an immense effect on the Raman signal. Since there is only one phase interface between the oil phase and the outer water phase, the refractive index of the outer water phase does not have a major influence. Here, the Raman signal depends to a large extent on the concentration of glycerol.

Although only one of the two hypotheses can be confirmed, it is proven on the basis of the measurement results shown in Figure 2-6 and the investigation of the residuals shown in Figure 2-7 that Raman spectroscopy is a suitable analysis method for double emulsions.

In chapter 3, the actual testing of the overall hypothesis GH1 is shown by means of the hypotheses H3.1 and H3.2. H3.1 postulates that the filling degrees of double emulsions, whose phases all have the same refractive index, can be precisely measured quantitatively. To test hypothesis H3.1, nine double emulsions whose emulsion phases all have the same refractive indices are analyzed. The double emulsions differ only in their filling degree, which ranges from 0 w-% to 40 w-%. Both spectrometrically and photometrically, the filling degrees can be measured with highest precision. Figure 3-5 and Figure 3-6 show the results of the measurement series. For both methods, there is a linear dependence between the set and the experimentally measured filling degrees. The corresponding Pearson coefficients of the linear trend lines are $R^2 = 0.9992$ for the spectrometric measurements and $R^2 = 0.9900$ for the photometric measurements. Accordingly, Hypothesis H3.1 is confirmed.

In addition, since the flow velocity of the double emulsion droplets is known, the oil droplet size can be determined via a temporally highly resolved measurement signal. This is tested on the basis of hypothesis H3.2. The photometric measurement signal has a resolution of 2ms, allowing a 1mm diameter droplet to be detected over fifty times as it passes through the laser.

As a result, the boundaries of each droplet can be clearly seen in the measurement signal, see Figure 3-9, and the associated droplet diameters can be calculated. Thus, hypothesis H3.2 is also confirmed.
The validity of the two hypotheses H3.1 and H3.2 also confirms the validity of the overall hypothesis GH1.
Supplement to the droplet size measurement, it is not possible to measure the inner droplet size, too. Within the oil droplet, the inner water droplets are densely packed in every spatial direction and approximately fifty times smaller than the diameter of the laser focus. Therefore, it is not possible to measure one single water droplet. It is the same situation as for dynamic or static light scattering measurements, see chapter **Fehler! Verweisquelle konnte nicht g efunden werden.**, whereby droplets must be diluted to be measured and the inner droplet size can only be measured prior to the second emulsification step. Furthermore, the oil droplet size is more important than the inner water droplet size, since more relevant emulsion properties, such as the viscosity or the sedimentation stability, change with changing oil droplet sizes.

5.3 Raman spectroscopy is suitable for studying the stability of double emulsions

The overall hypothesis GH2 is used to test whether the new measurement method can be used for stability studies on double emulsions. This was investigated in chapter 4 on the basis of hypotheses H4.1 and H4.2. Hypothesis H4.1 describes the dependency of the change in the filling degree of a double emulsion on the osmolality of its inner, aqueous double emulsion phase. To test this, the filling degree change of eight different double emulsions is measured continuously for 50 min each, combining two inner water phases with four different outer water phases. The osmolalities of the inner phase are 5788 mOsm/kg as well as 10255 mOsm/kg. The outer water phases have osmolalities between 6 mOsm/kg and 5581 mOsm/kg. Figure 4-7 and Table 4-2 show that the higher the osmolality of the inner water phase, the stronger the filling degree increases. Thus, hypothesis H4.1 is confirmed.
The second hypothesis H4.2 deals with the filling degree change as a function of the osmolality of the external water phase and states that the filling degree change increases with increasing osmolality of the outer water phase. This was investigated with the same eight different double emulsions used to test hypothesis H4.1. Figure 4-7 as well as Table 4-2, however, show a weaker filling degree change with increasing osmolality of the outer water phase, which makes hypothesis H4.2 invalid.
An explanation for this are the high osmolalities of the inner water phase. These are similar to or significantly higher than those of the outer water phase. As the osmolality of the outer water

phase increases, the difference between the two osmolalities decreases, and consequently there is a weaker driving force to change the degree of filling.
Regardless of the invalidity of hypothesis H4.2, the confirmed hypothesis H4.1 proves that the stability of double emulsions can be studied by Raman spectroscopy. Thus, the overall hypothesis GH2 is confirmed.

5.4 Comparison of the spectroscopic and photometric measurement methods

The studies presented in Chapters 3 and 4 allow to compare and evaluate the spectrometric as well as photometric measurement method. The main difference between the two methods is their temporal resolution. Photometric measurements were demonstrated with an integration time of 2 ms. Spectrometrically, the minimum integration time was 2 min. Thus, photometrically, each double emulsion droplet can be measured individually, while spectrometrically, many double emulsions are summarized in one measurement. However, it should be noted that shorter integration times are possible for measurements of single, stationary droplets, as shown in chapter 4.
Quantitatively, highly accurate measurements of the filling degrees are possible with both measurement methods. The slight difference between the Pearson coefficients in chapter 3.4 is caused by the different evaluation methods. For the evaluation of the spectrometric data, the software of the spectrometer manufacturer was used, while for the evaluation of the photometric data, a in-house developed software was used. For both methods, the evaluated Raman signal is the same.
With the additional information of the flow rate of the double emulsion droplets, it is possible to determine their diameter using the photometric data. This is not feasible based on the spectrometric data.
A final significant difference between the two measurement methods lies in the cost of the measurement equipment used. For the spectrometric measurements, a Raman spectrometer is essentially required. The Raman spectrometer "RNX1-532" from Kaiser Optical Systems used here is priced in the upper five-digit range. For each of the three photometric measurement channels, a CPM with associated bandpass filter, a laser and the beam splitters must be purchased. The costs for all of these were less than 20.000€ in this work. Components that are necessary for both methods, such as the measuring probe or components of the emulsification technology, are not included in this calculation.
Consequently, which method is finally selected depends on the one hand on the objective of the experiment – should the droplet diameters be determined? Is a high temporal resolution necessary? – and on the other hand on the available budget.

6 Outlook

This thesis shows the development of a new method for measuring the filling degree of double emulsions by Raman spectroscopy. To be able to use the method for as many applications as possible, further aspects should be investigated.

In chapter 2 it was shown that the difference of the refractive indices of the inner water phase and the oil phase has a decisive influence on the signal strength of the inner water phase. It is important to know the maximum difference between the two phases to obtain a valid measurement signal of the inner phase. This provides further knowledge about the extent to which it is permissible to intervene in the substance system of a double emulsion to make it accessible for the measurement method.

The measurements presented here were carried out in a microchannel on double emulsion droplets flowing isolated to the greatest possible extent. A transfer of many single droplets to droplet collectives, e.g. in a beaker, has not yet been investigated. A successful transfer would significantly extend the application range of the measurement method. However, a significant influence of the refractive index difference between the oil phase and the outer water phase is to be expected, so that a systematic investigation of the role of the refractive indices is also necessary for these phases.

Since this thesis focused on mostly fluorescence-free double emulsions, it is also necessary to investigate the use of fluorescent components. This is especially important with regard to double emulsions in the food industry, in which many fluorescent substances are used. There are several ways to study fluorescent samples using Raman spectroscopy. A common approach is to use a longer laser wavelength [30]. In addition, there is the Raman method "SERDS", which was specifically developed to handle fluorescent samples and is based on the use of two nearly equal excitation wavelengths [93].

7 Summary

Due to their complex, nested structure, double emulsions offer interesting opportunities for various applications. The main focus is on the encapsulation of value-adding, sensitive substances, which are dissolved in the inner phase and protected from environmental influences by the middle phase. Important areas of application for this are the food industry, the pharmaceutical industry and the cosmetics industry.
However, the complex structure of double emulsions also results in disadvantages. Due to the different interfaces, double emulsions tend to undergo several instabilities, which can cause double emulsions to separate into their individual phases. To better understand these instabilities and develop stable double emulsion formulations, they are the subject of numerous research efforts.
Some measurement techniques are already available for the analysis of double emulsions, which can measure the important structural parameters, such as the droplet sizes or the filling degree. However, these are often limited to off-line measurements and depend on compliance with specific boundary conditions. Therefore, there is a constant interest in new measurement techniques that can be used to analyze double emulsions during processing, transport, storage and application.
Raman spectroscopy offers a potential alternative. This optical measurement method is usually well suited for in-line or on-line measurements, is suitable for multicomponent systems due to its high selectivity and can investigate them both qualitatively and quantitatively.
This thesis deals with the development of a Raman spectroscopy-based measurement method which can measure the filling degree of double emulsions in-line. The development of such a measuring method places high demands on the double emulsion system and the measuring equipment used. The solutions developed for this thesis are described in detail in chapter 5.1.
The application of an optical measurement technique in a multiphase system, which has numerous phase interfaces, poses the challenge of minimizing the influence of light refraction at the phase interfaces. If the refraction is too strong, this could have a negative effect on the measurement result. Therefore, Chapter 2 systematically investigates the effect of different combinations of refractive indices of the three emulsion phases on the Raman signal strength of the inner water phase. The refractive index of the oil phase is 1.4027 and was not varied because of the limitation in oil soluble substances. Therefore, this refractive index serves as a reference for both water phases. During the measurements, the refractive indices of the inner water phase are varied between 1.3569 and 1.4200, the refractive indices of the outer water phase range between 1.3385 and 1.4317. Ammonium nitrate is dissolved in the inner water phase to be used as a tracer for the Raman measurement and for adjusting the refractive

index. For the same purpose, glycerol is added to the outer water phase. To ensure that the signal strength of the inner water phase is influenced only by the refractive indices, the concentration of ammonium nitrate and the filling degree are adjusted so that the same mass of ammonium nitrate is present in the inner water phase for all measurements.

The performed experiments have shown that, in addition to the differences in the refractive indices present, the number of phase interfaces at which the exciting laser is refracted has a decisive role.

Due to the very high number of inner water droplets, there are numerous phase interfaces between the inner water phase and the oil phase. If the refractive index of the inner water phase is gradually increased until it is equal to the refractive index of the oil phase, the Raman signal of the inner water phase also increases. If both refractive indices are equal, the maximum Raman signal is present. If the refractive index of the inner water phase is increased beyond this, the Raman signal decreases due to the occurring light refraction.

Since individual double emulsion droplets are analyzed in all experiments, only one phase interface is present between the outer water phase and the oil phase. Initially, the Raman signal shows the same behavior when the refractive index of the outer water phase is increased. If the refractive index is increased gradually up to that of the oil phase, the Raman signal strength of the inner water phase also increases. However, if the refractive index of the outer water phase is increased beyond that of the oil phase, the Raman signal of the inner water phase continues to increase constantly.

This proves that the refractive indices of the two water phases have an increasingly crucial role as the number of phase interfaces increases.

Chapter 3 shows the actual development of the measurement method for determining the filling degree of double emulsions. The measuring setup used is capable of measuring the filling degree both spectrometrically and photometrically. Spectrometrically, several hundred double emulsion droplets are analyzed during one measurement. Photometrically, each drop is measured individually. A total of nine double emulsions with filling degrees between 0% and 40% are analyzed, whereby their composition is not changed apart from the filling degree.

Both methods show a highly quantitative accuracy. For evaluation, the set filling degrees are compared with the measured filling degrees. For both methods, the measurement result increases linearly with the filling degree. The two Pearson coefficients of the associated linear trend lines are $R^2 = 0.9992$ (spectrometric) and $R^2 = 0.9900$ (photometric).

In addition, the oil droplet diameter of each double emulsion droplet can be measured from the photometric data. The required flow velocity of the droplets can be calculated from the known experimental conditions. Likewise, due to the short integration time of 2 ms, the exact measurement duration of all droplets is known. From the entirety of all calculated oil droplet diameters, their droplet size distribution can also be calculated.

A possible application of the method is shown in chapter 4. Here, the method is used to monitor filling degree changes within one double emulsion droplet due to water diffusion between the inner and outer water phases.
For this purpose, eight different double emulsions are studied, each emulsion having different aqueous phases. The composition of the aqueous phases is varied to obtain different osmolalities. Thereby, smaller osmolalities are always present in the outer water phase compared to the inner water phase.
During the measurement, a single double emulsion drop is monitored both photometrically and spectrometrically for 50 minutes. Due to the osmolalities present in both water phases, diffusion occurs from the outer water phase to the inner water phase. The filling degree of the double emulsion increases.
Again, both methods are able to reliably measure changes in the degree of filling quantitatively, although the photometric result is to be preferred due to the significantly shorter integration time.
The present work shows the successful development of a method to measure the filling degree of double emulsions by Raman spectroscopy.
Analyses of double emulsions by Raman spectroscopy have so far only been published for specific individual cases. Therefore, this work first investigates how the different refractive indices of a double emulsion affect the measurement result. Next, the actual methodology for filling degree measurement is demonstrated, before concluding with a study of diffusion monitoring within a double emulsion based on its filling degree.
Future research should address the question of the extent to which the present refractive indices of the emulsion phases involved can differ to be still analyzable with the presented method. A distinction should be made whether the emulsion droplets flow individually through a microchannel or are present in bulk in a beaker. In addition, the method should be made more robust against fluorescence in order to offer more potential applications for the food industry.

8 Zusammenfassung

Aufgrund ihrer komplexen, verschachtelten Struktur bieten Doppelemulsionen interessante Möglichkeiten für verschiedene Anwendungsfälle. Das Hauptaugenmerk liegt dabei auf der Verkapselung wertgebender, empfindlicher Substanzen, die in der inneren Phase gelöst sind und durch die mittlere Phase von Umgebungseinflüssen geschützt sind. Wichtige Anwendungsgebiete dafür sind die Lebensmittelindustrie, die pharmazeutische Industrie sowie die Kosmetikindustrie.

Die komplexe Struktur von Doppelemulsionen bringt allerdings auch Nachteile mit sich. Durch die verschiedenen Grenzflächen neigen Doppelemulsionen zu verschiedenen Instabilitäten, wodurch Doppelemulsionen in ihre einzelnen Phasen aufgetrennt werden können. Um diese Instabilitäten besser zu verstehen und stabile Doppelemulsionsfomulierungen zu entwickeln, sind diese Gegenstand zahlreicher Forschungsarbeiten.

Zur Analyse von Doppelemulsionen stehen bereits einige Messtechniken zu Verfügung, die die wichtigen Strukturparameter, wie die Tropfengrößen oder den Füllgrad, messen können. Allerdings sind diese häufig auf offline-Messungen beschränkt und sind auf die Einhaltung spezifischer Randbedingungen angewiesen. Daher besteht ein konstantes Interesse an neuen Messtechniken, mit denen Doppelemulsionen analysiert werden können.

Eine mögliche Alternative bietet die Raman-Spektroskopie. Diese optische Messmethode eignet sich üblicherweise gut für in-line oder on-line Messungen, ist aufgrund ihrer hohen Selektivität für Mehrkomponentensysteme geeignet und kann diese sowohl qualitativ als auch quantitativ untersuchen.

Daraus resultierend beschäftigt sich diese Arbeit mit der Entwicklung einer auf Raman-Spektroskopie basierender Messmethode, welche in-line den Füllgrad von Doppelemulsionen messen kann.

Die Entwicklung einer solchen Messmethode stellt hohe Anfoderungen an das verwendete Stoffsystem der Doppelemulsion sowie an die genutzte Messtechnik. Die Lösungen, welche für die jeweiligen Anforderungen gefunden wurden, werden in Kapitel 5.1 detailliert vorgestellt.

Die Anwendung einer optischen Messtechnik in einem Mehrphasensystem, welches über zahlreiche Phasengrenzflächen verfügt, bringt die Herausforderung mit sich, den Einfluss von Lichtbrechung an den Phasengrenzflächen zu minimieren. Ist dieser zu groß, könnte sich dies negativ auf das Messergebnis auswirken. Daher wird in Kapitel 2 systematisch untersucht, wie verschiedene Kombinationen von Brechungsindizes der drei Emulsionsphasen die Ramansignalstärke der inneren Wasserphase beeinflussen. Der Brechungsindex der Ölphase beträgt 1.4027 und wird auufgrund fehlender öllöslicher Substanzen nicht variiert. Damit bildet dieser Brechungsindex die Referenz für beide Wasserphasen. Während der Messungen

werden die Brechungsindizes der inneren Wasserphase zwischen 1.3569 und 1.4200 variiert, die Brechungsindizes der äußeren Wasserphase betragen zwischen 1.3385 und 1.4317. In der inneren Wasserphase liegt Ammoniumnitrat gelöst vor, welches als Tracer für die Ramanmessung sowie zum Einstellen der Brechungsindizes genutzt wird. Zum selben Zweck wird der äußeren Wasserphase Glycerin zugegeben. Damit die Signalstärke der inneren Wasserphase tatsächlich nur von den Brechungsindizes beeinflusst wird, werden die Konzentration von Ammoniumnitrat und der Füllgrad so eingestellt, dass bei allen Messungen die gleiche Masse an Ammoniumnitrat in der inneren Wasserphase vorliegt.
Die durchgeführten Versuche haben gezeigt, dass neben den Unterschieden der vorliegenden Brechungsindizes die Anzahl der Phasengrenzflächen, an denen der anregende Laser gebrochen wird, eine entscheidende Rolle innehat.
Zwischen der inneren Wasserphase und der Ölphase gibt es aufgrund der sehr hohen Anzahl an inneren Wassertropfen viele Phasengrenzflächen. Wird der Brechungsindex der inneren Wasserphase schrittweise erhöht, bis er gleich dem der Ölphase ist, nimmt das Ramansignal der inneren Wasserphase ebenfalls zu. Sind beide Brechungsindizes gleich, liegt das maximale Ramansignal vor. Wird der Brechungsindex der inneren Wasserphase darüber hinaus erhöht, sinkt das Ramansignal aufgrund der auftretenden Lichtbrechung ab.
Da bei allen Versuchen einzelne Doppelemulsionstropfen analysiert werden, liegt zwischen der äußeren Wasserphase und der Ölphase nur eine Phasengrenzfläche vor. Zunächst zeigt das Ramansignal bei Steigerung des Brechungsindex der äußeren Wasserphase das gleiche Verhalten. Wird der Brechungsindex schrittweise bis zu dem der Ölphase erhöht, erhöht sich ebenfalls die Ramansignalstärke der inneren Wasserphase. Wird der Brechungsindex der äußeren Wasserphase allerdings über den der Ölphase hinaus erhöht, nimmt das Ramansignal der inneren Wasserphase weiterhin stetig zu.
Dies beweist, dass die Brechungsindizes der beiden Wasserphasen mit zunehmender Anzahl an Phasengrenzflächen eine immer entscheidendere Rolle spielen.
Kapitel 3 zeigt die eigentliche Entwicklung der Messmethode zur Bestimmung des Füllgrades von Doppelemulsionen. Der genutzte Messstand ist dabei in der Lage den Füllgrad sowohl spektrometrisch als auch photometrisch zu messen. Spektrometrisch werden mehrere hundert Doppelemulsionstropfen während einer Messung analysiert. Photometrisch wird jeder Tropfen individuell gemessen. Insgesamt werden neun Doppelemulsionen mit Füllgraden zwischen 0% und 40% untersucht, wobei deren Zusammensetzung abgesehen vom Füllgrad nicht verändert wird.
Beide Methoden zeigen eine sehr hohe quantitative Güte. Zur Auswertung werden die eingewogenen Füllgraden mit den gemessenen Füllgraden verglichen. Bei beiden Methoden nimmt das Messergebnis mit dem Füllgrad linear zu. Die beiden Pearson-Koeffizienten der

zugehörigen linearen Trendlinien liegen bei R^2=0,9992 (spektrometrisch) sowie R^2=0,9900 (photometrisch).

Zudem kann aus den photometrischen Daten der Öltropfendurchmesser eines jeden Doppelemulsionstropfens gemessen werden. Die dafür nötige Fließgeschwindigkeit der Tropfen kann aus den bekannten Versuchsbedingungen berechnet werden. Ebenso ist aufgrund der kurzen Integrationszeit von 2ms die genaue Messdauer von allen Tropfen bekannt. Aus der Gesamtheit aller berechneten Öltropfendurchmesser lässt sich zusätzlich deren Tropfengrößenverteilung berechnen.

Eine mögliche Anwendung der Methode wird in Kapitel 4 gezeigt. Hier wird die Methode verwendet, um Füllgradänderungen innerhalb eines Doppelemulsionstropfens aufgrund von Wasserdiffusion zwischen der inneren und äußeren Wasserphase zu überwachen.

Dafür werden acht verschiedene Doppelemulsionen untersucht, wobei jede Emulsion über unterschiedliche wässrige Phasen verfügt. Die Zusammensetzung der wässrigen Phasen dahingehend variiert, um verschiedene Osmolalitäten zu erhalten. Dabei liegen in der äußeren Wasserphase stets kleinere Osmolalitäten als in der inneren Wasserphase vor.

Während der Messung wird ein einzelner Doppelemulsionstropfen für 50 Minuten sowohl photometrisch als auch spektrometrisch überwacht. Dabei kommt es aufgrund der vorliegenden Osmolalitäten in beiden Wasserphasen zur Diffusion von der äußeren Wasserphase in die innere Wasserphase. Der Füllgrad der Doppelemulsion nimmt zu.

Wieder sind beide Methoden in der Lage Füllgradänderungen quantitativ verlässlich zu messen, wobei das photometrische Ergebnis aufgrund der deutlich kürzeren Integrationszeit zu bevorzugen ist.

Die vorliegende Arbeit zeigt die erfolgreiche Entwicklung einer Messmethode, um mittels Raman-Spektroskopie den Füllgrad von Doppelemulsionen zu messen.

Analysen von Doppelemulsionen mittels Raman-Spektroskopie sind bis dahin nur für spezifische Einzelfälle veröffentlicht worden. Daher wird in dieser Arbeit zunächst untersucht, wie sich die unterschiedlichen Brechungsindizes einer Doppelemulsion auf das Messergebnis auswirken. Anschließend wird die eigentliche Methodik zur Füllgradmessung demonstriert, ehe abschließend eine Studie zur Diffusionsüberwachung innerhalb einer Doppelemulsion auf Basis von deren Füllgrad folgt.

Zukünftige Forschungsarbeiten sollten sich mit der Frage beschäftigen, inwieweit die vorliegenden Brechungsindizes der beteiligten Emulsionsphasen differieren dürfen, um mit der vorgestellten Methode noch analysiert werden zu können. Dabei ist zu unterscheiden, ob die Emulsionstropfen einzeln durch einen Mikrokanal strömen oder in bulk in einem Becherglas vorliegen. Außerdem sollte die Methode robuster gegen Fluoreszenz werden, um mehr Anwendungsmöglichkeiten für die Lebensmittelindustrie zu bieten.

9 Appendix

9.1 Appendix to chapter 3

Table A1. Details regarding the optical filters. * Edge wavelength. ** Laser 2000, Wessling, Germany. *** AHF analysentechnik AG, Tübingen, Germany.

Filter	Center Wavelength	FWHM	Supplier
Ammonium nitrate	564 nm	2	Laser 2000 **
Silicone oil	546 nm	12.9 nm	AHF ***
Reference	561 nm	2	Laser 2000
Long pass filter	542 nm *	-	AHF

Table A2. Weights of the inner water phase and oil phase as well as the resulting filling levels.

Filling Degree	0%	0.5%	1%	2%	5%	10%	20%	30%	40%
Mass W_1/g	0	1.00	2.00	4.00	10.01	20.02	40.03	60.12	111.53
Mass O/g		79.10	78.00	76.00	70.00	60.01	40.00	19.99	167.29
Filling degree/w-%	0	0.50	1.00	2.00	5.00	10.00	20.01	30.02	40.00

9.2 Appendix to chapter 4

Table B1: Details regarding the optical filters. *** Full width half maximum. ** Edge wavelength. *** AHF analysentechnik AG, Tübingen, Germany. **** Laser 2000, Wessling, Germany.

Filter	Center Wavelength	FWHM*	Supplier
Long pass filter	542 nm **	-	AHF ***
Silicone oil	546 nm	12.9 nm	AHF ***
Reference	561 nm	2	Laser 2000 ****
Ammonium nitrate	564 nm	2	Laser 2000 ****

10 Literatur

1. Gaulin A (1899) Appareil et Procédé pour la Stabilisation du Lait (295596)
2. Seifriz W (1925) Studies in emulsions III. Double reversal of oil emulsions occasioned by the same electrolyte. J. phys. Chem. (29):738–749
3. Leister N, Karbstein HP (2021) Influence of Hydrophilic Surfactants on the W1–W2 Coalescence in Double Emulsion Systems Investigated by Single Droplet Experiments. Colloids and Interfaces 5(2):21. doi:10.3390/colloids5020021
4. Muschiolik G, Dickinson E (2017) Double Emulsions Relevant to Food Systems: Preparation, Stability, and Applications. Compr Rev Food Sci Food Saf 16(3):532–555. doi:10.1111/1541-4337.12261
5. Leister N, Karbstein HP (2020) Evaluating the Stability of Double Emulsions—A Review of the Measurement Techniques for the Systematic Investigation of Instability Mechanisms. Colloids and Interfaces 4(1):8. doi:10.3390/colloids4010008
6. Köhler K (Hrsg) (2012) Emulgiertechnik. Grundlagen, Verfahren und Anwendungen, 3. Aufl. Behr, Hamburg
7. Orlando A, Franceschini F, Muscas C, Pidkova S, Bartoli M, Rovere M, Tagliaferro A (2021) A Comprehensive Review on Raman Spectroscopy Applications. Chemosensors 9(9):262. doi:10.3390/chemosensors9090262
8. Petersen M, Yu Z, Lu X (2021) Application of Raman Spectroscopic Methods in Food Safety: A Review. Biosensors (Basel) 11(6). doi:10.3390/bios11060187
9. Kortüm G (1969) Reflectance Spectroscopy. Principles, Methods, Applications. Springer International Publishing, New York, NY
10. Meyer T, Akimov D, Tarcea N, Chatzipapadopoulos S, Muschiolik G, Kobow J, Schmitt M, Popp J (2008) Three-dimensional molecular mapping of a multiple emulsion by means of CARS microscopy. J Phys Chem B 112(5):1420–1426. doi:10.1021/jp709643h
11. Leister N, Yan C, Karbstein HP (2022) Oil Droplet Coalescence in W/O/W Double Emulsions Examined in Models from Micrometer- to Millimeter-Sized Droplets. Colloids and Interfaces 6(1):12. doi:10.3390/colloids6010012
12. Mezzenga R, Folmer BM, Hughes E (2004) Design of double emulsions by osmotic pressure tailoring. Langmuir 20(9):3574–3582. doi:10.1021/la036396k
13. Saffarionpour S, Diosady LL (2021) Multiple Emulsions for Enhanced Delivery of Vitamins and Iron Micronutrients and Their Application for Food Fortification. Food Bioprocess Technol 14(4):587–625. doi:10.1007/s11947-021-02586-2

14. Sun BJ, Shum HC, Holtze C, Weitz DA (2010) Microfluidic melt emulsification for encapsulation and release of actives. ACS Appl Mater Interfaces 2(12):3411–3416. doi:10.1021/am100860b
15. Leister N, Vladisavljević GT, Karbstein HP (2022) Novel glass capillary microfluidic devices for the flexible and simple production of multi-cored double emulsions. J Colloid Interface Sci 611:451–461. doi:10.1016/j.jcis.2021.12.094
16. Teh S-Y, Lin R, Hung L-H, Lee AP (2008) Droplet microfluidics. Lab Chip 8(2):198–220. doi:10.1039/b715524g
17. Utada AS, Lorenceau E, Link DR, Kaplan PD, Stone HA, Weitz DA (2005) Monodisperse double emulsions generated from a microcapillary device. Science (New York, N.Y.) 308(5721):537–541. doi:10.1126/science.1109164
18. Datta SS, Abbaspourrad A, Amstad E, Fan J, Kim S-H, Romanowsky M, Shum HC, Sun B, Utada AS, Windbergs M, Zhou S, Weitz DA (2014) 25th anniversary article: double emulsion templated solid microcapsules: mechanics and controlled release. Adv Mater 26(14):2205–2218. doi:10.1002/adma.201305119
19. Theberge AB, Courtois F, Schaerli Y, Fischlechner M, Abell C, Hollfelder F, Huck WTS (2010) Microdroplets in microfluidics: an evolving platform for discoveries in chemistry and biology. Angew Chem Int Ed Engl 49(34):5846–5868. doi:10.1002/anie.200906653
20. Vladisavljević G, Al Nuumani R, Nabavi S (2017) Microfluidic Production of Multiple Emulsions. Micromachines 8(3):75. doi:10.3390/mi8030075
21. Rosano H, Gandolfo, F.G., Hidrot, J.-D.P. (1998) Stability of W1/O/W2 multiple emulsions influence of ripening and interfacial interactions. Colloids and Surfaces A: Physicochemical and Engineering Aspects (138):109–121
22. Neumann SM, van der Schaaf US, Karbstein HP (2018) Investigations on the relationship between interfacial and single droplet experiments to describe instability mechanisms in double emulsions. Colloids and Surfaces A: Physicochemical and Engineering Aspects 553:464–471. doi:10.1016/j.colsurfa.2018.05.087
23. Scherze I, Knöfel R, Muschiolik G (2005) Automated image analysis as a control tool for multiple emulsions. Food Hydrocolloids 19(3):617–624. doi:10.1016/j.foodhyd.2004.10.029
24. Schuch A, Köhler K, Schuchmann HP (2013) Differential scanning calorimetry (DSC) in multiple W/O/W emulsions. J Therm Anal Calorim 111(3):1881–1890. doi:10.1007/s10973-012-2751-2
25. Neumann SM, van der Schaaf US, Karbstein HP (2018) Structure stability and crystallization behavior of water in oil in water (WOW) double emulsions during their characterization by differential scanning calorimetry (DSC). J Therm Anal Calorim 133(3):1499–1508. doi:10.1007/s10973-017-6723-4

26. Guan X, Hailu K, Guthausen G, Wolf F, Bernewitz R, Schuchmann HP (2010) PFG-NMR on W 1 /O/W 2 -emulsions: Evidence for molecular exchange between water phases. Eur. J. Lipid Sci. Technol. 112(8):828–837. doi:10.1002/ejlt.201000022
27. Dieing T, Hollricher O, Toporski J (2011) Confocal Raman Microscopy. Springer Series in Optical Sciences, Bd 158. Springer Berlin Heidelberg, Berlin, Heidelberg
28. Geraldes CFGC (2020) Introduction to Infrared and Raman-Based Biomedical Molecular Imaging and Comparison with Other Modalities. Molecules 25(23). doi:10.3390/molecules25235547
29. Saletnik A, Saletnik B, Puchalski C (2021) Overview of Popular Techniques of Raman Spectroscopy and Their Potential in the Study of Plant Tissues. Molecules 26(6):1537. doi:10.3390/molecules26061537
30. Goldrick S, Lovett D, Montague G, Lennox B (2018) Influence of Incident Wavelength and Detector Material Selection on Fluorescence in the Application of Raman Spectroscopy to a Fungal Fermentation Process. Bioengineering (Basel) 5(4). doi:10.3390/bioengineering5040079
31. Smith E (2019) Modern Raman Spectroscopy. A Practical Approach, 2. Aufl. John Wiley et Sons, Incorporated, Newark
32. Kapusta P, Wahl M, Erdmann R (2015) Advanced Photon Counting, Bd 15. Springer International Publishing, Cham
33. Demtröder W (2007) Laserspektroskopie. Grundlagen und Techniken, 5. Aufl. Springer, Berlin, Heidelberg
34. Nachtmann M, Keck SP, Braun F, Eckhardt HS, Mattolat C, Gretz N, Scholl S, Rädle M (2018) A customized stand-alone photometric Raman sensor applicable in explosive atmospheres: a proof-of-concept study. J. Sens. Sens. Syst. 7(2):543–549. doi:10.5194/jsss-7-543-2018
35. Bai L, Huan S, Rojas OJ, McClements DJ (2021) Recent Innovations in Emulsion Science and Technology for Food Applications. J Agric Food Chem 69(32):8944–8963. doi:10.1021/acs.jafc.1c01877
36. Schuster S, Bernewitz R, Guthausen G, Zapp J, Greiner AM, Köhler K, Schuchmann HP (2012) Analysis of W1/O/W2 double emulsions with CLSM: Statistical image processing for droplet size distribution. Chemical Engineering Science 81:84–90. doi:10.1016/j.ces.2012.06.059
37. Budwig R (1994) Refractive index matching methods for liquid flow investigations. Exp Fluids 17(5):350–355. doi:10.1007/BF01874416
38. Wiederseiner S, Andreini N, Epely-Chauvin G, Ancey C (2011) Refractive-index and density matching in concentrated particle suspensions: a review. Exp Fluids 50(5):1183–1206. doi:10.1007/s00348-010-0996-8

39. Schalk R, Heintz A, Braun F, Iacono G, Rädle M, Gretz N, Methner F-J, Beuermann T (2019) Comparison of Raman and Mid-Infrared Spectroscopy for Real-Time Monitoring of Yeast Fermentations: A Proof-of-Concept for Multi-Channel Photometric Sensors. Applied Sciences 9(12):2472. doi:10.3390/app9122472
40. Kudelski A (2008) Analytical applications of Raman spectroscopy. Talanta (1):1–8. doi:10.1016/j.talanta.2008.02.042
41. Elizalde O, Leiza JR, Asua JM (2004) On-line monitoring of all-acrylic emulsion polymerization reactors by Raman spectroscopy. Macromol. Symp. 206(1):135–148. doi:10.1002/masy.200450211
42. He H, Sun D-W, Pu H, Chen L, Lin L (2019) Applications of Raman spectroscopic techniques for quality and safety evaluation of milk: A review of recent developments. Crit Rev Food Sci Nutr 59(5):770–793. doi:10.1080/10408398.2018.1528436
43. Zhang W, Ma J, Sun D-W (2021) Raman spectroscopic techniques for detecting structure and quality of frozen foods: principles and applications. Crit Rev Food Sci Nutr 61(16):2623–2639. doi:10.1080/10408398.2020.1828814
44. Da Jesus JISSd, Löbenberg R, Bou-Chacra NA (2020) Raman Spectroscopy for Quantitative Analysis in the Pharmaceutical Industry. Journal of Pharmacy & Pharmaceutical Sciences 23(1):24–46. doi:10.18433/jpps30649
45. Kollhoff RT, Kelemen K, Schuchmann HP (2015) Local Multiphase Flow Characterization with Micro Particle Image Velocimetry Using Refractive Index Matching. Chem. Eng. Technol. 38(10):1774–1782. doi:10.1002/ceat.201500318
46. Schalk R, Braun F, Frank R, Rädle M, Gretz N, Methner F-J, Beuermann T (2017) Non-contact Raman spectroscopy for in-line monitoring of glucose and ethanol during yeast fermentations. Bioprocess Biosyst Eng 40(10):1519–1527. doi:10.1007/s00449-017-1808-9
47. Tan C, McClements DJ (2021) Application of Advanced Emulsion Technology in the Food Industry: A Review and Critical Evaluation. Foods 10(4). doi:10.3390/foods10040812
48. Khan AY, Talegaonkar S, Iqbal Z, Ahmed FJ, Khar RK (2006) Multiple emulsions: an overview. Curr Drug Deliv 3(4):429–443. doi:10.2174/156720106778559056
49. Wang W, Zhang M-J, Chu L-Y (2014) Microfluidic approach for encapsulation via double emulsions. Current Opinion in Pharmacology 18:35–41. doi:10.1016/j.coph.2014.08.003
50. Iqbal M, Zafar N, Fessi H, Elaissari A (2015) Double emulsion solvent evaporation techniques used for drug encapsulation. Int J Pharm 496(2):173–190. doi:10.1016/j.ijpharm.2015.10.057
51. Muschiolik G (2007) Multiple emulsions for food use. Current Opinion in Colloid & Interface Science 12(4-5):213–220. doi:10.1016/j.cocis.2007.07.006

52. Schuch A, Wrenger J, Schuchmann HP (2014) Production of W/O/W double emulsions. Part II: Influence of emulsification device on release of water by coalescence. Colloids and Surfaces A: Physicochemical and Engineering Aspects 461:344–351. doi:10.1016/j.colsurfa.2013.11.044
53. Schuch A, Tonay AN, Köhler K, Schuchmann HP (2014) Influence of the second emulsification step during production of W/O/W multiple emulsions: Comparison of different methods to determine encapsulation efficiency in W/O/W emulsions. Can. J. Chem. Eng. 92(2):203–209. doi:10.1002/cjce.21834
54. Nabavi SA, Vladisavljević GT, Gu S, Ekanem EE (2015) Double emulsion production in glass capillary microfluidic device: Parametric investigation of droplet generation behaviour. Chemical Engineering Science 130:183–196. doi:10.1016/j.ces.2015.03.004
55. Bandulasena MV, Vladisavljević GT, Benyahia B (2019) Versatile reconfigurable glass capillary microfluidic devices with Lego® inspired blocks for drop generation and micromixing. J Colloid Interface Sci 542:23–32. doi:10.1016/j.jcis.2019.01.119
56. Nabavi SA, Vladisavljević GT, Bandulasena MV, Arjmandi-Tash O, Manović V (2017) Prediction and control of drop formation modes in microfluidic generation of double emulsions by single-step emulsification. J Colloid Interface Sci 505:315–324. doi:10.1016/j.jcis.2017.05.115
57. Bernewitz R, Dalitz F, Köhler K, Schuchmann HP, Guthausen G (2013) Characterisation of multiple emulsions by NMR spectroscopy and diffusometry. Microporous and Mesoporous Materials 178:69–73. doi:10.1016/j.micromeso.2013.02.049
58. Nachtmann M, Deuerling J, Rädle M (2020) Molecule Sensitive Optical Imaging and Monitoring Techniques-A Review of Applications in Micro-Process Engineering. Micromachines 11(4). doi:10.3390/mi11040353
59. Diaz D, Hahn DW (2020) Raman spectroscopy for detection of ammonium nitrate as an explosive precursor used in improvised explosive devices. Spectrochim Acta A Mol Biomol Spectrosc 233:118204. doi:10.1016/j.saa.2020.118204
60. Erckens RJ, Hosseini K, March WF, Jongsma FHM, Wicksted JP, Li HK, Hendrikse F (2002) Raman spectroscopy: noninvasive determination of silicone oil in the eye: potential applications for intraocular determination of biomaterials. Retina 22(6):796–799. doi:10.1097/00006982-200212000-00019
61. Mendelovici E, Frost RL, Kloprogge T (2000) Cryogenic Raman spectroscopy of glycerol. J. Raman Spectrosc. 31(12):1121–1126. doi:10.1002/1097-4555(200012)31:12<1121::AID-JRS654>3.0.CO;2-G
62. VANDERGRAAF S, SCHROEN C, BOOM R (2005) Preparation of double emulsions by membrane emulsification?a review. Journal of Membrane Science 251(1-2):7–15. doi:10.1016/j.memsci.2004.12.013

63. Benichou A, Aserin A, Garti N (2007) W/O/W double emulsions stabilized with WPI–polysaccharide complexes. Colloids and Surfaces A: Physicochemical and Engineering Aspects 294(1-3):20–32. doi:10.1016/j.colsurfa.2006.07.056
64. Lamba H, Sathish K, Sabikhi L (2015) Double Emulsions: Emerging Delivery System for Plant Bioactives. Food Bioprocess Technol 8(4):709–728. doi:10.1007/s11947-014-1468-6
65. Bernewitz R, Guthausen G, Schuchmann HP (2016) Imaging of Double Emulsions Imaging Technologies and Data Processing for Food Engineers. Springer, Cham, S 69–98
66. Bernewitz R, Schmidt US, Schuchmann HP, Guthausen G (2014) Structure of and diffusion in O/W/O double emulsions by CLSM and NMR–comparison with W/O/W. Colloids and Surfaces A: Physicochemical and Engineering Aspects 458:10–18. doi:10.1016/j.colsurfa.2014.01.002
67. Bernewitz R, Guan X, Guthausen G, Wolf F, Schuchmann HP (2011) PFG-NMR on Double Emulsions: a Detailed Look into Molecular Processes Magnetic Resonance in Food Science. Royal Society of Chemistry, Cambridge, S 39–46
68. Lutz R, Aserin A, Wicker L, Garti N (2009) Double emulsions stabilized by a charged complex of modified pectin and whey protein isolate. Colloids Surf B Biointerfaces 72(1):121–127. doi:10.1016/j.colsurfb.2009.03.024
69. Rantanen J (2007) Process analytical applications of Raman spectroscopy. J Pharm Pharmacol 59(2):171–177. doi:10.1211/jpp.59.2.0004
70. Chen X, Laughlin K, Sparks JR, Linder L, Farozic V, Masser H, Petr M (2015) In Situ Monitoring of Emulsion Polymerization by Raman Spectroscopy: A Robust and Versatile Chemometric Analysis Method. Org. Process Res. Dev. 19(8):995–1003. doi:10.1021/acs.oprd.5b00045
71. Hufnagel T, Rädle M, Karbstein HP (2022) Influence of Refractive Index Differences on the Signal Strength for Raman-Spectroscopic Measurements of Double Emulsion Droplets. Applied Sciences 12(18):9056. doi:10.3390/app12189056
72. Sela Y, Magdassi S, Garti N (1995) Release of markers from the inner water phase of W / O / W emulsions stabilized by silicone based polymeric surfactants. Journal of Controlled Release 33(1):1–12. doi:10.1016/0168-3659(94)00029-t
73. Eisinaite V, Duque Estrada P, Schroën K, Berton-Carabin C, Leskauskaite D (2018) Tayloring W/O/W emulsion composition for effective encapsulation: The role of PGPR in water transfer-induced swelling. Food Res Int 106:722–728. doi:10.1016/j.foodres.2018.01.042

74. Khadem B, Khellaf M, Sheibat-Othman N (2020) Investigating swelling-breakdown in double emulsions. Colloids and Surfaces A: Physicochemical and Engineering Aspects 585:124181. doi:10.1016/j.colsurfa.2019.124181
75. Khadem B, Sheibat-Othman N (2020) Modeling droplets swelling and escape in double emulsions using population balance equations. Chemical Engineering Journal 382:122824. doi:10.1016/j.cej.2019.122824
76. Garti N, Bisperink C (1998) Double emulsions: Progress and applications. Current Opinion in Colloid & Interface Science 3(6):657–667. doi:10.1016/s1359-0294(98)80096-4
77. McClements DJ (2015) Encapsulation, protection, and release of hydrophilic active components: potential and limitations of colloidal delivery systems. Advances in Colloid and Interface Science 219:27–53. doi:10.1016/j.cis.2015.02.002
78. McClements DJ, Jafari SM (2018) Improving emulsion formation, stability and performance using mixed emulsifiers: A review. Advances in Colloid and Interface Science 251:55–79. doi:10.1016/j.cis.2017.12.001
79. Dickinson E (2011) Double Emulsions Stabilized by Food Biopolymers. Food Biophysics 6(1):1–11. doi:10.1007/s11483-010-9188-6
80. Kanouni M, Rosano H, Naouli N (2002) Preparation of a stable double emulsion (W1/O/W2): role of the interfacial films on the stability of the system. Advances in Colloid and Interface Science 99(3):229–254. doi:10.1016/s0001-8686(02)00079-9
81. Yafei W, Tao Z, Gang H (2006) Structural evolution of polymer-stabilized double emulsions. Langmuir 22(1):67–73. doi:10.1021/la0523255
82. Nazir H, Zhang W, Liu Y, Chen X, Wang L, Naseer MM, Ma G (2014) Silicone oil emulsions: strategies to improve their stability and applications in hair care products. Int J Cosmet Sci 36(2):124–133. doi:10.1111/ics.12104
83. Garti N (1997) Progress in Stabilization and Transport Phenomena of Double Emulsions in Food Applications. LWT - Food Science and Technology 30(3):222–235. doi:10.1006/fstl.1996.0176
84. Regan JO, Mulvihill DM (2009) Water soluble inner aqueous phase markers as indicators of the encapsulation properties of water-in-oil-in-water emulsions stabilized with sodium caseinate. Food Hydrocolloids 23(8):2339–2345. doi:10.1016/j.foodhyd.2009.06.009
85. Hai M, Magdassi S (2004) Investigation on the release of fluorescent markers from w/o/w emulsions by fluorescence-activated cell sorter. Journal of Controlled Release 96(3):393–402. doi:10.1016/j.jconrel.2004.02.014
86. van Duynhoven JPM, Goudappel GJW, van Dalen G, van Bruggen PC, Blonk JCG, Eijkelenboom APAM (2002) Scope of droplet size measurements in food emulsions by

pulsed field gradient NMR at low field. Magn. Reson. Chem. 40(13):S51-S59. doi:10.1002/mrc.1115

87. (2013) Charakterisierung von Doppelemulsionen mittels NMR und CLSM-Struktur und Diffusion
88. Hufnagel T, Stoy R, Rädle M, Karbstein HP (2022) Measurement of the Filling Degree and Droplet Size of Individual Double Emulsion Droplets Using Raman Technologies. Chemosensors 10(11):463. doi:10.3390/chemosensors10110463
89. Guo S, Bocklitz T, Popp J (2016) Optimization of Raman-spectrum baseline correction in biological application. Analyst 141(8):2396–2404. doi:10.1039/c6an00041j
90. Hufnagel T, Leister N, Stoy R, Rädle M, Karbstein HP (2023) Research data to "Monitoring of osmotic swelling induced filling degree changes in WOW double emulsions using Raman technologies". Karlsruher Institut für Technologie (KIT)
91. Kuchenbecker P, Gemeinert M, Rabe T (2012) Inter-laboratory Study of Particle Size Distribution Measurements by Laser Diffraction. Part. Part. Syst. Charact. 29(4):304–310. doi:10.1002/ppsc.201000026
92. Poval™ K Kuraray Poval™ – Basic Physical Properties of PVOH Resin
93. Cordero E, Korinth F, Stiebing C, Krafft C, Schie IW, Popp J (2017) Evaluation of Shifted Excitation Raman Difference Spectroscopy and Comparison to Computational Background Correction Methods Applied to Biochemical Raman Spectra. Sensors (Basel) 17(8). doi:10.3390/s17081724

11 List of Figures

12 List of Tables

13 List of Publications

13.1 Peer-reviewed articles

Teumer, T.; Hufnagel, T.; Schäfer, T.; Schlarp-Horvath, R.; Karbstein, H.P.; Methner, F.; Rädle, M. *Entwicklung eines Partikelmesssystems zur Erfassung geringer Streulicht-Intensitäten optimiert für den Einsatz sehr schwacher Laserstrahlen*. Chem. Ing. Tech. **2019**, 91, 529–533.

Deuerling, J.; Manser, S.; Siber, J.; Keck, S.; Hufnagel, T.; Schmitt, L.; Medina, I.; Repke, J.-U.; Rädle, M. *Schnelle lokale Raman-Messung zur Untersuchung von Konzentrationsprofilen bei Mischvorgängen in Mikrokanälen*. Chem. Ing. Tech. **2019**, 83, 593.

Hufnagel, T.; Rädle, M.; Karbstein, H.P. *Influence of Refractive Index Differences on the Signal Strength for Raman-Spectroscopic Measurements of Double Emulsion Droplets*. *Appl. Sci.* **2022**, *12*, 9056. https://doi.org/10.3390/app12189056

Hufnagel, T.; Stoy, R.; Rädle, M.; Karbstein, H.P. *Measurement of the Filling Degree and Droplet Size of Individual Double Emulsion Droplets Using Raman Technologies*. *Chemosensors* **2022**, *10*, 463. https://doi.org/10.3390/chemosensors10110463

Hufnagel, T.; Leister, N.; Stoy, R.; Rädle, M.; Karbstein, H.P. *Monitoring of Osmotic Swelling Induced Filling Degree Changes in WOW Double Emulsions Using Raman Technologies*. *Chemosensors* **2023**, *11*, 206. https://doi.org/10.3390/chemosensors11040206

13.2 Poster presentations

Medina, I.; Teumer, T.; Strischakov, J.; Hufnagel, T.; Hohlen, A.; Schwede, C.; Melchin, T.; Scholl, S.; Rädle, M.; *Entwicklung optischer Sensoren zur Detektion der Belagbildung durch Reaktionsfouling*; Poster presentation held at the Jahrestreffen der ProcessNet-Fachgemeinschaft Prozess-, Apparate- und AnlagentechnikVirtuelle Tagung, 09.-10. November 2020

Teumer, T.; Moelyadi, I.; Hufnagel, T.; Stähle, P.; Rädle, M.; *Entwicklung eines optischen Sensors zur Detektion von schnellen Fällungsreaktionen bzw. Kristallwachstumsvorgängen in Mikrokanälen*; Poster presentation held at the 16. Kolloqium Prozessanalytik – Digital – 24.11.2020

Hufnagel, T.; Keck, S.; Schorz, S.; Rädle, M.; Ahlers, R.; *Raman – monitoring of water quality in waste water treatment plants: A novel method of highly sensitive Raman measurement for optimization of the waste water treatment process*; Poster presentation held at the EuroPACT 2021 – Digital – 24.11.2021

Teumer, T.; Wühler, F.; Moelyadi, I.; Hufnagel, T.; Lerche, D.; Rädle, M.; *Controlled dilution of micro- and nano-suspension as preparation for single particle measurements*; Poster presentation held at the EuroPACT 2021 – Digital – 24.11.2021